Improving the Foundation Layers for Concrete Pavements

TECHNICAL REPORT:

Pavement Foundation Layer Reconstruction – Iowa US 30 Field Study

March 2016

Sponsored by
Federal Highway Administration (DTFH 61-06-H-00011 (Work Plan #18))
FHWA TPF-5(183): California, Iowa (lead state), Michigan, Pennsylvania, Wisconsin

National Concrete Pavement Technology Center
Tech Center

CENTER FOR CEER EARTHWORKS ENGINEERING RESEARCH
IOWA STATE UNIVERSITY
Institute for Transportation

About the National CP Tech Center

The mission of the National Concrete Pavement Technology (CP Tech) Center is to unite key transportation stakeholders around the central goal of advancing concrete pavement technology through research, tech transfer, and technology implementation.

About CEER

The mission of the Center for Earthworks Engineering Research (CEER) at Iowa State University is to be the nation's premier institution for developing fundamental knowledge of earth mechanics, and creating innovative technologies, sensors, and systems to enable rapid, high quality, environmentally friendly, and economical construction of roadways, aviation runways, railroad embankments, dams, structural foundations, fortifications constructed from earth materials, and related geotechnical applications.

Disclaimer Notice

The contents of this report reflect the views of the authors, who are responsible for the facts and the accuracy of the information presented herein. The opinions, findings and conclusions expressed in this publication are those of the authors and not necessarily those of the sponsors.

The sponsors assume no liability for the contents or use of the information contained in this document. This report does not constitute a standard, specification, or regulation.

The sponsors do not endorse products or manufacturers. Trademarks or manufacturers' names appear in this report only because they are considered essential to the objective of the document.

Iowa State University Non-Discrimination Statement

Iowa State University does not discriminate on the basis of race, color, age, ethnicity, religion, national origin, pregnancy, sexual orientation, gender identity, genetic information, sex, marital status, disability, or status as a U.S. veteran. Inquiries regarding non-discrimination policies may be directed to Office of Equal Opportunity, Title IX/ADA Coordinator, and Affirmative Action Officer, 3350 Beardshear Hall, Ames, Iowa 50011, 515-294-7612, email eooffice@iastate.edu.

Iowa Department of Transportation Statements

Federal and state laws prohibit employment and/or public accommodation discrimination on the basis of age, color, creed, disability, gender identity, national origin, pregnancy, race, religion, sex, sexual orientation or veteran's status. If you believe you have been discriminated against, please contact the Iowa Civil Rights Commission at 800-457-4416 or the Iowa Department of Transportation affirmative action officer. If you need accommodations because of a disability to access the Iowa Department of Transportation's services, contact the agency's affirmative action officer at 800-262-0003.

The preparation of this report was financed in part through funds provided by the Iowa Department of Transportation through its "Second Revised Agreement for the Management of Research Conducted by Iowa State University for the Iowa Department of Transportation" and its amendments.

The opinions, findings, and conclusions expressed in this publication are those of the authors and not necessarily those of the Iowa Department of Transportation or the U.S. Department of Transportation Federal Highway Administration.

Technical Report Documentation Page

1. Report No. DTFH 61-06-H-00011 Work Plan 18	**2. Government Accession No.**	**3. Recipient's Catalog No.**
4. Title and Subtitle Improving the Foundation Layers for Concrete Pavements: Pavement Foundation Layer Reconstruction – Iowa US 30 Field Study		**5. Report Date** March 2016 **6. Performing Organization Code**
7. Author(s) David J. White, Pavana Vennapusa, Yang Zhang, Alex Johnson		**8. Performing Organization Report No.** InTrans Project 09-352
9. Performing Organization Name and Address National Concrete Pavement Technology Center and Center for Earthworks Engineering Research Iowa State University 2711 South Loop Drive, Suite 4700 Ames, IA 50010-8664		**10. Work Unit No. (TRAIS)** **11. Contract or Grant No.**
12. Sponsoring Organization Name and Address Federal Highway Administration U.S. Department of Transportation 1200 New Jersey Avenue SE Washington, DC 20590		**13. Type of Report and Period Covered** Technical Report **14. Sponsoring Agency Code** TPF-5(183)
15. Supplementary Notes Visit www.cptechcenter.org or www.ceer.iastate.edu for color PDF files of this and other research reports.		

16. Abstract

This technical project report is one of the field project reports developed as part of the TPF-5(183) and FHWA DTFH 61-06-H-00011:WO18 studies.

This report presents results and analysis of field and laboratory tests from a field study conducted on a US 30 reconstruction project in Boone County, Iowa. The project involved removal of the existing pavement, which showed severe pavement distresses; reconstruction of the pavement foundation layers (base, subbase, and subgrade); and placement of a new jointed plain cement pavement (JPCC).

Field testing was conducted by the Iowa State University (ISU) research team on the existing pavement prior to reconstruction work, on the new foundation layers, and on the newly constructed pavement. A detailed laboratory testing plan was executed on bulk samples of RPCC, RPCC/RAP, and subgrade layers. In situ LWD and DCP tests were conducted on the newly constructed foundation layers, and FWD tests were conducted after the pavement was placed. Temperature monitoring was conducted.

Results are detailed in the report.

17. Key Words concrete pavement—pavement foundation— mechanistic property—seasonal variation—in situ testing—subgrade		**18. Distribution Statement** No restrictions.	
19. Security Classification (of this report) Unclassified.	**20. Security Classification (of this page)** Unclassified.	**21. No. of Pages** 148	**22. Price**

Form DOT F 1700.7 (8-72) **Reproduction of completed page authorized**

IMPROVING THE FOUNDATION LAYERS FOR CONCRETE PAVEMENTS: PAVEMENT FOUNDATION LAYER RECONSTRUCTION – IOWA US 30 FIELD STUDY

Technical Report
March 2016

Research Team Members
Tom Cackler, David J. White, Jeffrey R. Roesler, Barry Christopher, Andrew Dawson, Heath Gieselman, and Pavana Vennapusa

Report Authors
David J. White, Pavana K. R. Vennapusa,
Yang Zhang, Alex Johnson
Iowa State University

Sponsored by
the Federal Highway Administration (FHWA)
DTFH61-06-H-00011 Work Plan 18
FHWA Pooled Fund Study TPF-5(183): California, Iowa (lead state), Michigan, Pennsylvania, Wisconsin

Preparation of this report was financed in part
through funds provided by the Iowa Department of Transportation
through its Research Management Agreement with the
Institute for Transportation
(InTrans Project 09-352)

National Concrete Pavement Technology Center and
Center for Earthworks Engineering Research
Iowa State University
2711 South Loop Drive, Suite 4700
Ames, IA 50010-8664
Phone: 515-294-8103
www.cptechcenter.org and www.ceer.iastate.edu

TABLE OF CONTENTS

LIST OF FIGURES

LIST OF TABLES

ACKNOWLEDGMENTS

This research was conducted under Federal Highway Administration (FHWA) DTFH61-06-H-00011 Work Plan 18 and the FHWA Pooled Fund Study TPF-5(183), involving the following state departments of transportation:

- California
- Iowa (lead state)
- Michigan
- Pennsylvania
- Wisconsin

The authors would like to express their gratitude to the National Concrete Pavement Technology (CP Tech) Center, the FHWA, the Iowa Department of Transportation (DOT), and the other pooled fund state partners for their financial support and technical assistance.

Chris Brakee, Melissa Serio, and several others with the Iowa Department of Transportation provided assistance in identifying the project, providing access to the project site, and obtaining project design information and specifications. Christianna White provided comments and editorial support. We greatly appreciate their help.

LIST OF ACRONYMS AND SYMBOLS

CBR	California bearing ratio
$DCP\text{-}CBR_{Subgrade}$	CBR of subgrade determined from DCP test
$DCP\text{-}CBR_{Subbase}$	CBR of subbase determined from DCP test
DPI	Dynamic penetration index
D_0	Deflection measured under the plate
D_1	Deflection measured on the unloaded slab
D_{10}	Grain size diameter corresponding to 10% passing by mass
D_{30}	Grain size diameter corresponding to 30% passing by mass
D_{60}	Grain size diameter corresponding to 60% passing by mass
E	Elastic modulus
E_{LWD}	Elastic modulus determined from 300 mm diameter plate Zorn light weight deflectometer
F	Shape factor
G_s	Specific gravity
I	Intercept
k	Modulus of subgrade reaction
k_{AASHTO}	Modulus of subgrade reaction determined following AASHTO (1993) procedure
k_{comp}	Composite modulus of subgrade reaction
k_{PCA}	Modulus of subgrade reaction estimated from CBR following PCA (1984) procedure
$k_{FWD\text{-}Dynamic}$	Dynamic modulus of subgrade reaction from FWD test
$k_{FWD\text{-}Static}$	Static modulus of subgrade reaction from FWD test
$k_{FWD\text{-}Static\text{-}Corr}$	Static modulus of subgrade reaction from FWD test correlated for slab size
k_1, k_2, k_3	Regression coefficients in “universal” model
LL	Liquid limit
M_r	Resilient modulus
n	Number of measurements
p	Number of parameters
PI	Plasticity index
PL	Plastic limit
P_a	Atmospheric pressure
R^2	Coefficient of determination
r	Plate radius
s_u	Undrained shear strength
w	Moisture content
w_{opt}	Optimum moisture content
ε	Axial strain
ε_p	Permanent strain
ε_f	Permanent strain at failure
ε_r	Resilient strain
γ_d	Dry unit weight
γ_{dmax}	Maximum dry unit weight
μ	Statistical mean or average

η	Poisson's ratio
σ	Statistical standard deviation
σ_B	Bulk stress
σ_c	Confining pressure
σ_d	Deviator stress
$\sigma_{d\ max}$	Maximum deviator stress
σ_0	Applied axial stress
$\sigma_1, \sigma_2, \sigma_3$	Principal stresses
τ_{oct}	Octahedral shear stress

EXECUTIVE SUMMARY

Quality foundation layers (the natural subgrade, subbase, and embankment) are essential to achieving excellent pavement performance. Unfortunately, many pavements in the United States still fail due to inadequate foundation layers. To address this problem, a research project, Improving the Foundation Layers for Pavements (FHWA DTFH 61-06-H-00011 WO #18; FHWA TPF-5(183)), was undertaken by Iowa State University (ISU) to identify, and provide guidance for implementing, best practices regarding foundation layer construction methods, material selection, in situ testing and evaluation, and performance-related designs and specifications. As part of the project, field studies were conducted in several in-service concrete pavements across the country that represented either premature failures or successful long-term pavements. A key aspect of each field study was to tie performance of the foundation layers to key engineering properties and pavement performance. In situ foundation layer performance data, as well as original construction data and maintenance/rehabilitation history data, were collected and geospatially and statistically analyzed to determine the effects of site-specific foundation layer construction methods, site evaluation, materials selection, design, treatments, and maintenance procedures on the performance of the foundation layers and of the related pavements. A technical report was prepared for each field study.

This report presents results and analysis of field and laboratory tests from a field study conducted on a US 30 reconstruction project in Boone County, Iowa. The project involved removal of the existing pavement which showed severe pavement distresses, reconstruction of the pavement foundation layers (base, subbase, and subgrade), and placement of a new jointed plain cement pavement (JPCC) on the east and west bound lanes of US 30 between mileposts 139.0 and 147.27. Field testing was conducted by the Iowa State University (ISU) research team on the existing pavement prior to reconstruction work, on the new foundation layers, and on the newly constructed pavement.

The existing pavement consisted of nominal 76 mm (3 in.) thick asphalt concrete (AC) overlay on nominal 229 mm (9 in.) thick portland cement concrete (PCC). The pavement layers were underlain by nominal 102 mm (4 in.) thick asphalt treated base (ATB). The existing pavement and the ATB layers were removed and the subgrade was undercut during the reconstruction process to place a nominal 410 mm (16 in.) thick modified subbase over the natural existing subgrade. The modified subbase layer consisted of 150 mm (6 in.) thick recycled portland cement concrete (RPCC) material or crushed limestone at the surface underlain by 260 mm (10 in.) thick mixture of RPCC and recycled asphalt pavement (RAP) material. A nominal 254 mm (10 in.) thick JPCP was placed on the newly constructed foundation layer.

Following is a summary of key findings from testing on the existing pavement:

- The existing pavement showed severe pavement distresses with reflective cracking and vertical upheave near joints, especially during winter. The Iowa DOT also reported incidents of damage to vehicle tires and problems with snowplow blade contact.
- Initial field investigations by the Iowa DOT rated the ride quality of the pavement section as “poor” based on pavement condition index (PCI) ranging between 54 and 56 on a 0-100 scale

(100 being good and 0 being failed condition).

- Core samples of the existing pavement were obtained near joints using 254 mm (10 in.) and 100 mm (4 in.) diameter diamond rotary bits. These core samples showed that the PCC and the ATB layers were severely deteriorated. Ice lenses and trapped water were presented at the interface of the HMA overlay and PCC, and PCC and ATB layers.
- The gravimetric moisture contents of PCC layer samples ranged between 12.5% and 20.4%. The PCC layer samples obtained from joints showed very little structural integrity.
- Vertical heaves ranging between 15 mm (0.6 in.) to 38 mm (1.5 in.) were measured at two four joints tested.

A detailed laboratory testing plan was executed on bulk samples of RPCC, RPCC/RAP, and subgrade layers. Laboratory testing included characterizing soil index properties, moisture-dry unit weight relationships, resilient modulus (M_r), permanent deformation and particle degradation behavior under cyclic triaxial loading, and frost-heave and thaw-weakening susceptibility. Following are some key findings from the laboratory study:

- Cyclic triaxial testing on RPCC/RAP material indicated that deviator stress and fines content have statistically significant influence on the permanent deformation behavior of the material. Relative density of the material was not found to be a statistically significant parameter for the range testing (85% to 95% relative density).
- Particle degradation due to cyclic loading was assessed by conducting particle-size analysis before and after cyclic triaxial loading on RPCC/RAP material samples. The particle-size analysis test results were used to determining breakage index (BI). Results indicated that the BI values varied between 0 and 5%, which is not considered significant.
- No significant difference or trend in the data was observed between relative density and M_r values on RPCC/RAP material samples. A similar observation was confirmed on recycled materials by other researchers.
- M_r test results on RPCC/RAP material showed that samples with about 12% fines content showed the largest M_r values and M_r values generally increased with increasing fines content at all relative densities.
- Based on M_r testing on the RPCC/RAP materials at 85 to 95% relative density, the k_1 regression coefficient values ranged between 706 and 1354 and was statistically significant for all samples, and the k_2 values ranged between 0.4 and 0.7 and was also statistically significant for all samples. The k_3 values ranged between -0.3 to 0.8 and were not always statistically significant.
- Undrained shear strength (s_u) testing on RPCC/RAP materials varied between 70 and 140 kPa. Samples that contained 6% fines showed the lowest s_u and the samples with natural 3.5% fines content showed the highest s_u. Difference in s_u among samples with varied relative density was small compared to difference among samples with different fines content.
- Freeze thaw testing on the subgrade material showed that moisture contents after testing were about 0 to 2% higher in the material after the freeze-thaw cycles, compared to its initial moisture content. The clayey subgrade material tested was rated as medium for frost-heave susceptibility and as high for thaw-weakening susceptibility.
- Freeze that testing on the RPCC material showed that the moisture contents after testing

increased by 2 to 6% in all the samples compared to its initial moisture content. The material was rated as medium for frost-heave susceptibility and as negligible for thaw-weakening susceptibility.

In situ LWD and DCP tests were conducted on the newly constructed foundation layers to determine the mechanistic properties of the foundation layers for comparison with the assumed design values. FWD tests were conducted after the pavement was placed. A summary of the field test results are as follows:

- CBR values were lower in the top 150 mm (6 in.) of RPCC modified subbase layer than the bottom 10 in. of RPCC/RAP modified subbase layer, and the subgrade was very variable. The average CBR of the RPCC modified subbase layer was about 11, the average CBR of the RPCC/RAP layer was about 69, and the subgrade CBR (for the top 300 mm) was about 14. The CBR of the weakest layers within the subgrade was about 7.
- LWD test results indicated the elastic modulus varied between 11 and 79 MPa in the longitudinal direction, it varied between 19 and 100 MPa in the transverse direction. The tests were conducted transversely across the pavement width to capture the variability observed at the surface with aggregate segregation. The higher moduli values corresponded well with areas where more fines were present at the surface.
- The *k* values determined from the FWD test ($k_{\text{FWD-Static-Corr}}$) were lowest and were closer to the assumed design *k* value. On average, the average $k_{\text{FWD-Static-Corr}}$ value was about 0.95 times the design *k* value.
- The *k* values determined from $\text{CBR}_{\text{SG-Weak}}$ (i.e., CBR of the weakest layer in the subgrade) using the correlations shown in PCA (1984) ($k_{\text{PCA(1984)}}$) were also closer to the assumed design *k* value. The average $k_{\text{PCA(1984)}}$ calculated from CBR_{SG} (i.e., average CBR of the top 300 mm of the subgrade) was about 1.4 times higher than the design *k* value.
- The *k* values calculated using the empirical relationships between CBR and *k* from AASHTO (1993) ($k_{\text{AASHTO(1993)}}$) were about 2 to 4 times higher than the design *k* value.
- Comparisons of $k_{\text{FWD-Static-Corr}}$ and CBR_{SG} with published relationships are presented in this report. A similar comparison was provided with $\text{CBR}_{\text{SG-Weak}}$ values. These comparisons suggest that the relationships are generally in line with the published data in the literature when $\text{CBR}_{\text{SG-Weak}}$ are considered, but not with CBR_{SG}. Nevertheless, the CBR versus *k* relationships show significant scatter and present significant uncertainty in predictions, so designers must use caution when using such correlations. Developing site-wide or local correlations can provide better confidence in empirical relationships.

Key findings from the temperature monitoring results are as follows:

- Freeze-thaw cycles decreased with depth as expected. The number of freeze-thaw cycles at the surface ranged between 60 and 82 cycles and decreased to about 5 to 10 cycles near the bottom of the pavement. The number of cycles decreased to less than 3 at 0.7 m depth and no freeze-thaw cycles were observed at depths greater than 1.1 m during the monitoring period.
- The maximum frost depth of 1.1 m was observed during 2012-2013 winter, and in the remaining three winters of the monitoring period (2011-2015), the frost penetration depth reached around 0.6 to 0.8 m.

- The temperature measurements obtained across the pavement width did not show significant temperature differences (< 1^{o}C) between the areas beneath the driving lanes and the shoulders, which suggests that no snow cover insulation effects were observed at this site.

CHAPTER 1. INTRODUCTION

This report presents results and analysis of field and laboratory tests from a field study conducted on the US 30 reconstruction project in Boone County in Iowa. The project involved removal of the existing pavement which showed severe pavement distresses, reconstruction of the pavement foundation layers (base, subbase, and subgrade), and placement of a new jointed plain cement pavement (JPCC) on the east and west bound lanes of US 30 between mileposts 139.0 and 147.27. Field testing was conducted by the Iowa State University (ISU) research team on the existing pavement prior to the reconstruction work, and on the newly constructed pavement and the foundation layers.

According to the historical as-built records provided Iowa DOT (2009), the existing pavement consisted of nominal 76 mm (3 in.) thick asphalt concrete (AC) overlay on nominal 229 mm (9 in.) thick portland cement concrete (PCC). The pavement layers were underlain by nominal 102 mm (4 in.) thick asphalt treated base (ATB). The existing pavement and the ATB layers were removed and the subgrade was undercut during the reconstruction process to place a nominal 410 mm (16 in.) thick modified subbase over the natural existing subgrade. The modified subbase layer consisted of 150 mm (6 in.) thick recycled portland cement concrete (RPCC) material or crushed limestone at the surface underlain by 260 mm (10 in.) thick mixture of RPCC and recycled asphalt pavement (RAP) material. A nominal 254 mm (10 in.) thick JPCP was placed on the newly constructed foundation layer. Thickness design of the new pavement was conducted by the Iowa DOT according to the PCA (1984) method, by assuming a modulus of subgrade reaction (k) value for the foundation layer.

Field testing on the existing pavement was conducted in February 2010 (winter/frozen condition), prior to the reconstruction work. The existing pavement showed severe pavement distresses with reflective cracking and vertical upheave near joints, especially during winter. The Iowa DOT also reported incidents of damage to vehicle tires and problems with snowplow blade contact. Initial field investigations by the Iowa DOT rated the ride quality of the pavement section as “poor” based on pavement condition index (PCI) ranging between 54 and 56 on a 0-100 scale (100 being good and 0 being failed condition). Core samples of the existing pavement were obtained near joints using 254 mm (10 in.) and 100 mm (4 in.) diameter diamond rotary bits. These core samples were visually inspected, and then were sealed and sent to laboratory for additional testing. Visual inspections were conducted to evaluate the joint deterioration and vertical heave profiles were measured longitudinally across the joints.

The ISU research team was present on the project site after the foundation layer construction was completed in June 2011. In situ light weight deflectometer (LWD) and dynamic cone penetrometer (DCP) tests were conducted on the foundation layer to obtain mechanistic properties of the new foundation layers for comparison with the assumed design values. At one location, the pavement foundation layers were instrumented with thermocouple temperature sensors to monitor seasonal temperature variations in the foundation layer with depth and temperature variations across the pavement width. The vertical temperature variations were monitored to assess frost depth and freezing/thawing periods, and the temperature variations

across the pavement width were monitored to assess the influence of snow cover on the shoulder on the mainline pavements.

A few months after the pavement construction was completed, falling weight deflectometer (FWD) tests were conducted on the pavement near mid-panel and joints where the foundation layer testing was previously conducted. DCP tests were also conducted in the foundation layers by drilling holes in the pavement. Results from FWD and DCP tests were analyzed and compared with the assumed *k* values in thickness design.

In addition to field testing, a detailed laboratory testing plan was executed on bulk samples of RPCC, RPCC-RAP, and subgrade materials. Laboratory testing included characterizing soil index properties, moisture-dry unit weight relationships, resilient modulus (M_r), permanent deformation and particle degradation behavior under cyclic triaxial loading, and frost-heave and thaw-weakening susceptibility. M_r tests were conducted on the modified subbase materials collected from the project site to assess the influence of relative density and fines content on the M_r values and the constitutive model parameters to predict the M_r values. Permanent deformation and particle degradation behavior was assessed using repeated load cyclic triaxial testing using 1,000 to 100,000 cycles. Frost-heave tests were conducted using a setup specially fabricated at (ISU) for this research project to assess the foundation materials susceptibility to frost-heave by exposing samples to two freeze-thaw cycles. Thaw-weakening susceptibility ratings of the foundation materials were determined by conducting California bearing ratio (CBR) tests on compacted samples before and after two thawing cycles.

This report contains seven chapters. Chapter 2 provides background literature review pertaining to joint deterioration and seasonal variations. Chapter 3 presents an overview of the laboratory and in situ testing methods used in this project. Chapter 4 presents results from laboratory testing. Chapter 5 presents results from in situ testing and analysis and compares the laboratory and in situ measured values with the design assumed values. Chapter 6 presents key findings and conclusions from this study.

The findings from this report should be of significant interest to researchers, practitioners, and agencies who deal with design, construction, and maintenance aspects of PCC pavements. Results from this project provide one of several field project reports being developed as part of the TPF-5(183) and FHWA DTFH 61-06-H-00011:WO18 studies.

CHAPTER 2. LITERATURE REVIEW

Pavements in northern climates are subjected to severe temperature variations with freezing and thawing cycles. Stable support conditions and good drainage in the foundation layers are key to provide good ride quality and long-term performance of the pavement layers. This chapter presents brief background and literature review related the topics of joint deterioration, sub-surface drainage, and subsurface temperature variations and seasonal variations in mechanistic properties in the pavement and foundation layers.

Joint Deterioration

Taylor (2011) and Taylor et al. (2012) conducted investigations of joint deterioration in concrete pavement and reported that the onset of pavement distress is related to micro-cracking near the joints where water is trapped (Figure 1), which eventually leads to loss of materials. Taylor reported that two causes of pavement deterioration are being investigated: "1) freezing-related deterioration caused by concrete saturation and 2) mechanical deterioration" (Taylor 2011, 2).

Water trapped near joints contributes to freezing-related deterioration. Two main factors result in trapped water near joints, the lack of proper sealing (or a failed seal) near joints and poor drainage of underlying base layers. Pavements that are subjected to longer saturation periods, concretes with marginal air void systems, and high usage of de-icing salts contribute to freezing-related deteriorations. These type of deteriorations progress rapidly once the damage starts (Taylor 2011). Zhang et al. (2015) reported that in jointed portland cement concrete (JPCC) pavements, low permeability in base layers beneath the pavements correlates with joint deterioration.

Figure 1. Typical shadowing with trapped water and micro-cracks (Taylor 2011)

According to Taylor (2011), mechanical deterioration is typically narrow and shallow, and typically starts near the edge of the slab and propagations along the joint. Poor maintenance of sawing equipment and/or inappropriate sawing practices contribute to mechanical deterioration, but are difficult to observe immediately after sawing although they will be accelerated due to weathering. Table 1 summarizes prevention, mitigation, and repair strategies for joint deterioration problems from information provided in Taylor (2011).

Table 1. Prevention and mitigation and repair strategies for joint deterioration

Prevention	Use concrete mixtures that are well proportioned using appropriate materials. Pay attention to the air void system. Ensure that fresh concrete is well cured. Allow water to leave the hardened concrete.
Mitigation and Repair	Apply surface sealants to the faces of and near existing joints to reduce ingress of water into the concrete. Consider limiting the type of de-icing salts to sodium chloride. Partial / full depth repairs of the joints may be required if the serviceability of the pavement is compromised. Pay attention to maintenance of drainages systems. Consider retrofitting edge-drains to improve drainage.

Li et al. (2012) investigated the relationship between water absorption and critical saturation degree and freezing-related joint deterioration. Three groups of concrete specimens with 0.42 water-cement ratio and volumetric 6%, 10%, and 14% air content were cured for 28 days. Li et

al. (2012) reported that 86–88% was the critical degree of saturation. When the degree of saturation was greater than this value, freezing-related joint damage was found in all specimens within 1 to 6 freeze-thaw cycles. The addition of an air entraining agent significantly delayed the time for specimens to reach the critical degree of saturation (88%) from 4–6 days to 3–6 years. However, the results indicated that the addition of the air entraining agent did not reduce the potential for freezing-related joint deterioration.

Jones et al. (2013) analyzed concrete pavement joint deterioration and focused on freeze-thaw damage mechanisms, de-icing salts, and laboratory testing results on field cores. Air void system analysis, optical microscopy analysis, freeze-thaw resistance testing, resistance to chloride ion penetration (RCP) testing, and scanning electronic microscopy (SEC) examinations were conducted in laboratory on cores from field. The results indicated that concrete near deteriorated joints was always associated with poor air void systems, numerous micro-cracks presenting as infilling of the air voids, higher rates of absorption, high RCP values, and low values of freeze-thaw durability factors. Although de-icing salts could help to melt snow and ice on pavement, de-icing may contribute to pavement distress. High concentrations of salts attract water that keeps pavements moist combined with insufficient drainage of this trapped water results in joint deterioration.

Sub-surface Drainage

It is widely accepted that undrained water within the pavement system increases the risk of distress in pavements due to freezing, thawing, erosion, and reduction in effective stresses under dynamic loading. As discussed above, trapped undrained water in the base layer can contribute to joint deterioration. Zhang et al. (2015) documented a case study that compared the performance of joints with subsurface permeability based on field testing conducted on a pavement in Iowa. A borehole permeameter (Figure 2) developed at Iowa State University was used to measure permeability at two sealed distressed, one sealed sound, and one unsealed sound joint locations. Tests were conducted in summer and winter for comparison. The permeability at the sound joint was twice the value of the distressed joints in summer, while the permeability from these two locations was close at low level in winter. The results indicated that deteriorated joints had relatively low permeable base layers, which probably contributed to water being trapped at the joints. In frozen conditions, a significant decrease in sub-surface permeability was observed. An interesting finding on the gradation analysis of the base materials under joints was that it presented relatively more fines content than that from mid-panel locations, which indicated a loss of materials from the distressed joints.

Figure 2. Borehole permeameter setup developed by Iowa State University (Zhang et al. 2013)

Seasonal Freeze-Thaw Cycles in Pavements and Foundation Layers

As part of a study of soil stabilization, Hoover et al. (1962) constructed and examined a pavement test section built on US 117 in Jasper County, Iowa during October 1957. They computed 0^{o}C isotherms and estimated frost depths using the Modified Berggren Formula and U.S. Weather Bureau information. They also estimated the number of freeze-thaw cycles that occurred during each winter cycle, as shown in Figure 3 to Figure 5.

When pavement structures are exposed to frost heaving and thaw weakening, the mechanical properties can be significantly affected by the seasonal changes in temperature and soil moisture conditions (Simonsen and Isacsson 1999). Simonsen and Isacsson reviewed the available literature on the effects of freezing and thaw weakening on pavement structures. The stiffness of supporting layers typically increases when frozen because soil particles in the base and subbase materials are frozen together and ice lens have formed in the subgrade materials, which result in an increase in bearing capacity. The damage caused by freezing is due to differential frost heave and thermal cracks in asphalt cement (AC) layers. According to Simonsen and Isacsson (1999), once pavements begin to thaw in the spring, bearing capacity can be drastically reduced because of increased saturation in the supporting layers. They reported that drainage in pavement systems is very important in general, but it is even more important in cold regions because increases in moisture content in foundation layers when water from thawing ice causes high pore water pressures to develop that lead to reductions in effective stress that influences shear stress and bearing capacity. Further, water that results from melting ice becomes trapped between the pavement material and the remaining frozen layers below (Simonsen and Isacsson 1999).

Simonsen and Isacsson (1999) also reported that less severe winters produce conditions for greater amounts of heave for given depths of frost because slow frost penetration rates can result in more ice lenses being formed. This slow frost penetration leads to the majority of the ice accumulating near the surface of the pavement foundation layers. Once the ice begins to melt, there is a rapid release of water that can create detrimental support conditions. On the other hand, severe winters result in deeper frost penetration, which means that the main concentrations of ice are deeper in the pavement foundation. Even though there may be more ice present, the effect of the melting ice on the pavement is less rapid and spread over a longer period of time. If drainage of the pavement system is high enough, the effects of additional water on the system will be lessened. The ability of the system to drain is related to the fines content of the materials.

According to Johnson (2012), thawing typically progresses from the pavement surface down and results in conditions where melted water can become trapped between the pavement surface and the frozen layers below. In this condition, where thawing is rapid, the drainage path is constrained in the vertical direction so transverse drainage paths must be available. When this occurs, transverse drainage can be cut off. If slower thawing takes place, the thawing front will work its way from the lower layers up and water will be allowed to drain. The thaw depth affects the amount of settlement that will take place and the rate of thawing affects the magnitude of change in pore water pressure. The amount of settlement that takes place depends on ice lens formation, soil density, pore water pressures, and soil compressibility.

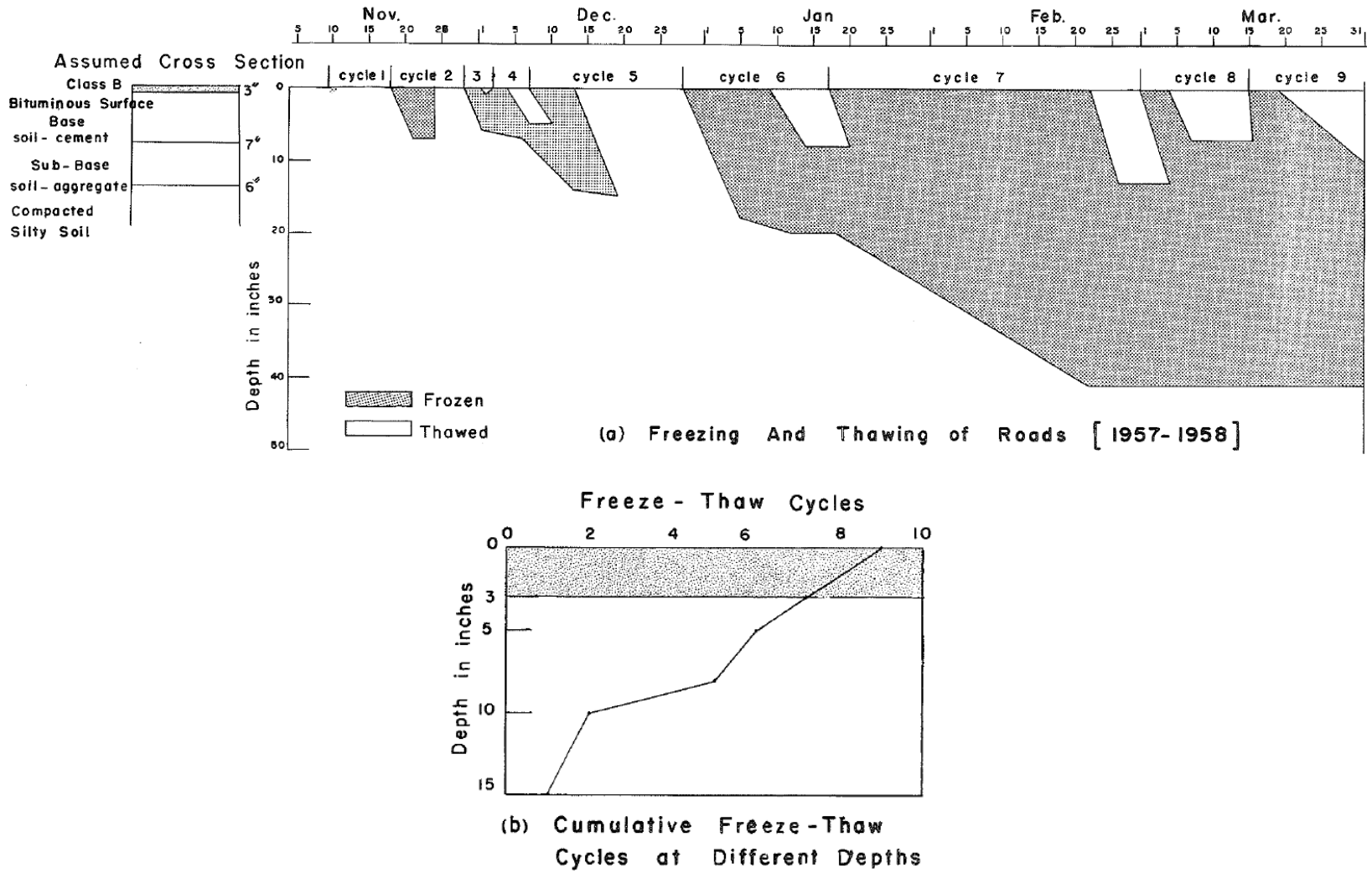

Figure 3. Winter 1957–1958: Computed frozen zones (top) and cumulative freeze-thaw cycles (bottom) (Hoover et al. 1962)

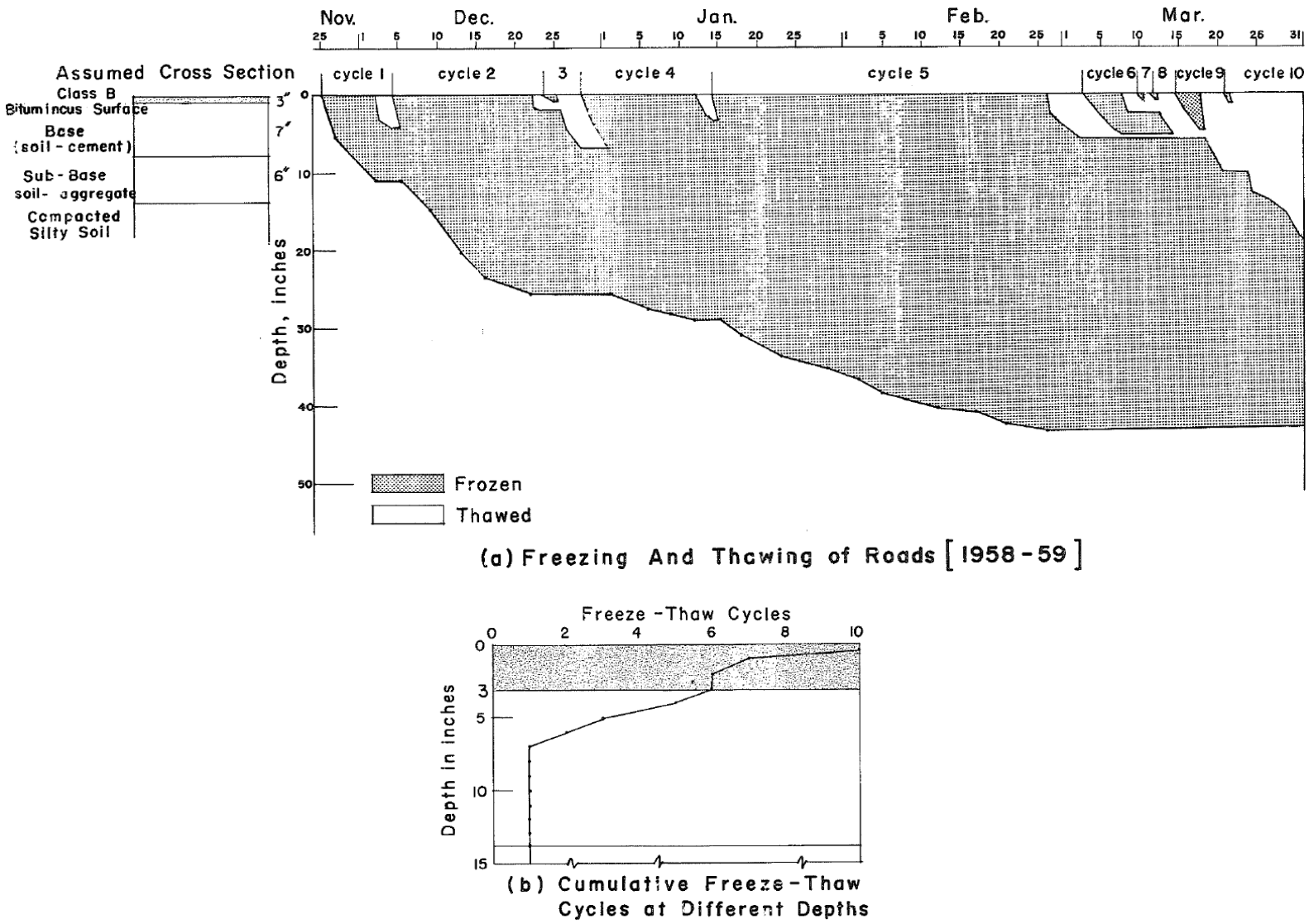

Figure 4. Winter 1958–1959: Computed frozen zones (top) and cumulative freeze-thaw cycles (bottom) (Hoover et al. 1962)

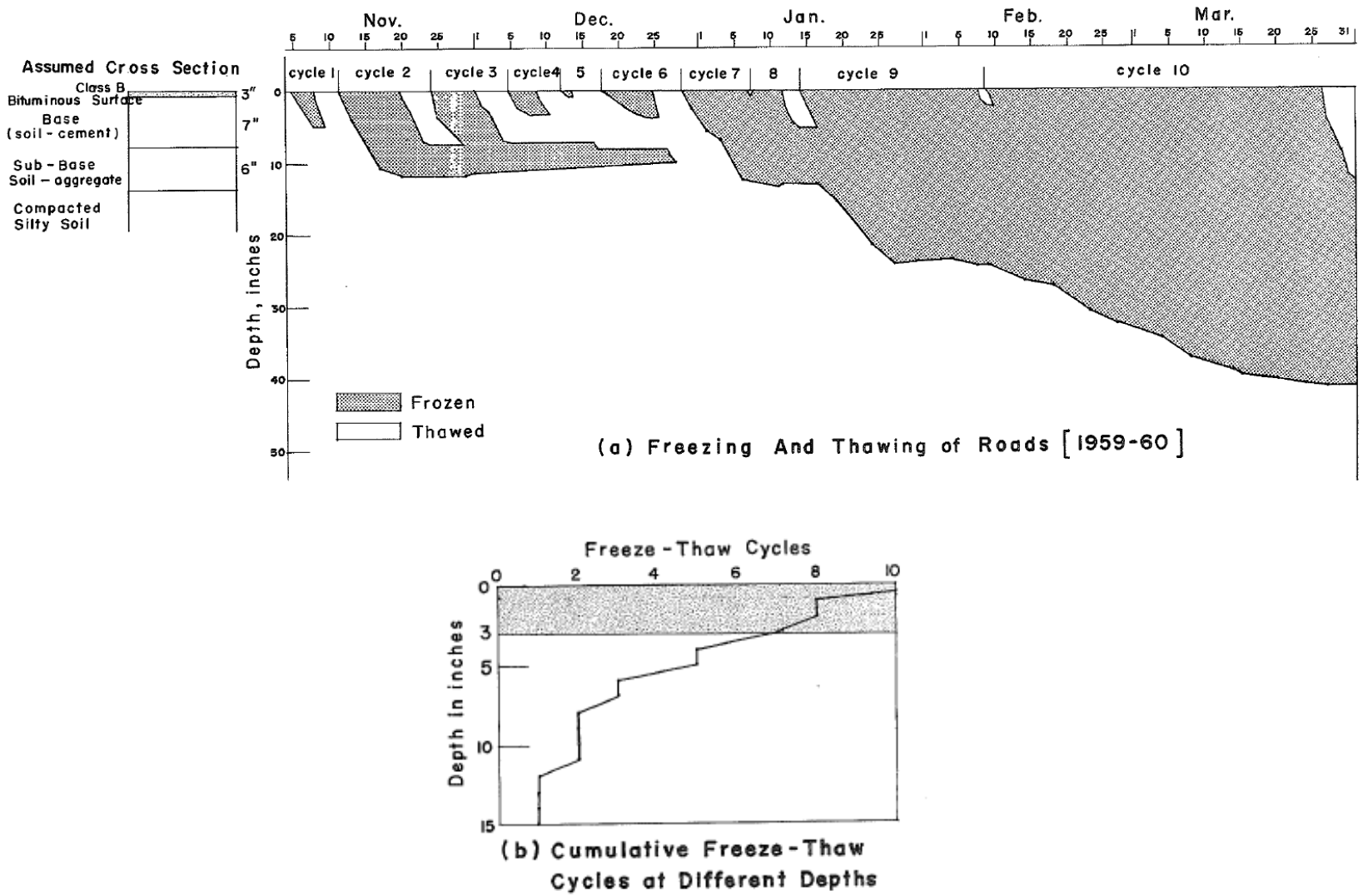

Figure 5. Winter 1959–1960: Computed frozen zones (top) and cumulative freeze-thaw cycles (bottom) (Hoover et al. 1962)

Simonsen and Isacsson (1999) identified the following factors that can impact the amount of thaw-weakening damage on pavement systems: road structure, frost susceptibility, subgrade conditions, temperature, precipitation, and traffic. They found that the length of recovery from thaw weakening is dependent on the frost depth, soil type, water content, and drainage conditions, and that, depending on drainage conditions, it can take weeks to months to fully recover. Andersland and Ladanyi (2004) suggested that load restrictions can be used to reduce pavement damage during periods of thaw weakening, but that load restrictions are most commonly used on flexible pavements because most rigid pavements were determined to be able to resist the loss of strength during thawing.

Simonsen and Isacsson (1999) described that when pavement foundation layers are deformed under traffic loads, most of the deflection rebounds once loads have been removed. The remaining deformation that does not rebound is called permanent deformation and occurs when excess water is present. Spring thawing conditions present the ideal opportunity for permanent deformation to occur. When base materials are saturated, vehicle loads are initially placed on pore water. When the pore water is loaded it makes the base material unstable and can cause upward stress that can cause cracks in the pavement system. After this process occurs many times, it can cause holes in the pavement layer and a loss of base material; this is especially true for AC pavements. Salour and Erlingsson (2012) found that when the base course is saturated, there can be a pumping of fines in the base course that eventually leads to a weaker and less drainable material than what was initially designed.

Another type of failure can occur when the subgrade is frost susceptible and has been frozen (Simonsen and Isacsson 1999). Once the subgrade begins to thaw and pore water pressures increase due to the additional water, the subgrade is displaced and is unable to sustain loads that are applied from the upper pavement layers. When the subgrade is displaced, a loss of support for the pavement layer occurs that can cause deformations in the pavement. Salour and Erlingsson (2012) found that the relative damage on AC pavements caused by traffic loading during thaw weakening is 1.5 to 3 times higher than the average annual damage.

Andersland and Ladanyi (2004) reported that determining the 0°C isotherm is an approach to analyze temperature variations in pavement focusing on freezing and thawing periods in pavement layers (Figure 6). Frozen and thawed zones versus time can be estimated from the isotherm depth. Determination of this isotherm presents the maximum frost penetrations and the periods that pavements are susceptible to break-up. This period is defined as the time when the upper pavement layers are thawed while the lower layers are still frozen. Thawed water from upper layers cannot drain into lower frozen layers due to the low permeability. In these conditions, the bearing capacity of foundations may significantly decrease, and the upper pavements become more fragile under traffic loads. Andersland and Ladanyi (2004) reported that these fragile conditions are a problem that pavement engineers need to identify, which is the primary reason why spring load restrictions should be implemented in seasonal frost regions (Ovik et al. 2000; NDDOT 2015).

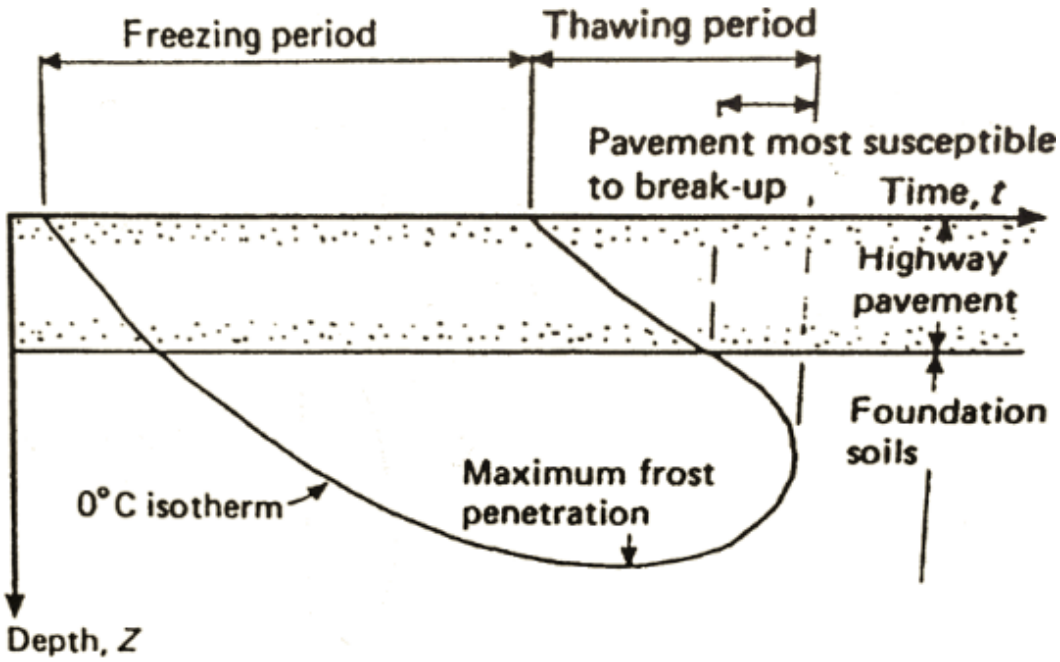

Figure 6. Model of seasonal ground freezing and thawing periods beneath pavement (Andersland and Ladanyi 2004)

Seasonal Variations in Pavement Foundation Mechanistic Properties

In situ testing during different seasons to determine mechanistic properties of pavement foundation layers such as strength and M_r or *k* is critical for thickness design because these properties of pavement foundations change in response to climatic conditions (Lary et al. 1984, Konrad and Roy 2000). Pavement design guides take this into consideration (AASHTO 1993; AASHTO 2008). For example, AASHTO (1993) suggests adjusting the design M_r of roadbed soil based on the durations of periods of freezing and thawing and in summer. AASHTO (1993) provides suggested values for use in design when subgrade is in frozen, thawed, and summer conditions. AASHTO (2008) deals with seasonal variations in a more sophisticated manner that accounts for local climatic modeling data and laboratory test measurements to adjust design modulus values for seasonal variations.

The next section is a summary of the literature about field investigations into frost heave, followed by a review of the literature about thaw weakening.

Frost Heave

In a study at MnROAD (Lukanen et al. 2006), frost pins were placed in sections of AC and portland cement concrete (PCC). The AC sections had sand, clay, and granular base as foundation materials. The PCC sections had a granular base with either sand or clay underneath.

The frost pins were placed at 50 ft intervals in the five 500-ft test sections and observed over a four-year period. The results revealed uneven heave across each of the sections. This differential heave affects pavement ride and performance. Differential heave can greatly increase pavement roughness and occurs when material types or properties change (e.g., a change from cut to fill or an area with increased moisture content) (Joint Departments of the Army and Air Force 1985).

Many states require a 3–5 ft subcut into the subgrade, which consists of removing the subgrade material and recompacting it in place, a process that helps create a uniform subgrade that will reduce differential heave. The test sections at MnROAD were undercut 5 ft but still showed signs of differential heave. The sections with clay subgrade in the pavement structure showed the greatest amount of frost heave. Also the AC on clay sections showed an increase in the International Roughness Index (IRI) as the subgrade heaved. The AC on sand sections showed smaller increases in IRI because the subgrade had small amounts of heave. Although the PCC section with a clay subgrade heaved significantly, the PCC sections showed no increases in IRI. Lukanen et al. (2006) reported that ride quality is minimally related to differential frost heave in the subgrade and many other factors can affect the IRI in addition to frost heave. They concluded that current empirical design and mechanistic empirical design processes do not account for differential frost-heave movements.

Thaw Weakening

Increased moisture content in supporting layers during thawing weakens pavement structures (Janoo and Berg 1996). This additional water in pavement structures reduces the bearing capacity of the pavement system because reduced strength of the supporting layers. The strength of AC pavements is largely dependent on the temperature, this results in large variations in strength during the high temperature swings that occur during freezing and thawing periods. PCC can also be negatively affected during thawing periods because of curling effects that are caused by high temperature differentials in the pavement layer. The curling can occur at the edges and corners of the pavement which will affect the load transfer efficiency. Janoo and Berg (1996) conducted a study of the effects of thaw weakening on PCC for airfields. They conducted falling weight deflectometer (FWD) tests and measured temperatures in the pavement structure. Frost depths were determined based on where the temperature was 0°C. An example of their frost depth versus time can be seen in Figure 7.

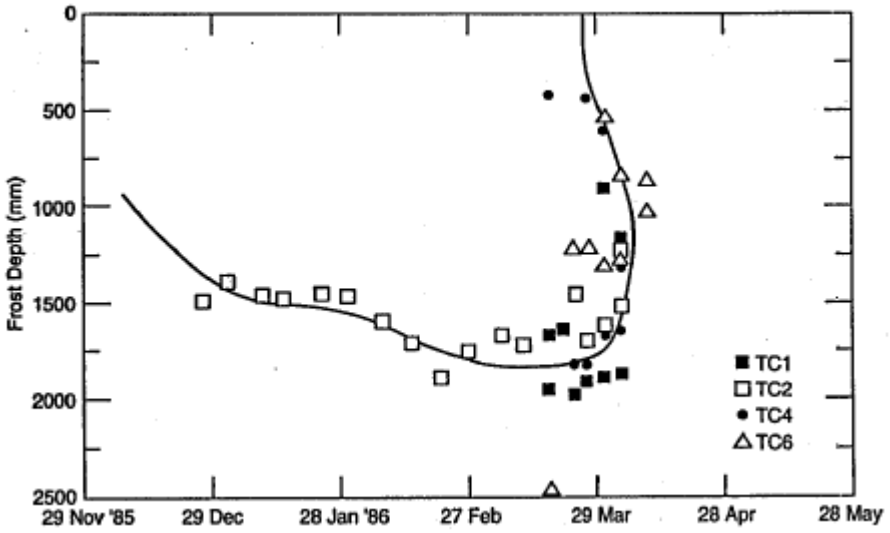

Figure 7. Frost penetration plot (Janoo and Berg 1996)

Janoo and Berg (1996) used the FWD deflection basin area index parameter to analyze the effects of thaw weakening. An example of the data can be seen in Figure 8 where the higher the basin area measurement, the lower the strength of the pavement structure. They measured joint load transfer efficiency (LTE), which is a measure of how well the load is distributed from one PCC slab to the next. They found that the LTE typically decreased as the temperature increased as the beginning of the spring thaw. However, as thawing progressed, the LTE began to increase (Figure 9).

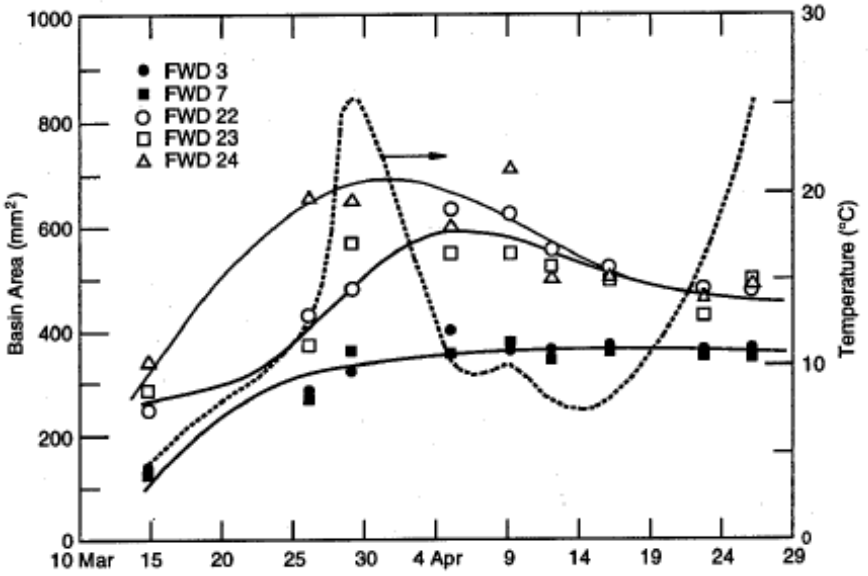

Figure 8. Change in basin area during spring thaw (Janoo and Berg 1996)

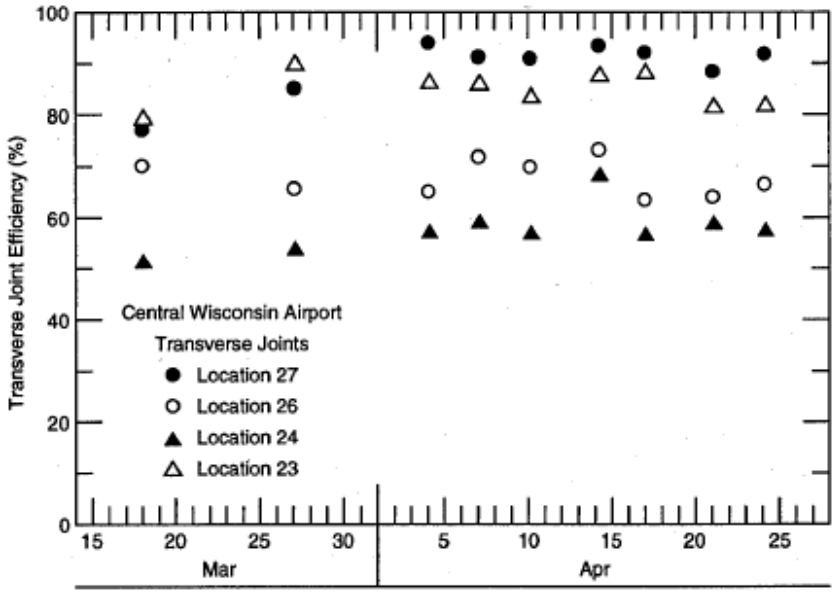

Figure 9. Joint transfer efficiency during spring thaw (Janoo and Berg 1996)

Drumm and Meier (2003) compiled seasonal test data from sites across North America. The research was conducted as a part of the Long Term Pavement Performance (LTPP) Seasonal Monitoring Program (SMP). They collected data from temperature sensors, moisture sensors, and FWD tests. They discussed that the temperature in PCC does not affect the performance as much as the gradient in the PCC slab. Curling of the slabs can result of the temperature gradient. Upward curling will occur when the temperature is cooler on the top compared to the bottom (i.e., at night) and downward curling can occur when the temperature on the top is warmer than the bottom (i.e., during day). When the temperature in the slab is colder, the joints open which can result in reduced load transfer efficiencies. Reductions in load transfer efficiencies can also be caused by curling. FWD testing can be performed at the edge of slabs to observe daily and seasonal changes in load transfer efficiency due to curling and opening of joints. FWD deflections, from increasing loads, from the slab edges and the center of slab can be compared. If the deflections have a near linear relationship between the drop height and response, it is an indication that the slab is in good contact with the underlying layers. Any deviations from linear can indicate curling.

Drumm and Meier (2003) mentioned that it is a typical misunderstanding that granular base material do not undergo thaw weakening. This is a result of a strong base material requiring a significant amount of fines, which as discussed can decrease the permeability and increase the frost-heave potential. They found, from several sources, that there is no relationship between amount of rainfall and subgrade moisture content variation. Joint faulting in PCC, can be a result of pumping (i.e., loss of material), frost heave, or expansive subgrade soils.

Drumm and Meier stated that, “even under the best of circumstances, FWD backcalculation is as much an art as it is a science” (2003, p. 4–5). Spring thaw and recovery moduli were difficult to backcalculate because the pavement structure was not adequately modeled by the elastic layer

theory that was used. Because it is difficult for theory to represent a soft saturated layer trapped between a much stiffer base material and the frost subgrade that lies below they recommended that advanced modeling would be required to represent this situation. The backcalculated moduli during frozen periods are typically too high and inconsistent. They found that it was difficult to determine when slab curling was or was not affecting the results, and recommended that deflection basins be used rather than backcalculated moduli to determine the effects of frost action on the pavement system.

Drumm and Meier (2003) used the following indices at Mn/ROAD to assess spring thaw conditions: SCI, BDI, and D_0. The FWD indices are defined in Table 2. These indices are expected to decrease during frozen periods (Figure 10). A stress level of 550 kPa was used in the study because it corresponds to a stress level that is typically used in pavement design. With the data available, they were not able to detect a significant thaw-weakening period. They hypothesized that it was a result of one or a combination of the following factors: thaw weakening occurred between their site visits, the subgrade soils were not frost susceptible, or the pavements were designed to minimize the effects of thaw weakening. The LTPP SMP sites were only visited once a month. Drumm and Meier analyzed FWD results on AC pavements from the U.S. Army Frost Effects Research Facility and other locations that were collected on a daily basis during thawing and reported that the effects of thawing could be seen from SCI and SDI indices.

Table 2. FWD indices (Drumm and Meier 2003)

Parameter	Formula
AREA	$6 * [(D_0/D_0) + (2*D_{305}/D_0) + (2*D_{610}/D_0) + (D_{914}/D_0)]$
Deflection at load plate (D_0)	D_0
Deflection at 1524 mm (D_{1524})	D_{1524}
Base curvature index (BCI)	$D_{610} - D_{914}$
Surface curvature index (SCI)	$D_0 - D_{305}$
Basin damage index (BDI)	$D_{305} - D_{610}$
Partial area (PA), m^2	$[(D_{457}+D_{610})/2*0.153] + [(D_{610}+D_{914})/2*0.304] + [(D_{914}+D_{1524})/2*0.610]$
Subgrade damage index (SDI)	$D_{610} - D_{1524}$
Subsurface index (SI)	$D_{305} - D_{1524}$

D_x is the surface deflection measured x mm from the loading plate.

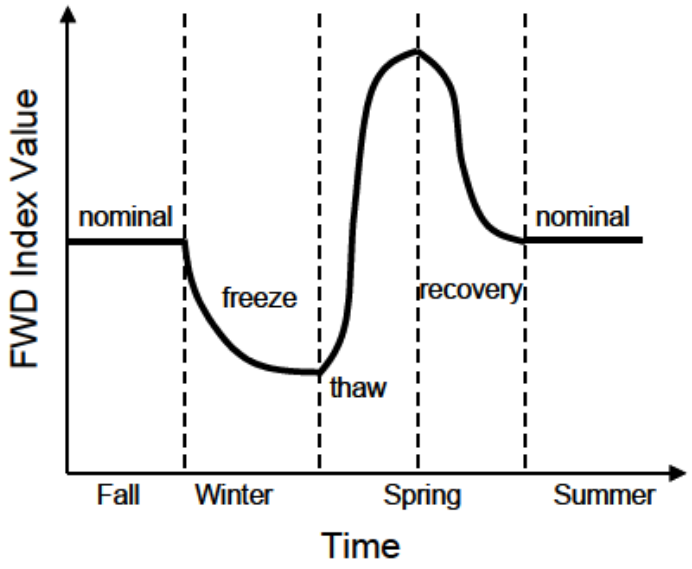

Figure 10. Expected seasonal variation of FWD indices (Drumm and Meier 2003)

Jong et al. (1998) performed a study to develop a method for determining when load restrictions should be implemented. The data collected measured air and subsurface temperatures, subsurface water contents, water phase changes, and pavement moduli. Thermocouples and thermistors were used to measure temperature, time domain reflectometry probes were used to determine water contents and phase changes, and FWD tests were used to determine the pavement moduli. Flexible pavements (i.e., AC pavements) were tested over an 18 month period on three secondary highways. They found that the thermocouples, thermistors, and time domain reflectometry probes all resulted in approximately the same frost depth profiles (Figure 11). They

presented the structural capacity of the pavement in the form of FWD deflection basins and backcalculated FWD moduli. An example of the FWD deflection basin can be seen in Figure 12. The basins show that the deflection is very low during winter and very high during spring, with the deflections for the summer period falling in between.

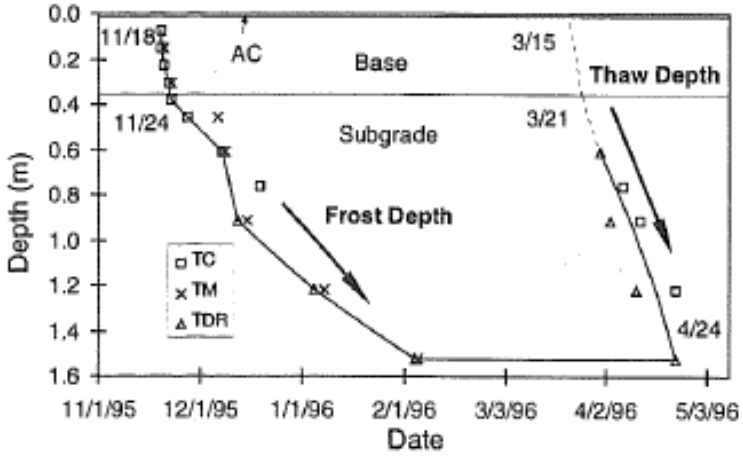

Figure 11. Frost depth measured with thermocouples, thermistors, and time domain reflectometry probes (Jong et al. 1998)

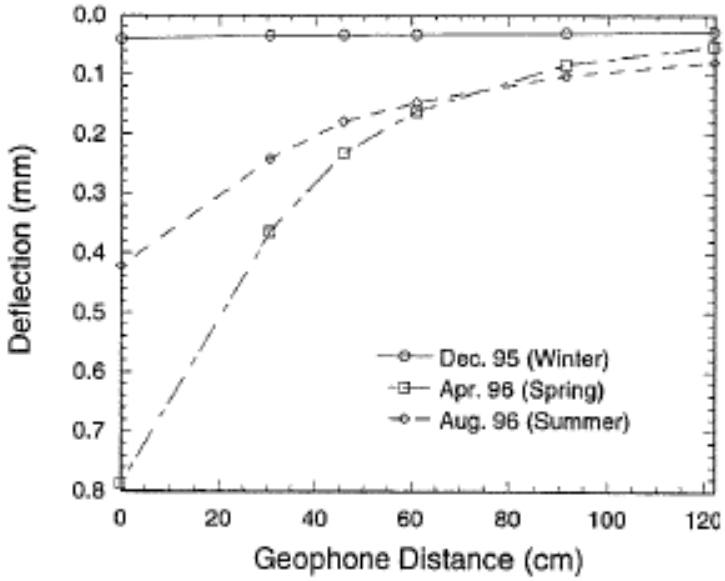

Figure 12. Changes in seasonal FWD deflection basins (Jong et al. 1998)

Jong et al. (1998) performed FWD tests at approximately 15 m intervals and found that overall; the modulus did not vary significantly for the intervals tested, so it was assumed that one interval could be used to represent the test section. They found that the moduli of the base and subgrade continued to weaken, after thawing began, until both layers were completely thawed (Figure 13). The thaw weakening stage lasted approximately one month and continued to recover for an

additional four months. Figure 13 also shows that the subgrade has a higher modulus than the base for a brief period during thawing.

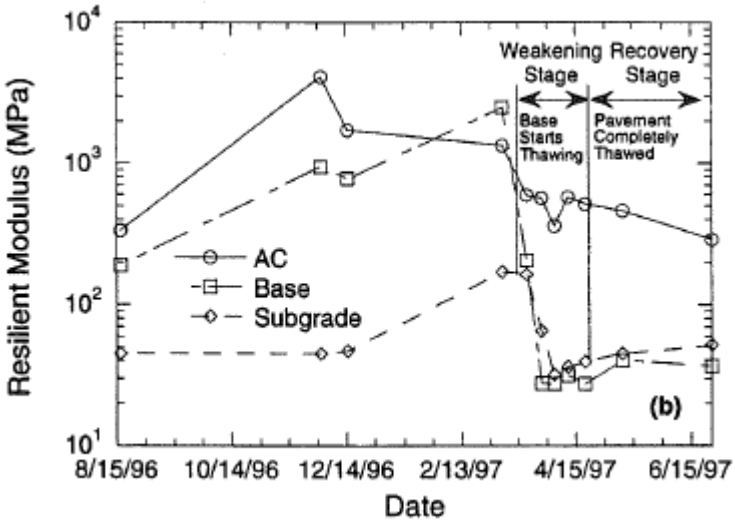

Figure 13. Changes in seasonal resilient modulus (Jong et al. 1998)

Newcomb and Birgisson (1999) presented a profile (Figure 14) of typical deflection response over a year that indicates that the deflection response from applied loads is reduced during periods of freezing and then drastically increases during the following thaw period. They examined findings from other studies and concluded that the critical period during thawing is when water is trapped in the base layer between the pavement and the frozen subgrade.

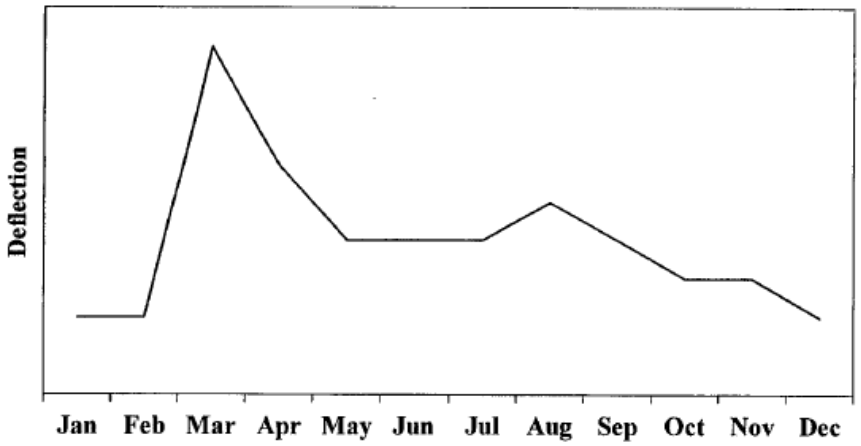

Figure 14. Typical pavement deflection response due to seasonal changes (Newcomb and Birgisson 1999)

The effect on the resilient modulus can be seen in (Figure 15). The result of water being trapped in the base course is that the modulus of the subgrade is actually higher than that of the base course for a short time, which supports Jong et al. (1998).

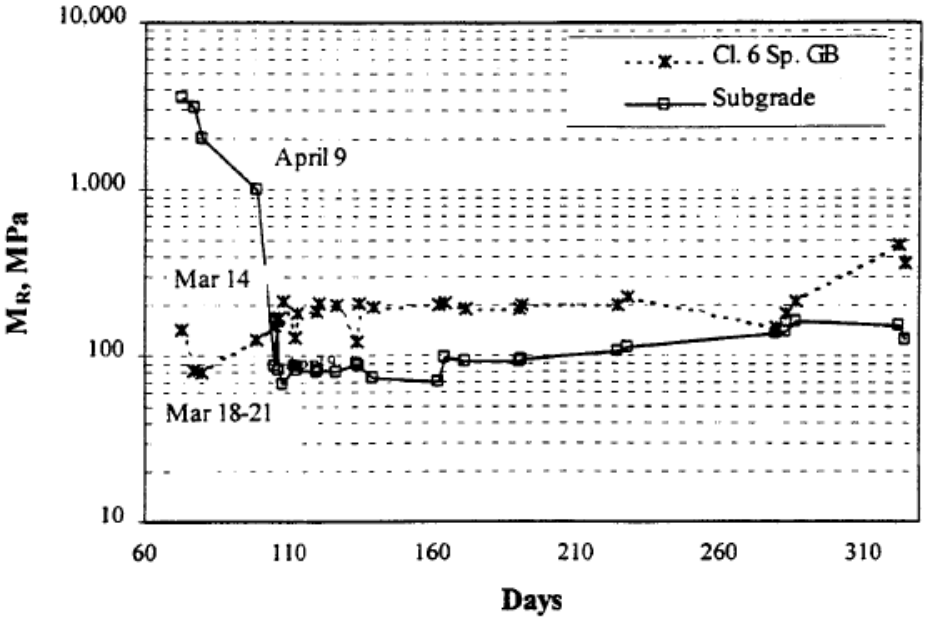

Figure 15. Seasonal changes in the resilient moduli of base and subgrade layers (Newcomb and Birgisson 1999)

As a part of the ROADEX II Project in Northern Europe, the effects of thaw weakening on low volume gravel roads were studied (Saarenketo and Saara 2005). They used DCP test results to determine the changes in stiffness and thickness of pavement layers and to determine the depths to layer interfaces and the location of the frost line. They backcalculated a modulus, based on the shear strength, from the DCP data. Figure 16 shows the DCP moduli being used to track the thawing process. They concluded that the DCP test is very useful for monitoring frost depth and stiffness of the road structures, but that it has problems penetrating stiff base courses so it is not suitable for observing well-built roads.

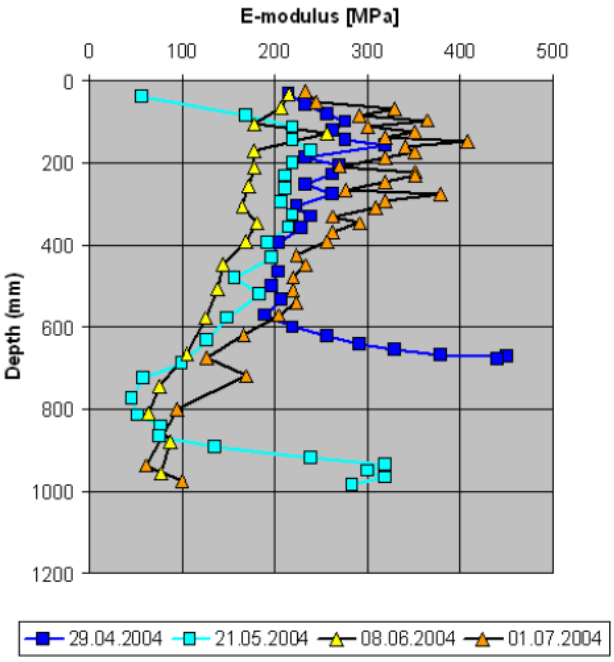

Figure 16. Tracking thawing process by using DCP backcalculated moduli (Saarenketo and Saara 2005)

Baladi et al. (2009) reported seasonal changes in pavement subgrade M_r values. More than 500 groups of FWD test results, including those conducted in that study and those collected over the previous 20 years, were used to determine layer moduli. The backcalculated *k* values from FWD deflections per empirical AREA method were converted to M_r based on AASHTO (1993). The converted M_r values were also correlated with previous data to consider limitations in applying the AASHTO (1993) conversion process to determine effects on subbase and base layers. FWD tests were conducted on two PCC and one ACC pavement test sections in Michigan during fall and spring. The results indicated that during thawing, the subgrade M_r values under the PCC pavements were 30–50% less than in the fall, but subgrade M_r values under the ACC pavement were similar in both seasons.

Becker et al. (2014) investigated the freeze-thaw performance of stabilized pavement foundations in Iowa from October 2012 to April 2013 by comparing the CBR and elastic modulus in the fall and after the spring thaw. Although several stabilization methods had been used, in comparison with the fall CBR values, the spring CBR of both granular subbase (CBR_{SB}) and subgrade (CBR_{SG}) decreased. Becker et al. (2014) reported that the thawed CBR_{SG} was as low as 10% of the values measured during summer/fall. Results of elastic modulus testing indicated the thawed stiffness of the composite foundation layers decreased by 20–90% compared to values observed in summer/fall.

CHAPTER 3. EXPERIMENTAL TEST METHODS

This chapter summarizes the laboratory and in situ testing methods used in this study.

Laboratory Testing Methods and Data Analysis

Particle-Size Analysis and Index Properties

Samples from granular subbase and subgrade layers were collected from the field and were carefully sealed and transported to the laboratory for testing. Particle-size analysis tests on the OGDC material samples were performed in accordance with ASTM C136-06 *Standard test method for sieve analysis of fine and coarse aggregates.* Particle-size analysis tests on the sand subbase and subgrade materials were conducted in accordance with ASTM D422-63 *Standard Test Method for Particle-Size Analysis of Soils.*

Atterberg limit tests (i.e., liquid limit—LL, plastic limit—PL, and plasticity index—PI) were performed in accordance with ASTM D4318-10 *Standard test methods for liquid limit, plastic limit, and plasticity index of soils* using the dry preparation method. The results from particle-size analysis and Atterberg limits tests were used to classify the materials on the unified soil classification system (USCS) in accordance with ASTM D2487-10 *Standard Practice for Classification of Soils for Engineering Purposes (Unified Soil Classification System)* and AASHTO classification system in accordance with ASTM D3282-09 *Standard Practice for Classification of Soils and Soil-Aggregate Mixtures for Highway Construction Purposes.*

Specific gravity tests were performed on materials finer than No. 4 sieve, in accordance with ASTM D854-10 *Standard test methods for specific gravity of soil solids by water pycnometer*. For materials with coarse particles (i.e., retained on No. 4 sieve), specific gravity was determined in accordance with ASTM C127-07 *Standard test method for relative density (specific gravity) and absorption of coarse aggregate.*

Two laboratory compaction tests were used to determine the relationship between dry density and moisture content for the soils obtained from the field. Subgrade soil compaction characteristics were determined using standard and modified Proctor compaction methods in accordance with ASTM D698-07 *Standard test methods for laboratory compaction characteristics of soil using standard effort* and ASTM D1557-07 *Standard test methods for laboratory compaction characteristics of soil using modified effort*, respectively. Maximum and minimum index density tests were performed using a vibratory table on subbase materials in accordance with ASTM D4253-00 *Standard test methods for maximum index density and unit weight of soil using a vibratory table* and D4254-00 *Standard test methods for minimum index density and unit weight of soils and calculation of relative density.* Moisture-unit weight relationships of subbase materials were determined by performing maximum index density tests by incrementally increasing the moisture content by approximately 1.5% for each test.

Resilient Modulus and Cyclic Triaxial Testing Sample Preparation

Samples for M_r tests and repeated load cyclic triaxial testing were prepared according to AASHTO T307-99. Homogeneous samples of subbase materials were tested for resilient modulus (M_r) and unconsolidated undrained (UU) shear strength generally following the AASHTO T-307 procedure—granular base/subbase Type I material. Samples were prepared using the vibratory compaction method as described in AASHTO T-307. Prior to compaction, materials were moisture-conditioned and allowed to mellow for at least 3 to 6 hours. A 101.6 mm (4 in.) diameter split mold was used to compact the sample (Figure 17) in five lifts of equal mass and thickness using an electric rotary hammer drill and a circular steel platen placed against the material (Figure 18). Calipers were used to verify consistent compaction layer thicknesses (Figure 18).

Figure 17. Split mold, steel platen (4 in. diameter), and vibratory hammer for compaction of subbase material samples

Figure 18. Compaction of subbase material samples in the split mold (left) and verification of thickness of each lift using calipers (right)

Resilient Modulus and Shear Strength Triaxial Testing

M_r and UU tests were performed using the Geocomp automated M_r test setup (Figure 19) in accordance with AASHTO T-307. The setup consists of a Load Trac-II load frame, an electrically controlled servo valve, an external signal conditioning unit, and a computer with a network card for data acquisition. The system uses a real-time adjustment of proportional-integral-derivative (PID) controller to adjust the system control parameters as the stiffness of the sample changes to apply the target loads during the test. Figure 19 shows the triaxial test chamber used in this study. The chamber is set up for both 71 mm (2.8 in.) and 101.6 mm (4 in.) diameter samples. Two linear voltage displacement transducers (LVDTs) are mounted to the piston rod to measure resilient strains in the sample during the test.

M_r tests were performed following the AASHTO T-307 conditioning and loading sequences suggested for base and subgrade materials (Table 3). Each load cycle consisted of a 0.1 second haversine-shaped load pulse followed by a 0.9 second rest period. M_r is calculated as the ratio of the applied cyclic deviator stress (σ_d) and resilient strain (ε_r). The σ_d and ε_r values from a typical stress-strain cycle during the test are shown in Table 2. The average σ_d and ε_r of the last five cycles of a loading sequence are used in M_r calculations. After M_r testing, UU shear strength testing was performed on each sample by applying a confining pressure of 34.5 kPa (5 psi) to the base material samples.

Figure 19. Triaxial chamber (left) and triaxial chamber, load frame, and computer equipment for resilient modulus tests (right)

Table 3. Resilient modulus test sequences and stress values for base/subbase materials (AASHTO T-307)

Sequence No.	Confining Pressure kPa	psi	Max. Axial Stress kPa	psi	No. of cycles
0	103.4	15	103.4	15	500–1000
1	20.7	3	20.7	3	100
2	20.7	3	41.4	6	100
3	20.7	3	62.1	9	100
4	34.5	5	34.5	5	100
5	34.5	5	68.9	10	100
6	34.5	5	103.4	15	100
7	68.9	10	68.9	10	100
8	68.9	10	137.9	20	100
9	68.9	10	206.8	30	100
10	103.4	15	68.9	10	100
11	103.4	15	103.4	15	100
12	103.4	15	206.8	30	100
13	137.9	20	103.4	15	100
14	137.9	20	137.9	20	100
15	137.9	20	275.8	40	100

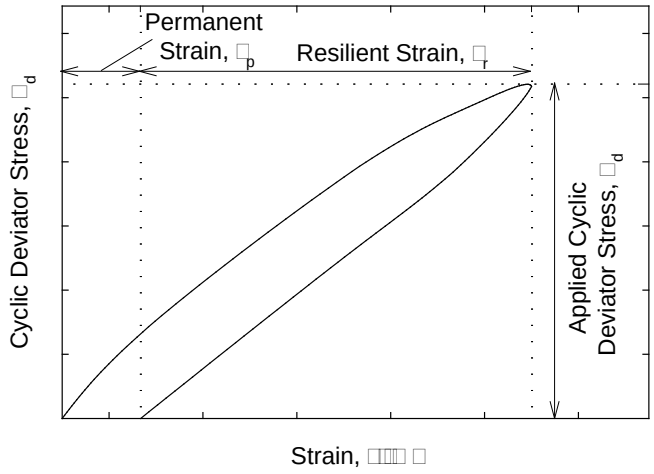

Figure 20. Graphical representation of one load cycle in M_r testing

Resilient Modulus Data Analysis

M_r values are used in pavement design as a measure of stiffness of unbound materials in the pavement structure. The M_r parameter is a highly stress-dependent parameter. Many non-linear constitutive models have been proposed that incorporate the effects of stress levels and predict M_r values. Most soils exhibit the effects of increasing stiffness with increasing bulk stress and decreasing stiffness with increasing shear stress (Andrei et al. 2004). A non-linear constitutive

model (also called the "universal" model) proposed by Witczak and Uzan (1988) (Equation 1) was used in this study

$$M_r = k_1 P_a \left(\frac{\sigma_B}{P_a} \right)^{k_2} \left(\frac{\tau_{oct}}{P_a} + 1 \right)^{k_3} \quad (1)$$

where P_a = atmospheric pressure (MPa); σ_B = bulk stress (MPa) = $\sigma_1 + \sigma_2 + \sigma_3$; τ_{oct} = octahedral shear stress (MPa) = $\{[(\sigma_1-\sigma_2)^2+(\sigma_2-\sigma_3)^2+(\sigma_3-\sigma_1)^2]^{1/2}\} / 3$; σ_1, σ_2, σ_3 = principal stresses; and k_1, k_2, k_3 = regression coefficients. The k_1 coefficient is proportional to M_r and therefore is always > 0. The k_2 coefficient explains the behavior of the material with changes in the volumetric stresses. Increasing volumetric stresses increases the M_r value and therefore the k_2 coefficient should be ≥ 0. The k_3 coefficient explains the behavior of the material with changes in shear stresses. Increasing shear stress softens the material and yields a lower M_r value; therefore, the k_3 coefficient should be ≤ 0.

The R^2 values determined for this model were adjusted for the number of regression parameters using Equation 2

$$R^2(\text{Adjusted}) = 1 - \left[\frac{(1 - R^2)(n-1)}{n-p-1} \right] \quad (2)$$

where *n* = the number of data points and *p* = the number of regression parameters.

Cyclic Triaxial Testing

Permanent Deformation Behavior Assessment

Cyclic triaxial tests were conducted to assess the permanent deformation behavior of the granular materials three methods referenced in this report as the ISU 100k, ISU 1k, and NCHRP 598 (Saeed 2008) methods. The loading sequences for the three methods are summarized in Table 4. Testing was conducted on subbase material samples prepared at different relative densities and fines contents to assess their influence on the permanent deformation behavior. Permanent defamation (ε_p) was quantified as accumulated permanent axial strain which is the ratio of the amount of unrecoverable change in sample height to the original sample height (Figure 20).

The ISU 100k test included 4 loading sequences with 25,000 cycles in each sequence under constant confining stress and axial stress. Samples were considered as failed for both ISU 100k and ISU 1k tests when an axial strain of 5% was reached in the sample, per AASHTO T307-99 specification.

The NCHRP 598 test proposed by Saeed (2008) specifically for recycled aggregate materials consists of 1 preconditioning (PC) sequence and 10 loading sequences with same confining

pressure and various cyclic stresses. Samples were considered failed when the samples reached 10% permanent strain.

Table 4. Repeated load triaxial test sequences

Sequence No.	Confining Pressure (kPa)	Confining Pressure (psi)	Maximum Axial Stress (kPa)	Maximum Axial Stress (psi)	No. of Cycles
ISU 1k test					
1	103.4	15.0	68.9	10.0	1,000
ISU 100k test					
1	103.4	15.0	68.9	10.0	25,000
2	103.4	15.0	68.9	10.0	25,000
3	103.4	15.0	68.9	10.0	25,000
4	103.4	15.0	68.9	10.0	25,000
NCHRP 598 test					
PC	103.4	15.0	68.9	10.0	50
1	103.4	15.0	68.9	10.0	1000
2	103.4	15.0	137.9	20.0	1000
3	103.4	15.0	275.8	40.0	1000
4	103.4	15.0	413.7	60.0	1000
5	103.4	15.0	551.6	80.0	1000
6	103.4	15.0	689.5	100.0	1000
7	103.4	15.0	827.4	120.0	1000
8	103.4	15.0	965.3	140.0	1000
9	103.4	15.0	1103.2	160.0	1000
10	103.4	15.0	1241.1	180.0	1000

Note: PC = preconditioning sequence

The sample displacements were measured using two LVDTs. The measurements were averaged to determine the accumulated ε_p at the end of each loading cycle. After the permanent strains of all load applications were calculated, the permanent strains were plotted with number of load cycles to observe the change in the accumulated permanent strains with increasing loading cycles. The accumulated permanent strain versus number of load cycles for ISU 100k and ISU 1k tests were plotted as single parabola curves with increasing number of loading cycles because constant confining pressure and cyclic stress were applied in each test. The accumulated permanent strains obtained in NCHRP 598 tests were plotted as stair-step parabola curves with increasing number of load cycles because increasing deviator stress and constant confining pressure were applied in these tests.

The data obtained was used to fit into a ε_p prediction model proposed by Barksdale (1972), which basically indicates a linear relationship between the accumulated permanent strain and logarithm number of load applications (Equation 3).

$$\varepsilon_{1,p} = a + b \cdot log(N) \quad (3)$$

where: $\varepsilon_{1,p}$ = accumulated permanent axial strain; N= number of load repetitions; and a and b = regression parameters.

This equation was modified to predict the permanent strain obtained in the NCHRP 598 tests according to the applied deviator stresses as Equation 4:

$$\varepsilon_{1,p} = k_1 + k_2 \cdot \sigma_d + k_3 \cdot \sigma_d^2 + \left[k_4 + \frac{k_5 \cdot (e^{k_6 \cdot \sigma_d} - 1)}{k_6}\right] \cdot \log_{10}[N - 1000 \cdot (S - 1)] \quad (4)$$

where: $\varepsilon_{1,p}$ = accumulated permanent axial strain; N = number of load cycles; S = number of load sequences; k_1, k_2, k_3, k_4, k_5, and k_6 = regression parameters; and σ_d = deviator stress (kPa).

Aggregate Particle Degradation Behavior Assessment

Mechanical sieve analyses were conducted according to ASTM D422-63 to assess degradations of aggregate particles after cyclic triaxial tests, using an index parameter called as breakage index (BI). BI is defined as the change in particle size distributions (Figure 21) of the tested materials due to test loadings, and was proposed by Indraratna et al. (2005) to quantify ballast degradations under cyclic loading. BI is calculated using Equation 5:

$$BI = \frac{A-B}{B} \quad (5)$$

where: BI = breakage index; A = area between the particle size distribution curve after permanent deformation test and the 0% passing base line; and B = area between the particle size distribution curve of the original materials and the 0% passing base line (Figure 21).

If the original particle size distribution curve is below the particle size distribution curve after permanent deformations (see Figure 21), the difference between two curves indicates that particles broke down to smaller particles. Particle degradation can be caused due to loads applied during compaction and cyclic loading.

Each degradation test included two mechanical sieve analyses tests: one on materials before permanent deformation testing and another after the test.

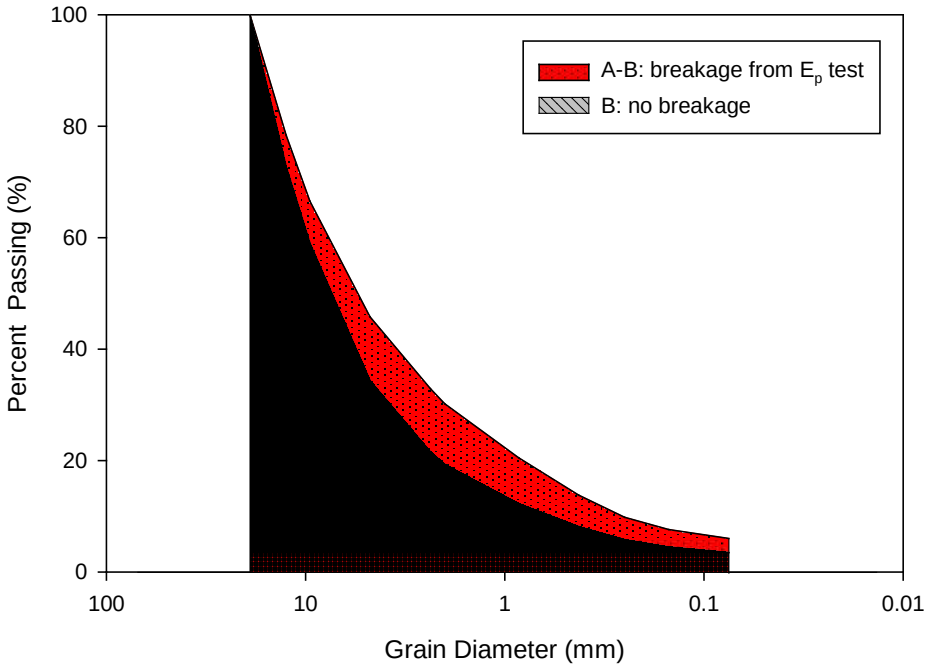

Figure 21. Example of calculating breakage index (BI)

Frost Heave and Thaw Weakening Tests

The frost heave and thaw weakening test was performed in general accordance with ASTM D5918-06 *Standard test methods for frost heave and thaw weakening susceptibility of soils*. The test is used to classify the frost heave and thaw weakening susceptibility of soils based on the heave rate and the thawed CBR values determined from the test. The heave rate and post-test F/T CBR values are compared with a classification system provided in the standard to determine the susceptibility ratings Table 5. It must be noted that the test results can only be used to compare the relative frost heave and thaw weakening susceptibility between material types and cannot be used to directly determine the amount of frost heave or thaw weakening in situ in a pavement system.

Table 5. Frost susceptibility classifications (ASTM D5918-06)

Frost Susceptibility Classification	Heave Rate (mm/day)	Thawed CBR (%)
Negligible	<1	>20
Very low	1 to 2	20 to 15
Low	2 to 4	15 to 10
Medium	4 to 8	10 to 5
High	8 to 16	5 to 2
Very High	>16	<2

The custom-made test setup fabricated at Iowa State University is shown in a cross-sectional diagram Figure 22 and a three-dimensional view in Figure 24.

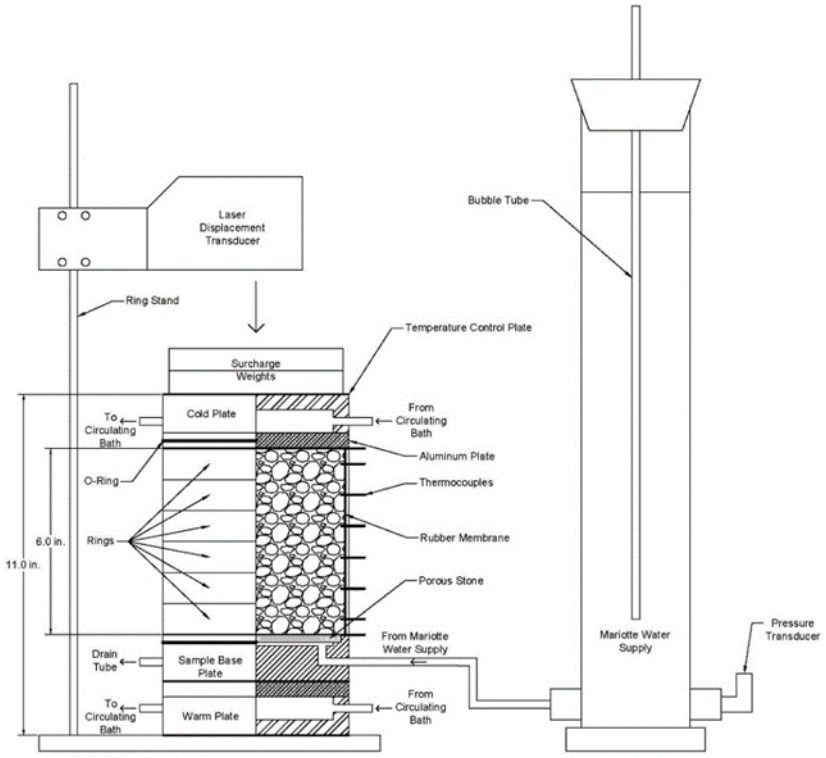

Figure 22. Illustration of frost-heave and thaw-weakening test assembly

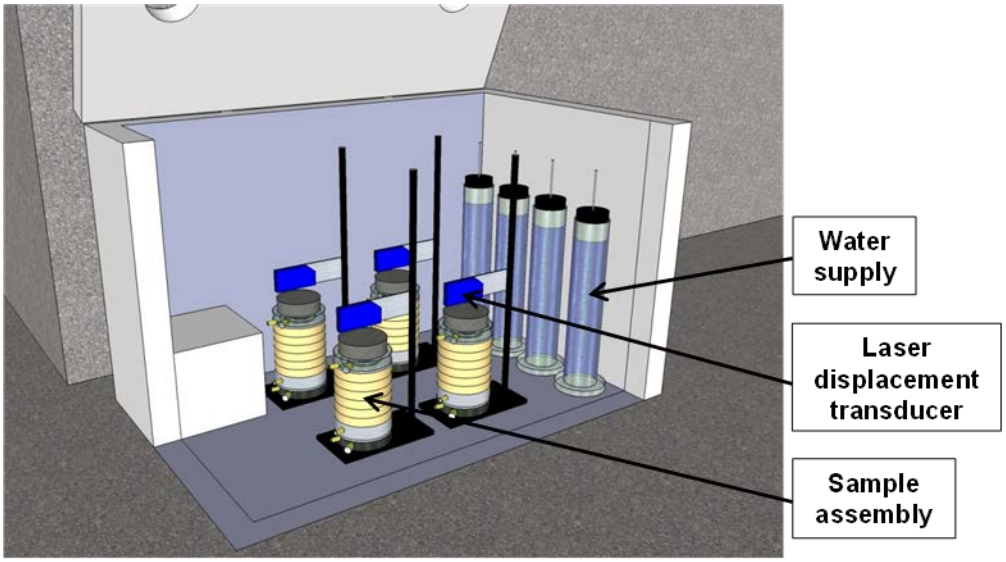

Figure 23. Three dimensional CAD illustration of frost-heave and thaw-weakening test assembly

The samples were 146 mm (5.75 in.) in diameter and 152 mm (6 in.) in height and were compacted inside six rings with a rubber membrane between the soil and the rings. The compaction mold setup is shown in Figure 24 and Figure 25.

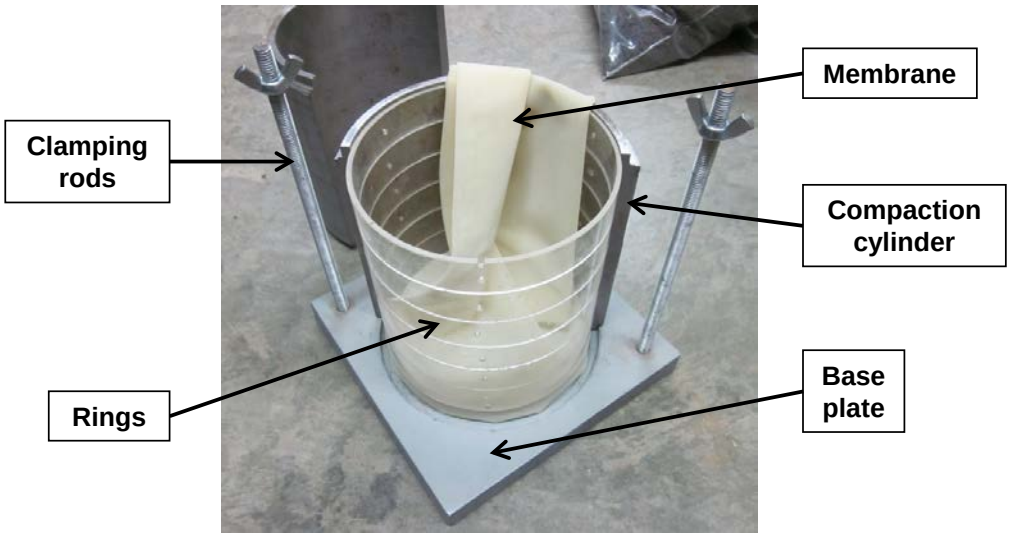

Figure 24. Inside view of the frost-heave and thaw-weakening test compaction mold with six rings

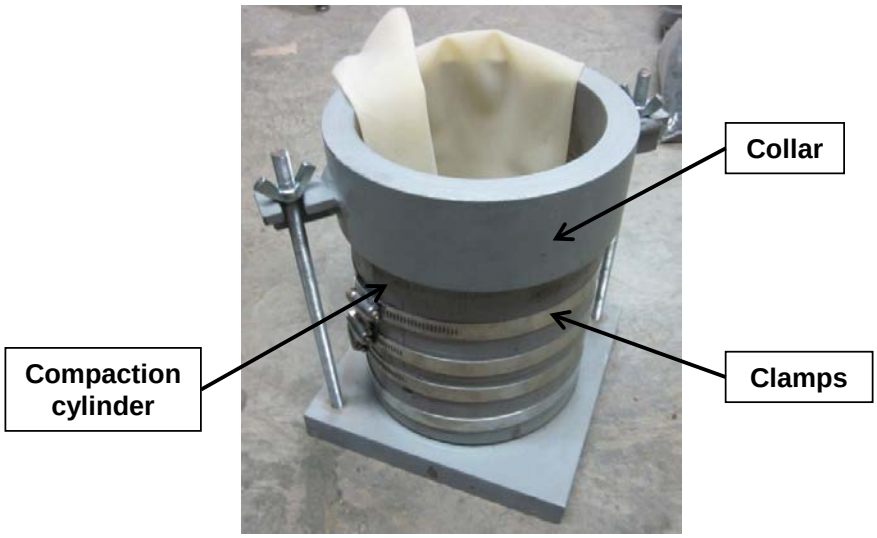

Figure 25. Frost-heave and thaw-weakening test compaction mold setup with collar

A water supply was made available at a level of 13 mm (0.5 in.) above the bottom of the sample using a Mariotte tube as illustrated in Figure 26, to saturate the sample. A surcharge weight was applied to the sample to simulate the loading of a typical pavement section. During the test, laser transducers installed on a ring stand and a bracket above the sample were used to obtain heave and consolidation measurements, and thermocouples installed in the sample obtained the temperature profile (Figure 22). The laser transducers used in this study had a measurement range of 50 mm and a resolution of 0.75 μm. The lasers and thermocouples were connected to a data acquisition system that recorded the temperature in one-minute intervals.

The tests were carried out by exposing four soil samples to two F/T cycles over a five day period. The samples were placed in a temperature controlled chest freezer (Figure 24) and then frozen and thawed by changing the temperature at the top and bottom of the samples using temperature controlled water baths (Figure 26). The programmable water baths used in this study had an operating range of -30°C to +200°C; were adjustable to ±0.01°C; and were filled with a 50% ethylene glycol-water solution. Insulating tape was wrapped around the flexible tubing between the water baths and the temperature control end plates to help reduce temperature variations in the solution. The target top and bottom of the sample temperatures (Figure 27) were programmed into the water baths and the actual temperatures were measured during the test. An example of the measured temperatures at the top and bottom of the sample is shown in Figure 28.

Figure 26. Temperature control water baths used to freeze and thaw samples

Results indicated that the measured temperatures were higher during freezing and lower during thawing than the target values. This discrepancy likely occurred because of temperature losses in the glycol solution when transported from the temperature control baths to the temperature control end plates (although care was taken to reduce these variations as indicated above). Once the test sequence was completed, CBR test was performed on the thawed samples in accordance with ASTM D1883-07 and a moisture content profile of the sample was determined by carefully trimming the thawed sample to desired depths.

The heave rates of the samples were determined from the slope of the heave versus time plot as illustrated in Figure 28. For a period of about 24 hours for both 1st and 2nd freezing cycles. ASTM D5918 specifies determining heave rate during the first eight hours of each freezing cycle. However, a few samples that were obtained from other research project sites did not heave during the first eight hours, and the samples that did heave during the first eight hours showed similar heave rates over the 8 hour and the 24 hour periods. To be consistent in comparing measurements from different project sites, the research team decided to present the heave rate over the 24 hour period.

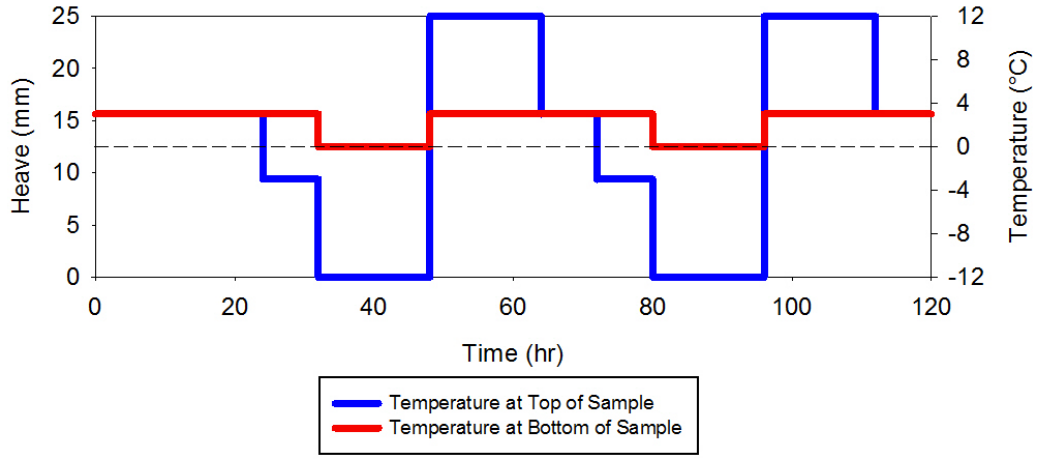

Figure 27. Target top and bottom temperatures with time per ASTM D5918-06 during F/T cycles

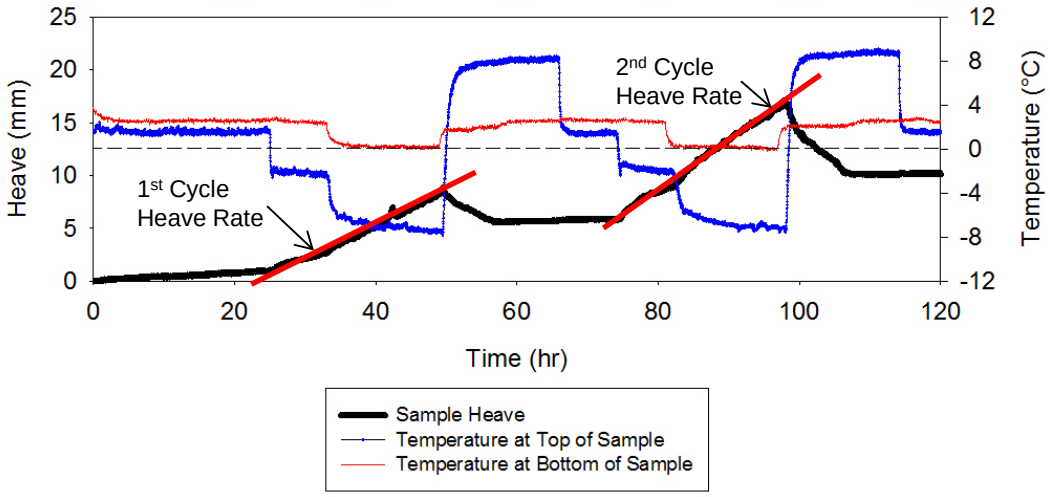

Figure 28. Example of measured top and bottom temperatures during F/T cycles and determination of heave rate for 1st and 2nd freezing cycles

In Situ Testing

Dynamic Cone Penetrometer

DCP tests (Figure 30) were performed in accordance with ASTM D6951-03 *Standard Test Method for Use of the Dynamic Cone Penetrometer in Shallow Pavement Applications* to determine dynamic penetration index (DPI) and calculate California bearing ratio (CBR) using Equation 6 or 7, as appropriate.

$$CBR\ (\%) = \frac{292}{DPI^{1.12}} \text{ for all soils with CBR} > 10 \quad (6)$$

$$CBR\ (\%) = \frac{1}{(0.017019 \times DPI)^2} \text{ when CBR} < 10 \text{ on CL soils} \quad (7)$$

The DPI of each layer was calculated as the ratio of the cumulative number of blows for each layer and the depth of the layer. These DPI values were used to determine the average CBR of each layer using the equations shown above. CBR of subgrade layers is denoted as CBR_{SG} and CBR of subbase layers is denoted as CBR_{SB} in this report. There were two modified subbase layers in this field study, RPCC and an RPCC/RAP mixture. The CBR of the two layers are distinguished as $CBR_{SB\text{-}RPCC}$ and $CBR_{SB\text{-}RPCC/RAP}$. The subgrade layer CBR (CBR_{SG}) was determined for the top 300 mm (12 in.) of the subgrade to represent properties of the reworked subgrade. Also, previous research White and Vennapusa (2014) indicated that a weak 75 mm (3 in.) layer within the subgrade can influence the FWD results. Therefore, $CBR_{SG\text{-}Weak}$ was also determined using the procedure illustrated as an example in Figure 29.

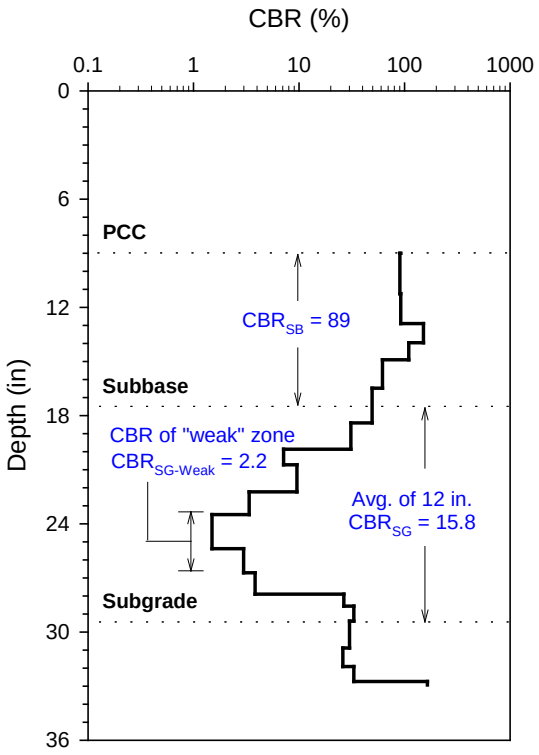

Figure 29. Example determination of average CBR of top 12 in. of subgrade and CBR of the "weak" layer within the subgrade

Zorn Light Weight Deflectometer

Zorn LWD tests were performed on subbase and subgrade layers to determine elastic modulus (Figure 30). The LWD was setup with 300 mm diameter plate and 71 cm drop height. The tests were performed following manufacturer recommendations (Zorn 2003) and the elastic modulus values were determined using Equation 8:

$$E = \frac{(1-\eta^2)\sigma_0 r}{D_0} \times F \quad (8)$$

where E = elastic modulus (MPa); D_0 = measured deflection under the plate (mm); η = Poisson's ratio (0.4); σ_0 = applied stress (MPa); r = radius of the plate (mm); and F = shape factor depending on stress distribution (assumed as 8/3) (see Vennapusa and White 2009). The results are reported as $E_{LWD\text{-}Z3}$ (where Z represents Zorn LWD and 3 represents 300 mm diameter plate).

Figure 30. DCP testing (left) and Zorn LWD testing (right)

Kuab Falling Weight Deflectometer

Falling weight deflectometer (FWD) tests were conducted using a Kuab FWD setup with a 11.81 in. diameter loading plate by applying one seating drop and three loading drops. The applied loads varied from about 27 kN (6,000 lb) to 54 kN (12,000 lb) in the three loading drops. The actual applied loads were recorded using a load cell, and deflections were recorded using seismometers mounted on the device, per ASTM D4694-09 *Standard Test Method for Deflections with a Falling-Weight-Type Impulse Load Device.* The FWD plate and deflection sensor setup and a typical deflection basin are shown in Figure 31. To compare deflection values from different test locations at the same applied contact stress, the values at each test location were normalized to a 40 kN (9,000 lb) applied force.

FWD tests were conducted at the center of the PCC slab panels and at the joints. Tests conducted at the joints were used to determine joint load transfer efficiency (LTE) and voids beneath the pavement based on "zero" load intercept values. Tests conducted at the center were used to determine modulus of subgrade reaction (*k*) values and the intercept values. The procedure used to calculate these parameters are described below.

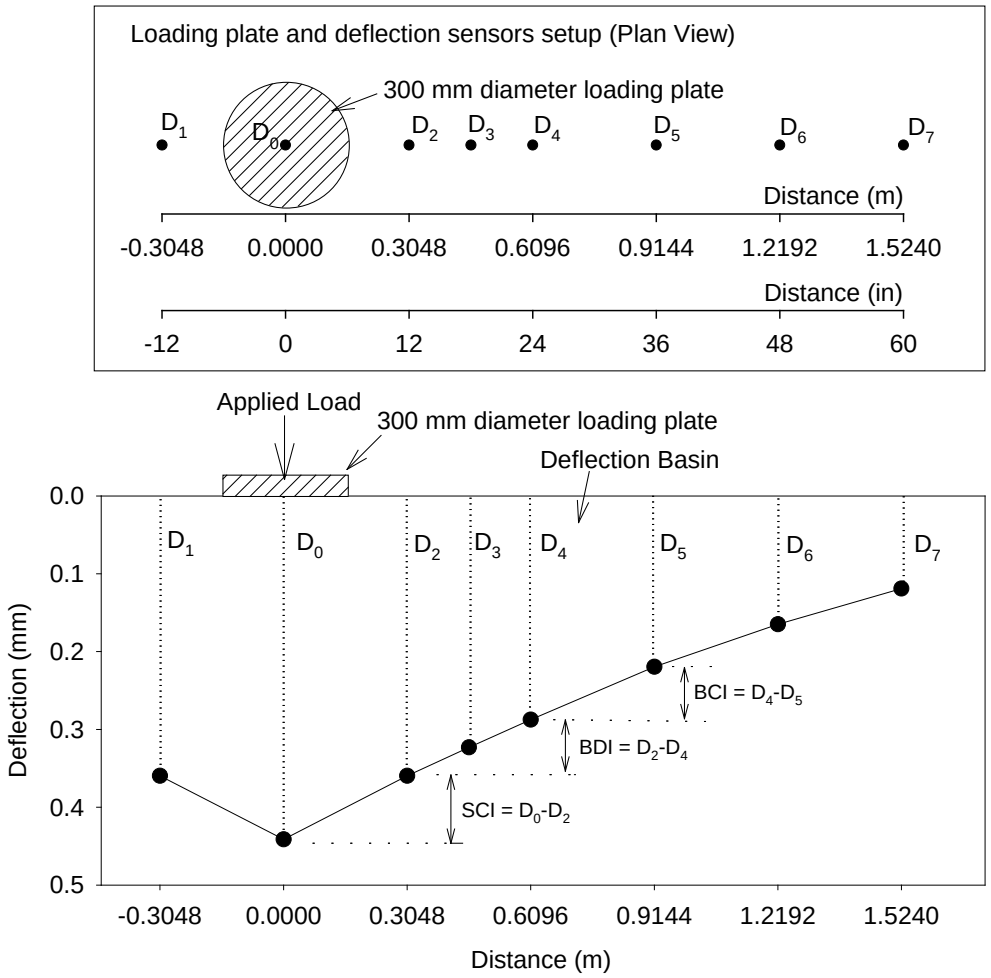

Figure 31. FWD deflection sensor setup used for this study and an example deflection basin with SCI, BDI, and BCI calculation procedure

LTE was determined by obtaining deflections under the plate on the loaded slab (D_0) and deflections of the unloaded slab (D_1) using a sensor positioned about 305 mm (12 in.) away from the center of the plate (Figure 31). The LTE was calculated using Equation 8.

$$LTE(\%) = \frac{D_1}{D_0} \times 100 \tag{8}$$

Voids underneath pavements can be detected by plotting the applied load measurements on the x-axis and the corresponding deflection measurements on the y-axis, and plotting a best fit linear regression line as illustrated in Figure 32, to determine the "zero" load intercept (I) values. AASHTO (1993) suggests I = 0.05 mm (2 mils) as a critical value for void detection. According to von Quintus and Simpson (2002), if I = −0.01 and +0.01 mm, then the response would be considered elastic. If I > 0.01 then the response would be considered deflection hardening, and if I < −0.01 then the response would be considered deflection softening.

Pavement layer temperatures at different depths were obtained during FWD testing, in accordance with the guidelines from Schmalzer (2006). The temperature measurements were used to determine equivalent linear temperature gradients (T_L) following the temperature-moment concept suggested by Jannsen and Snyder (2000). According to Vandenbossche (2005), the I-values are sensitive to temperature induced curling and warping affects. Large positive temperature gradients (i.e., when surface is warmer than bottom) that cause the panel corners to curl down result in false negative I-values. Conversely, large negative gradients (i.e., when surface is cooler than bottom) that cause the panel corners to curl upward result in false positive I-values. Interpretation of I-values therefore should consider the temperature gradient. Concerning LTE measurements for doweled joints, the temperature gradient is reportedly not a critical factor Vandenbossche (2005).

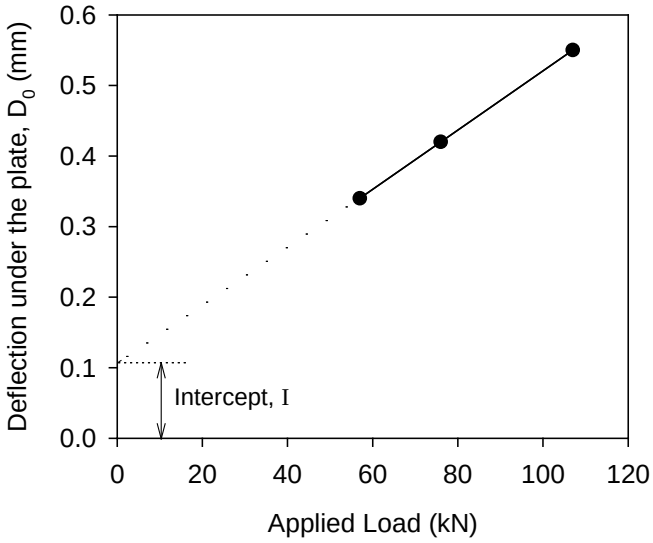

Figure 32. Void detection using load-deflection data from FWD test

The *k* values were determined using the $AREA_4$ method described in AASHTO (1993). The AREA method was first proposed by Hoffman and Thompson (1981) for flexible pavements and has since been applied extensively for concrete pavements (Darter et al. 1995). Since the *k* value determined from FWD test represents a dynamic value, it is referred to here as $k_{FWD\text{-}Dynamic}$. Deflections obtained from four sensors, i.e., D_0, D_2, D_4, and D_5 (see Figure 31) are used in the $AREA_4$ calculation. $AREA_4$ is calculated using Equation 9 and has dimensions of length (in.), as it is normalized with deflections under the center of the plate (D_0):

$$AREA_4 = 6 + 12 \times \left(\frac{D_2}{D_0} \right) + 12 \times \left(\frac{D_4}{D_0} \right) + 6 \times \left(\frac{D_5}{D_0} \right) \quad (9)$$

where D_0 = deflections measured directly under the plate (in.); D_2 = deflections measured at 305 mm (12 in.) away from the plate center (in.); D_4= deflections measured at 610 mm (24 in.) away from the plate center (in.); and D_5 = deflections measured at 914 mm (36 in.) away from the plate center (in.). AREA method can also be calculated using different sensor configurations and setups, i.e., using deflection data from 3, 5, or 7 sensors and those methods are described in detail in the literature (Stubstad et al. 2006, Smith et al. 2007).

In the early research conducted using the AREA method, the ILLI-SLAB finite element program was used to compute a matrix of maximum deflections at the plate center and the AREA values by varying the subgrade *k*, the modulus of the PCC layer, and the thickness of the slab (ERES Consultants, Inc. 1982). Measurements obtained from FWD tests were then compared with the ILLI-SLAB program results to determine the *k* values through back calculation. Later, in the 1990s to replace the back calculation procedure, Barenberg and Petros (1991) and Ioannides (1990) proposed a forward solution procedure based on Westergaard's solution for loading on an infinite plate. This forward solution presented a unique relationship between AREA value (for a given load and sensor arrangement) and the dense liquid radius of relative stiffness (L) in which subgrade is characterized by the *k* value. The radius of relative stiffness (L) is estimated using Equation 10:

$$L = \left[\frac{\ln\left(\frac{x_1 - AREA_4}{x_2} \right)}{x_3} \right]^{x_4} \quad (10)$$

where $x_1 = 36$; $x_2 = 1812.279$; $x_3 = -2.559$; $x_4 = 4.387$. It must be noted that the x1 to x4 values vary with the sensor arrangement and these values are only valid for the AREA4 sensor setup. Once the L value is known, the $k_{FWD\text{-}Dynamic}$ value can be estimated using Equation 11:

$$k_{FWD-Dynamic}(pci) = \frac{PD_0^*}{D_0 L^2} \quad (11)$$

where P = applied load (lb); D_0 = deflection measured at plate center (inches); and D_0* = non-dimensional deflection coefficient calculated using Equation 12:

$$D_0^* = a \cdot e^{-be^{-cL}} \quad (12)$$

where a = 0.12450; b = 0.14707; and c = 0.07565. It must be noted that these equations and coefficients are valid for an FWD setup with an 11.81 in. diameter plate.

The advantages of the AREA method are the ease of use without any back calculations and its use of multiple sensor data. The disadvantages are that the process assumes the slab and the subgrade are horizontally infinite. This assumption leads to an underestimation of the *k* value. Crovetti (1993) developed the following slab size corrections for a square slab based on finite element analysis conducted using the ILLI-SLAB program, for use in the $k_{\text{FWD-Dynamic}}$ (Eq. 11):

$$Adjusted\ D_0 = D_0\left(1 - 1.15085e^{-0.71878\left(\frac{L'}{L}\right)^{0.80151}}\right) \quad (13)$$

$$Adjusted\ L = L\left(1 - 0.89434e^{-0.61662\left(\frac{L'}{L}\right)^{1.04831}}\right) \quad (14)$$

where L′ = slab size (smaller dimension of a rectangular slab, length or width). This procedure also has limitations: (1) it considers only a single slab with no load transfer to adjacent slabs, and (2) it assumes a square slab. The square lab assumption is considered to produce sufficiently accurate results when the smaller dimension of a rectangular slab is assumed as L′ (Darter et al. 1995). Darter et al. 1995 suggested using $L' = \sqrt{Length \times Width}$ to further refine the slab size corrections. There are no established procedures reported to date on correcting for load transfer to adjacent slabs, which remains as a limitation of this method. In this project, $k_{\text{FWD-Dynamic}}$ values corrected for slab size are reported as $k_{\text{FWD-Dynamic-Corr}}$.

AASHTO (1993) suggests dividing the $k_{\text{FWD-Dynamic}}$ value by a factor of 2 to determine the equivalent $k_{\text{FWD-Static}}$ value. The origin of this factor 2 dates back to Foxworthy's work in the 1980s. Foxworthy (1985) reported comparisons between the $k_{\text{FWD-Dynamic}}$ values obtained using Dynatest model 8000 FWD and the Static *k* values (Static k_{PLT}) obtained from 30 in. diameter plate load tests (Foxworthy did not report the exact procedure followed to calculate the Static k_{PLT}). Foxworthy used the AREA-based back calculation procedure using the ILLI-SLAB finite element program. Results obtained from Foxworthy's study are shown in Figure 33, and are based on 7 FWD tests conducted on PCC pavements with slab thicknesses varying from about 10 in. to 25.5 in. and plate load tests conducted on the foundation layer immediately beneath the pavement over a 4 ft x 5 ft test area. A few of these sections consisted of a 5 to 12 in. thick base course layer and some did not. The subgrade layer material consisted of CL soil from Sheppard Air Force Base in Texas, SM soil from Seymour-Johnson Air Force Base in North Carolina, and from McDill Air Force base in Florida (soil type was unspecified). No slab size correction was performed on this dataset.

Data from Foxworthy (1985) yielded a logarithmic relationship between the dynamic and the static *k* values. On average, the $k_{\text{FWD-Dynamic}}$ values were about 2.4 times greater than the Static k_{PLT} values. Darter et al. (1995) indicated that the factor 2 is reasonable based on results from other test sites (Figure 33). Darter et al. (1995) also compared FWD test data from eight

long term pavement performance (LTPP) test sections with the Static k_{PLT} values and reported factors ranging from 1.78 to 2.16, with an average of about 1.91. The $k_{FWD\text{-}Dynamic}$ values used in that comparison were corrected for slab size.

For the analysis conducted in this research project, the $k_{FWD\text{-}Dynamic\text{-}Corr}$ values were divided by 2 and are reported as $k_{FWD\text{-}Static\text{-}Corr}$ values.

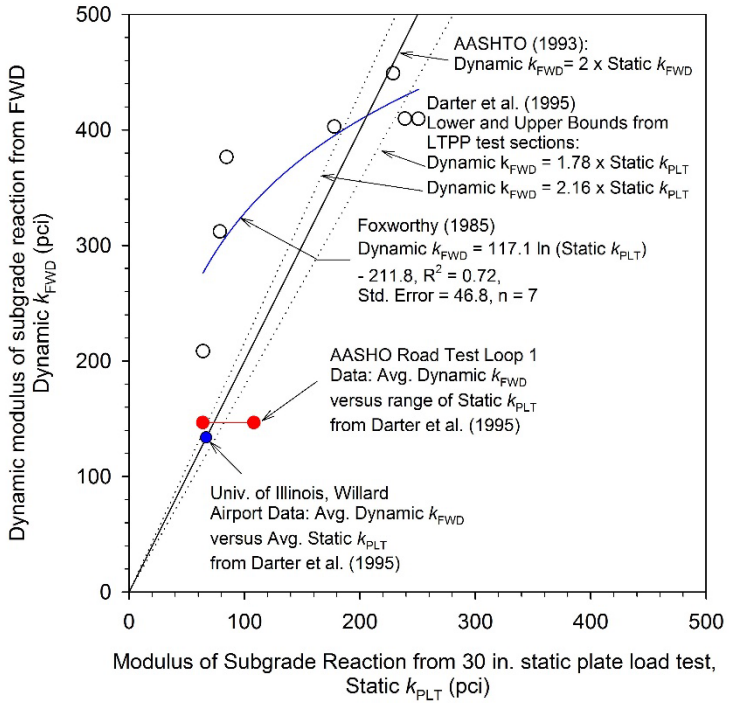

Figure 33. Static k_{PLT} values versus Dynamic k_{FWD} measurements reported in literature

Determination of *k* Values

Subgrade *k* values were determined directly from field measurements using FWD testing, empirical relationships from DCP test measurements, and empirical relationships from laboratory measurements. All of these values are compared in this report with reference to the design assumed value. The *k* values determined using different procedures and the notations are listed below:

- $k_{FWD\text{-}Static\text{-}Corr}$ – determined from the FWD test and corrected for slab size.
- $k_{AASHTO(1993)}$ – determined using Equation 8, where M_r is determined from DCP-$CBR_{Subgrade}$ using charts provided in AASHTO (1993) (see Appendix A) or directly from laboratory measurements.

$$k_{AASHTO(1993)} = \frac{M_r}{19.4} \tag{15}$$

Note: as shown in Eq. 8, units for M_r are [psi] and k are [psi/in]; multiply the right side of the equation by 39.6 for units of M_r in [MPa] and k in [kPa/mm]

- $k_{PCA(1984)}$ – determined from CBR using charts provided in PCA (1984) (see Appendix A).

Pavement Temperature Monitoring

Thermocouple temperature sensors were installed at about mile 143.68 on US30 EB lane, east of the 500th Avenue Overpass Bridge. Type T thermocouple wires were used to make the sensors. Sensors were installed vertically from about 0.15 m to about 1.2 m below the top of the modified subbase layer. All vertical sensors were located at the center line. Sensors were also installed horizontally at a depth of about 0.15 m below the modified subbase layer surface, to measure temperature variations horizontal across the pavement width and the shoulder. A pavement and foundation layer cross-section along with the vertical and horizontal temperature sensor locations are shown in Figure 34. Pictures of installation are shown in Figure 35 and Figure 36. The sensors were connected to a CR5000 Campbell Scientific datalogger to continuously record data (every 10 minutes). The datalogger was outfitted with a chargeable 12 volt battery that was charged by a solar panel.

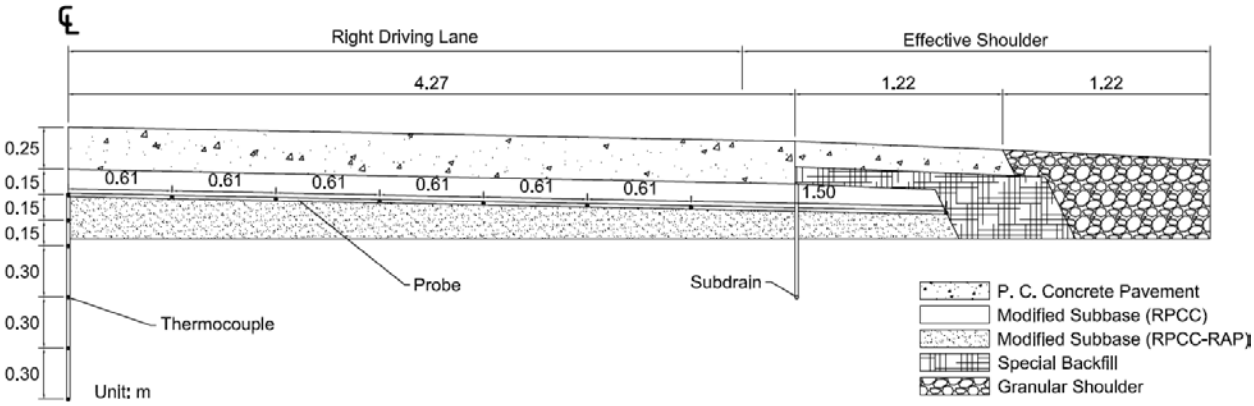

Figure 34. Profile of temperature probe installation

Figure 35. Preparation of a vertical hole to install temperature sensors down to about 1.2 m below surface

Figure 36. Vertical and horizontal temperature probes (left) and temperature data acquisition setup (right)

CHAPTER 4. LABORATORY TESTING RESULTS

Laboratory test results of subgrade and subbase layer samples collected from the field are presented in this chapter.

Particle Size Analysis and Index Properties

A summary of the soil index properties for the subgrade, RPCC/RAP modified subbase, and crushed limestone subbase collected from the project site are shown in Table 6. The particle size distributions for the materials are shown in Figure 37 through Figure 39.

Table 6. Summary of IA US-30 soil index properties

Soil index property	Subgrade	RPCC/RAP modified subbase	RPCC modified subbase
USCS classification	SC	GP-GM	GP-GM
AASHTO classification	A-6(2)	A-1-a	A-1-a
Coefficient of uniformity (c_u)	—	34.3	44.3
Coefficient of curvature (c_c)	—	0.93	4.48
D_{10} (mm)	—	0.232	0.273
D_{30} (mm)	0.020	1.31	3.85
D_{60} (mm)	0.286	7.97	12.1
Gravel size (%) (> 4.75 mm)	11.0	51.0	67.0
Sand size (%) (4.75 – 0.074 mm)	46.0	43.0	28.0
Silt size (%) (0.074 – 0.002 mm)	24.0	4.0	5.0
Clay size (%) (≤ 0.002 mm)	19.0	2.0	0.0
Passing 0.074 mm (%)	43.0	6.0	5.2
Passing 0.02 mm (%)	31.3	4.6	2.3
Liquid limit (LL)	27	NP	NP
Plasticity index (PI)	15	NP	NP
Specific gravity (G_s)	2.63	2.52	2.57
Optimum moisture content (%) standard Proctor	11.9	10.3	—
Maximum dry unit weight (kN/m^3) standard Proctor	18.71	19.30	—

NP:not plastic; — Test not performed

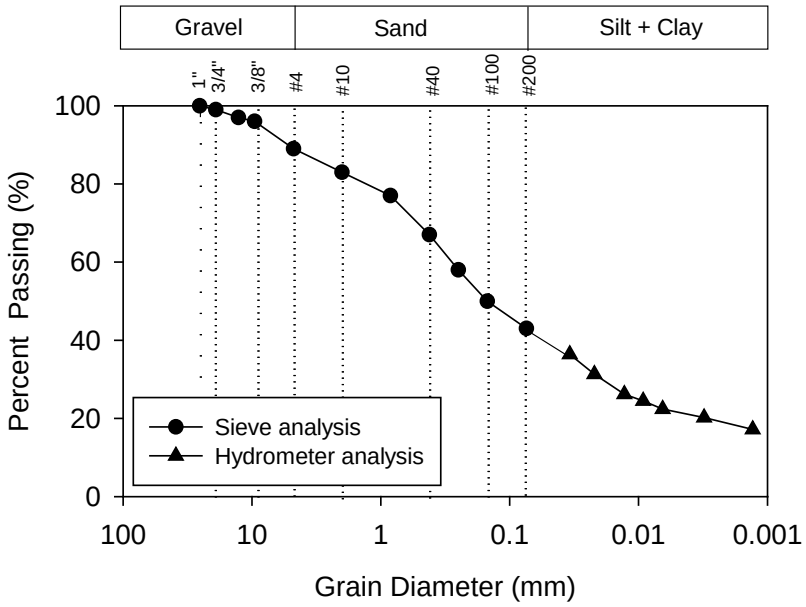

Figure 37. IA US-30 clayey sand subgrade particle size distribution

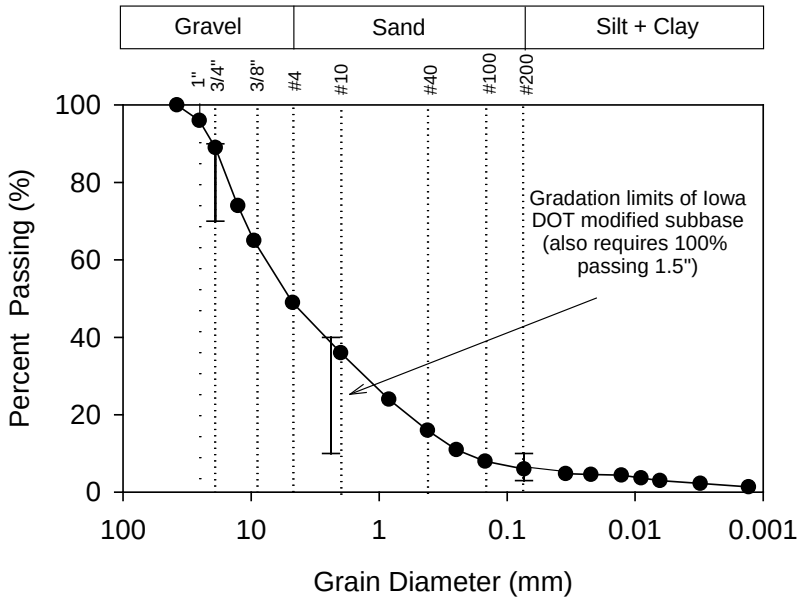

Figure 38. IA US-30 RPCC/RAP modified subbase particle size distribution

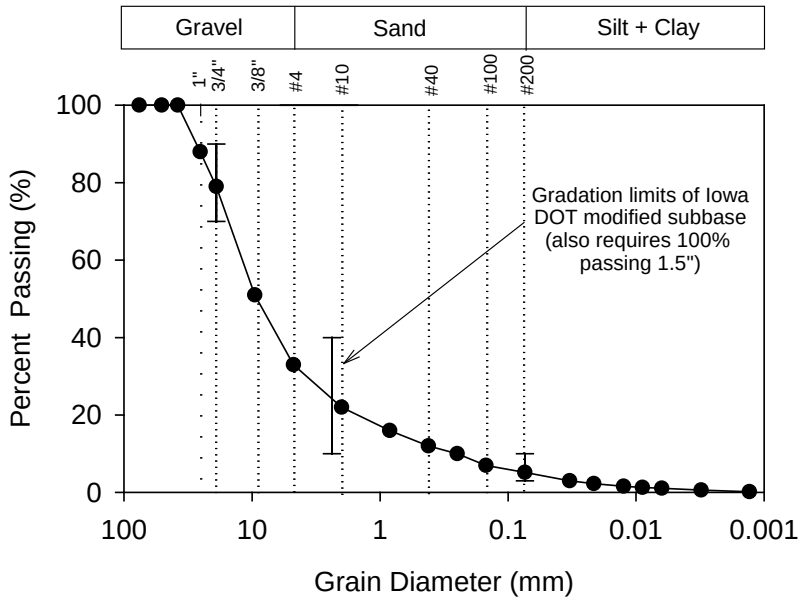

Figure 39. IA US-30 RPCC modified subbase particle size distribution

Permanent Deformation

Three test methods, ISU 100k, ISU 1k, and NCHRP 598 tests were followed to assess the permanent deformation (ε_p) behavior of the modified subbase materials in this study. ISU 100k and 1k tests were conducted on RPCC material and NCHRP 598 tests were conducted on RPCC/RAP material. Tests were conducted at different relative densities (RD), deviator stresses (σ_d), and at varying fines content (F_{200}) in the RPCC material. The RDs were varied between 80% and 95%; deviator stresses were varied between 20.7 and 103.4 kPa in the 100k and 1k tests and 68.9 to 1241 kPa in the NCHRP 598 tests; and fines content were varied between 0 and 12%. Each test was conducted on a unique sample that was prepared to meet the target values of designed sample characteristics and the actual values of the sample characteristics were determined. A unique test number was assigned for each test to avoid repeated descriptions of samples characteristics.

The target and actual characteristics of the ISU 100k tests on RPCC samples are provided in

Table 7. Similarly, the characteristics of the ISU 1k tests and NCHRP 598 tests on RPCC samples are provided in Table 8 and Table 9, respectively.

Table 7. Target and actual characteristics of ISU 100k tests on RPCC samples

Test	F_{200} (%)		w (%)		RD (%)		γ_d (kN/m^3)	
no.	Target	Actual	Target	Actual	Target	Actual	Target	Actual
D-A8	natural	6.2	10.0	8.1	95.0	104.1	17.14	17.61
D-A9				9.6	90.0	100.4	16.90	17.42
D-A10				9.9	90.0	99.4	16.90	17.37
D-A11				9.8	90.0	99.4	16.90	17.37
D-A12				9.6	90.0	99.8	16.90	17.39
D-A13				10.1	90.0	99.2	16.90	17.36
D-A14				10.1	80.0	88.7	16.44	16.85
D-A15				9.8	85.0	95.0	16.67	17.15

Table 8. Target and actual characteristics of ISU 1k tests on RPCC samples

Test	F_{200} (%)		w (%)		RD (%)		γ_d (kN/m^3)	
no.	Target	Actual	Target	Actual	Target	Actual	Target	Actual
D-B1	natural	5.6	10.0	9.65	95.0	103.7	17.14	17.59
D-B2				10.15	90.0	99.4	16.90	17.37
D-B3				9.59	90.0	100.4	16.90	17.42
D-B4				9.88	90.0	101.0	16.90	17.45
D-B5				9.84	90.0	100.0	16.90	17.40
D-B6				10.51	90.0	98.0	16.90	17.30
D-B7				10.11	80.0	89.2	16.44	16.87
D-B8				10.05	85.0	94.4	16.67	17.12

Table 9. Target and actual characteristics of NCHRP 598 tests on RPCC/RAP samples

Test	F_{200} (%)		w (%)		RD (%)		γ_d (kN/m^3)	
No.	Target	Actual	Target	Actual	Target	Actual	Target	Actual
D-C25	0.0	0.8	6.0	5.7	85.0	88.5	15.26	15.36
D-C26	natural	3.5	6.0	7.5	85.0	77.0	16.12	15.97
D-C27	6.0	6.0	6.0	6.0	85.0	86.1	16.76	16.81
D-C28	12.0	12.4	6.0	6.0	85.0	86.3	17.54	17.60
D-C29	0.0	0.8	6.0	5.8	90.0	93.3	15.41	15.51
D-C30	natural	3.5	6.0	7.5	90.0	81.2	16.22	16.05
D-C31	6.0	6.0	6.0	6.0	90.0	91.3	16.96	17.01
D-C32	12.0	12.4	6.0	6.2	90.0	90.7	17.74	17.77
D-C33	0.0	0.8	6.0	5.5	95.0	99.0	15.56	15.69
D-C34	natural	3.5	6.0	6.4	95.0	95.4	16.44	16.33
D-C35	6.0	6.0	6.0	6.2	95.0	95.6	17.17	17.19
D-C36	12.0	12.4	6.0	6.0	95.0	96.4	17.95	18.01

The accumulated ε_p at the end of ISU 1k tests and ISU 100k tests performed at different σ_d are summarized in Table 10 and Table 11, respectively. The ε_p values for all tests were very small ($0.10 \pm 0.04\%$) and did not show a clear trend or influence of σ_d or RD.

The accumulated ε_p at the end of each NCHRP 598 test sequence (labeled S1 to S10) was calculated and is summarized in Table 12. As suggested by Saeed (2008), tests were terminated if ε_p = 10% was achieved. All samples showed > 10% permanent strain before the 9th test sequence which involved applying a 1,103 psi deviator stress.

Table 10. ε_p (%) at the end of the tests for RPCC samples (ISU 1k)

Test no.	ε_p at the test end %	σ_c kPa	psi	σ_d kPa	psi
D-B1	0.09	103.4	15.0	20.7	3.0
D-B2	0.03	103.4	15.0	20.7	3.0
D-B3	0.05	103.4	15.0	41.4	6.0
D-B4	0.12	103.4	15.0	62.1	9.0
D-B5	0.10	103.4	15.0	82.7	12.0
D-B6	0.12	103.4	15.0	103.4	15.0
D-B7	0.03	103.4	15.0	20.7	3.0
D-B8	0.07	103.4	15.0	20.7	3.0

Table 11. ε_p (%) at the end of the tests for RPCC samples (ISU 100k)

Test no.	ε_p at the test end %	σ_c kPa	psi	σ_d kPa	psi
D-A8	0.02	103.4	15.0	20.7	3.0
D-A9	0.06	103.4	15.0	20.7	3.0
D-A10	0.07	103.4	15.0	41.4	6.0
D-A11	0.13	103.4	15.0	62.1	9.0
D-A12	0.11	103.4	15.0	82.7	12.0
D-A13	0.11	103.4	15.0	103.4	15.0
D-A14	0.003	103.4	15.0	20.7	3.0
D-A15	0.06	103.4	15.0	20.7	3.0

Table 12. ε_p (%) at all load sequences end for RPCC/RAP samples (NCHRP 598)

Test No.	S1	S2	S3	S4	S5	S6	S7	S8	S9	S10
D-C25	0.076	0.362	1.352	2.694	4.624	7.440	—	—	—	—
D-C26	0.011	0.051	0.196	0.599	2.102	6.459	—	—	—	—
D-C27	0.022	0.141	0.741	1.685	2.953	4.445	7.122	—	—	—
D-C28	0.006	0.039	0.130	0.404	0.971	1.704	2.816	5.258	—	—
D-C29	0.078	0.330	1.336	2.620	4.122	6.496	—	—	—	—
D-C30	0.016	0.062	0.194	0.500	1.635	4.388	8.894	—	—	—
D-C31	0.024	0.146	0.711	1.558	2.568	3.770	5.395	7.695	—	—
D-C32	0.015	0.050	0.162	0.404	0.895	1.622	2.572	4.262	—	—
D-C33	0.066	0.279	1.073	2.208	3.789	5.756	10.176	—	—	—
D-C34	0.017	0.071	0.255	0.639	1.802	3.740	7.217	—	—	—
D-C35	0.016	0.075	0.389	1.001	1.845	2.905	4.272	6.610	—	—
D-C36	0.007	0.031	0.106	0.240	0.551	1.078	1.772	3.002	—	—

Notes: — means the test ended at this load sequence or previous load sequence with ε_p > 10%.

Permanent deformation test results for ISU 100k and ISU 1k tests at different deviator stresses are presented in Figure 40 and Figure 41, respectively. Similarly, the results on samples tested at same deviator stresses but with different RD are presented in Figure 42 and Figure 43. Results from NCHRP 598 tests at different fines content and RD are shown in Figure 44 to Figure 50.

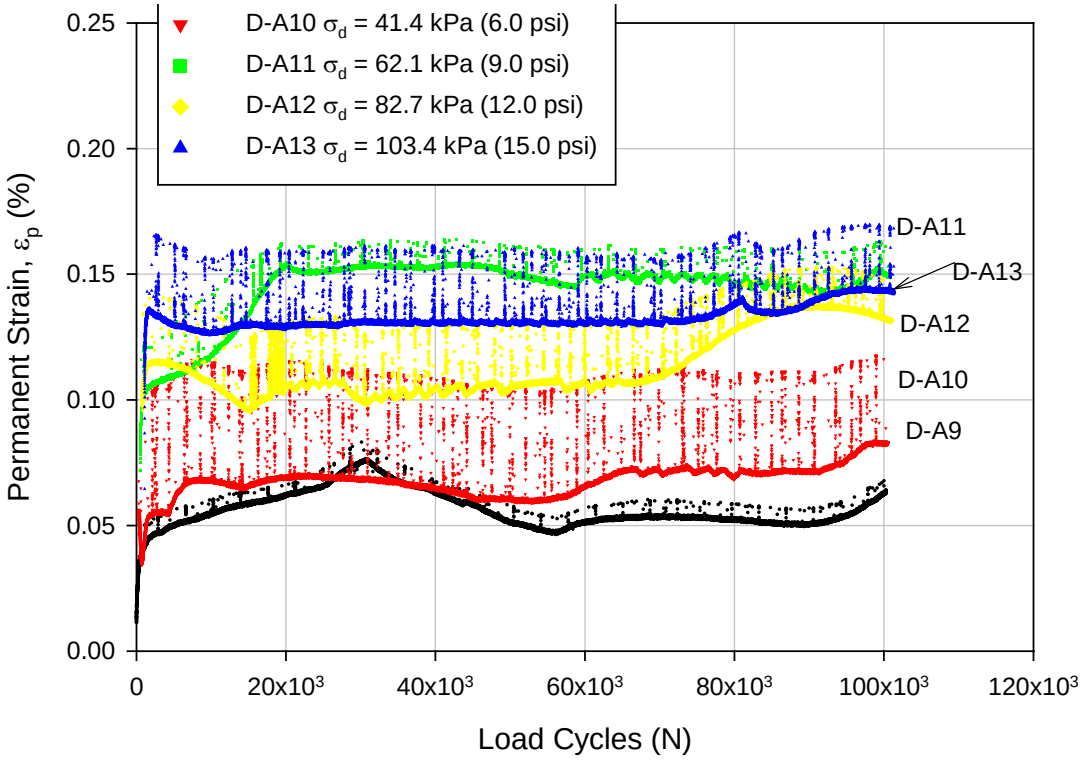

Figure 40. ε_p at 90% target RD for RPCC samples (ISU 100k)

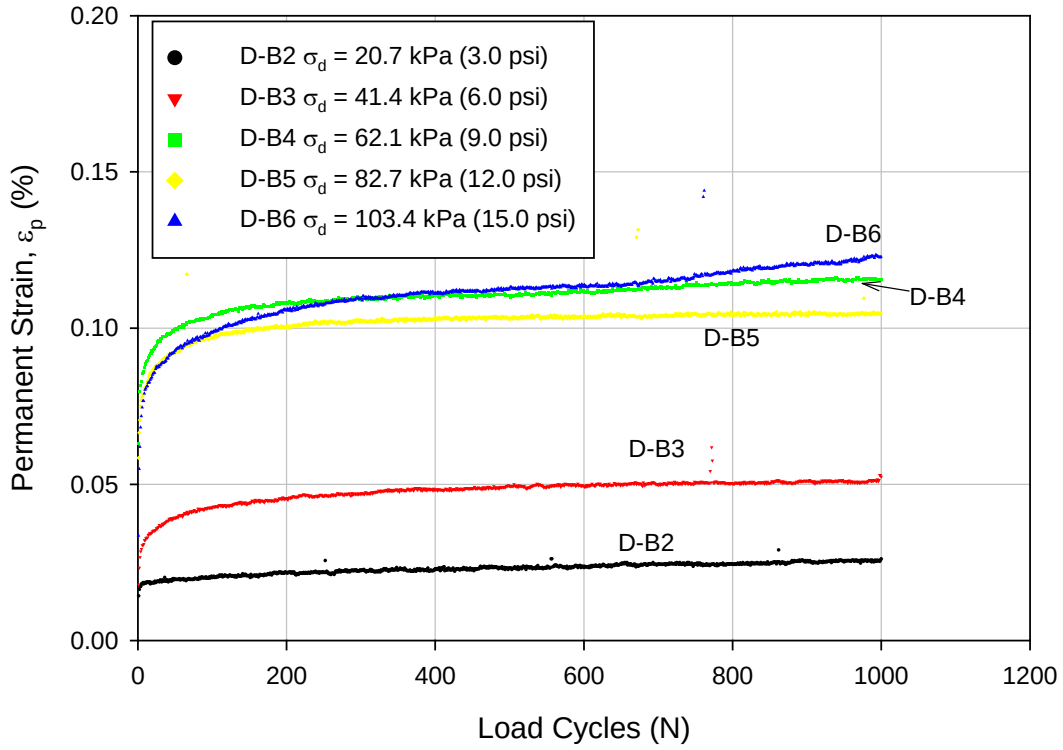

Figure 41. ε_p at 90% target RD for RPCC samples (ISU 1k)

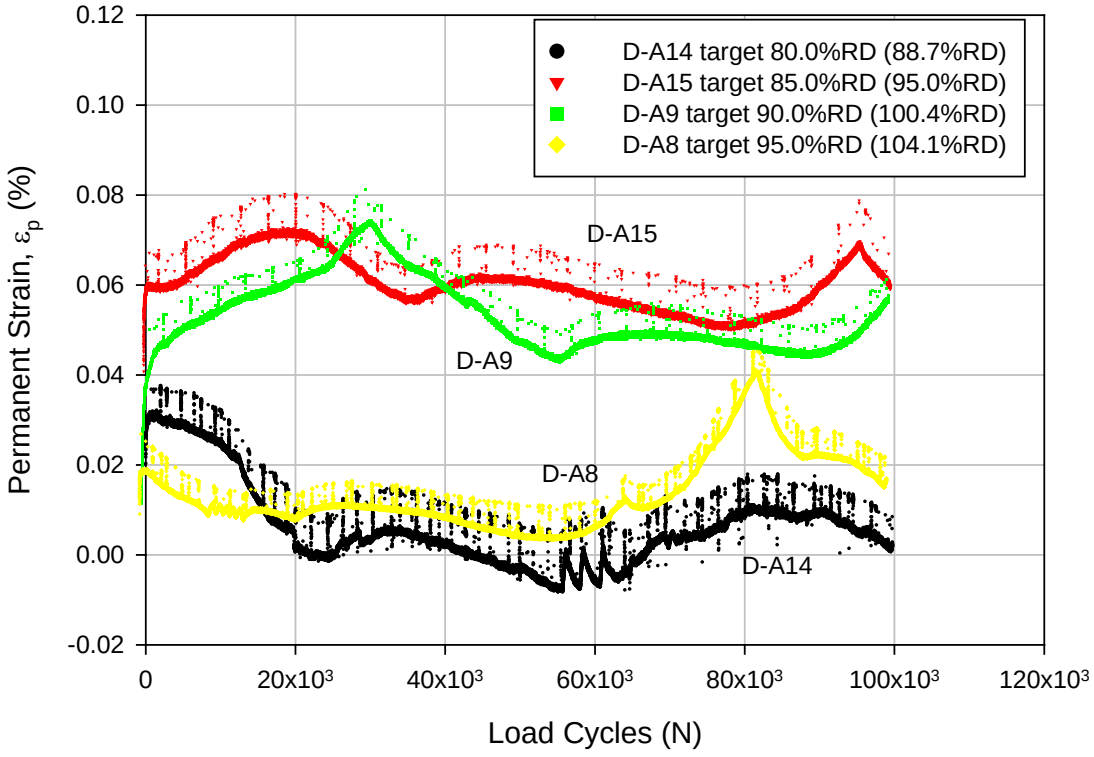

Figure 42. ε_p at 20.7 kPa (3.0 psi) σ_d for RPCC samples (ISU 100k)

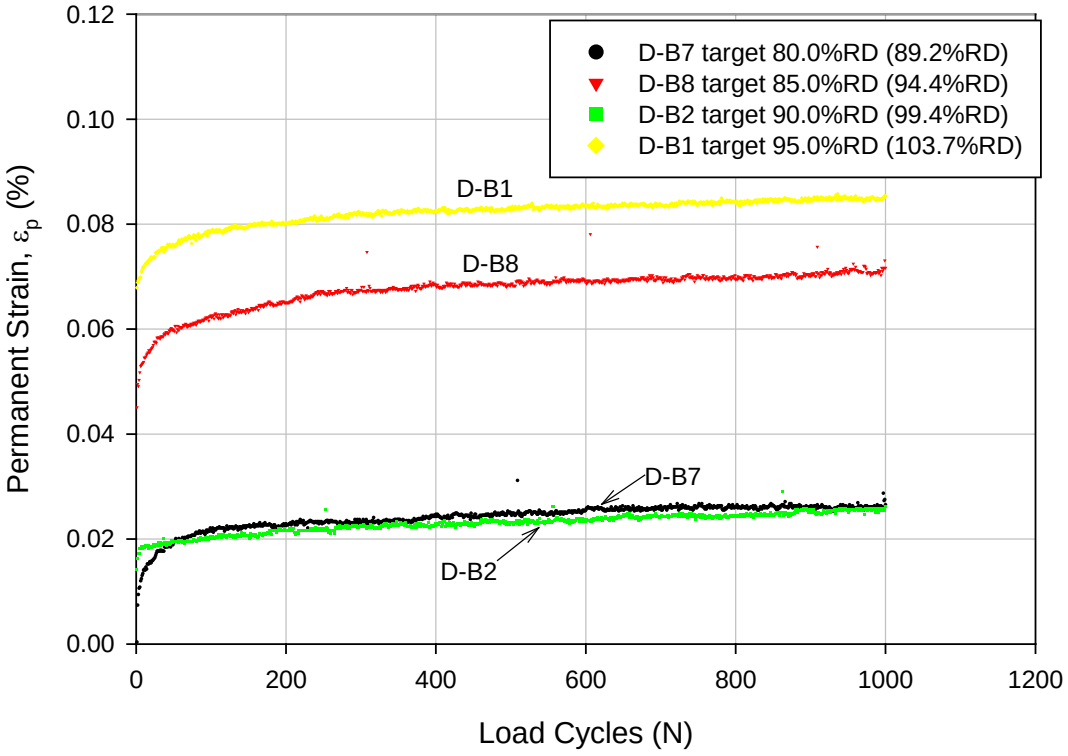

Figure 43. ε_p at 20.7 kPa (3.0 psi) σ_d for RPCC samples (ISU 1k)

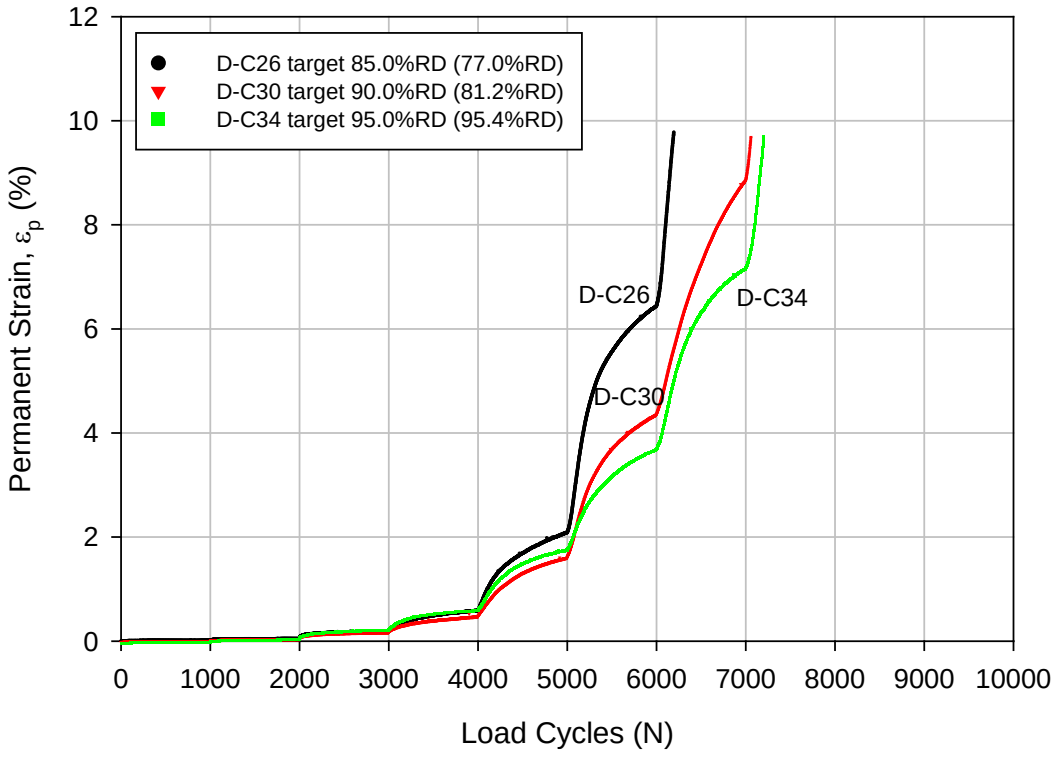

Figure 44. ε_p at 3.5% (natural) F_{200} for RPCC/RAP samples (NCHRP 598)

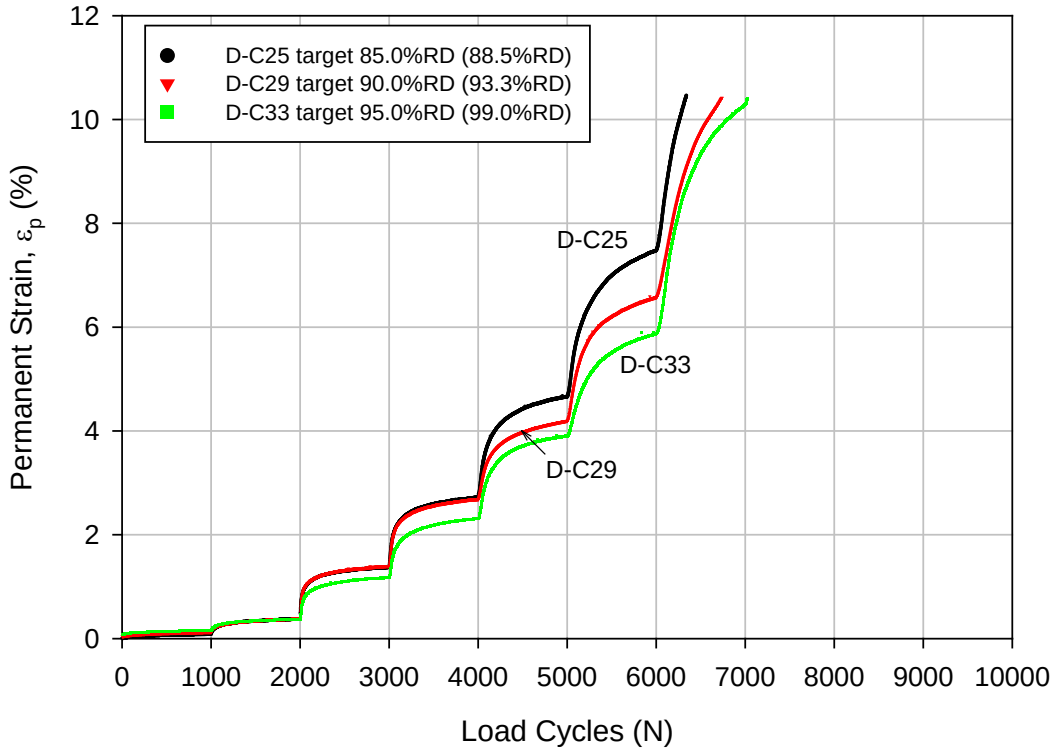

Figure 45. ε_p at 0.8% F_{200} for RPCC/RAP samples (NCHRP 598)

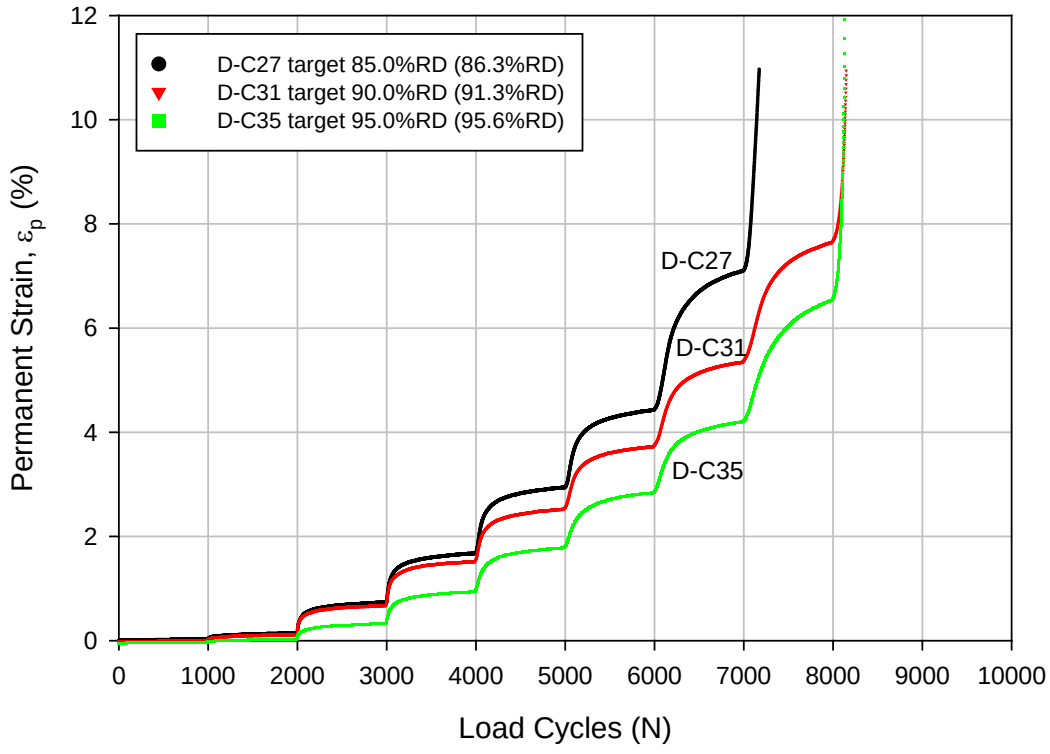

Figure 46. ε_p at 6.0% F_{200} for RPCC/RAP samples (NCHRP 598)

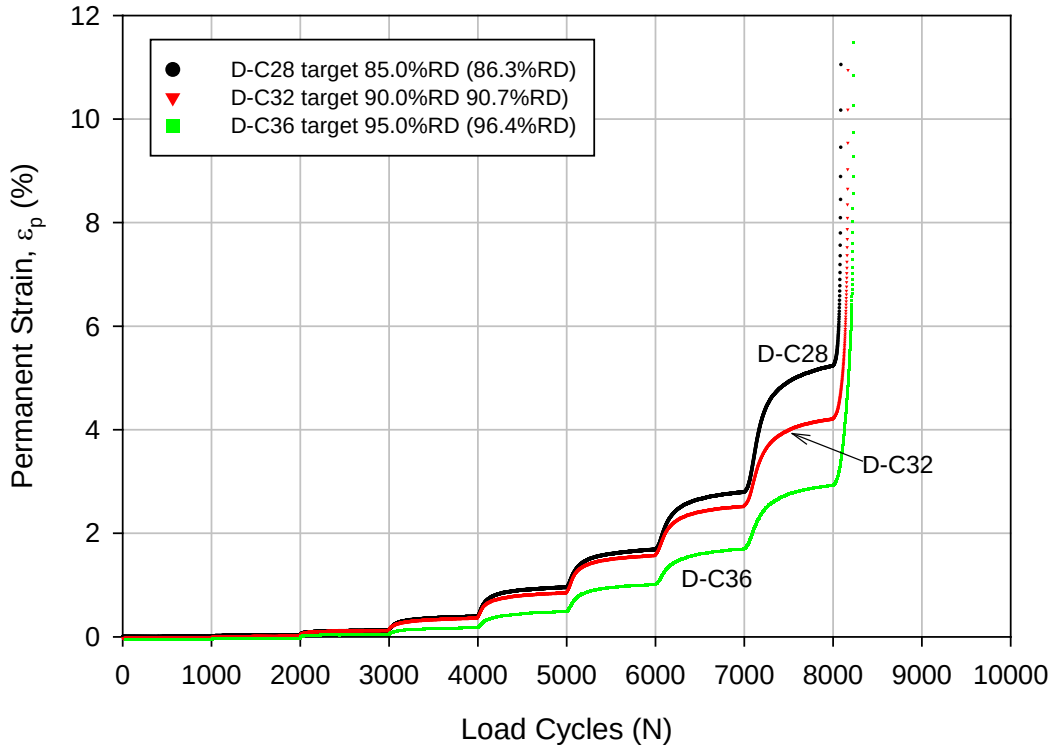

Figure 47. ε_p at 12.4% F_{200} for RPCC/RAP samples (NCHRP 598)

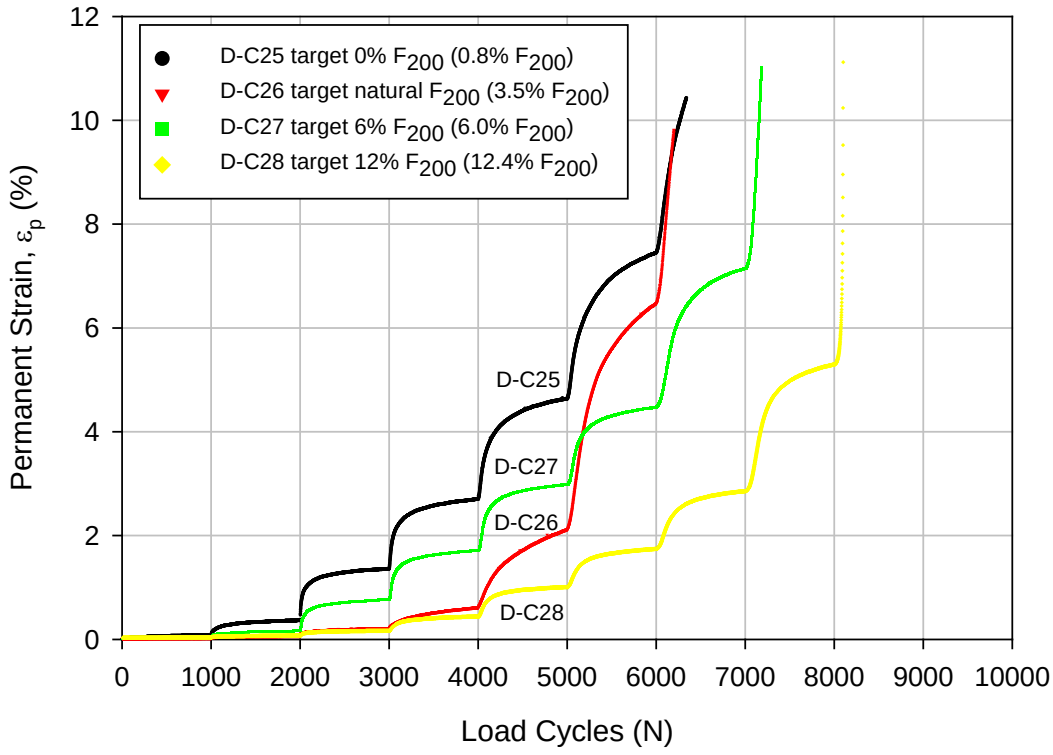

Figure 48. ε_p at 85% target RD for RPCC/RAP samples (NCHRP 598)

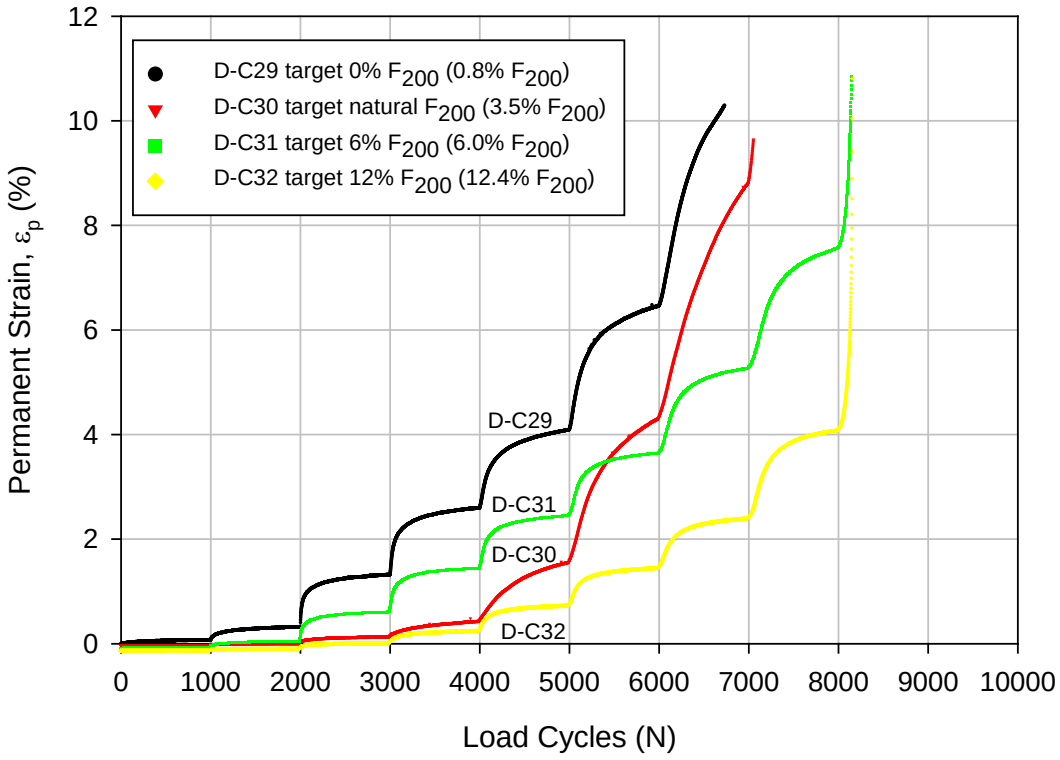

Figure 49. ε_p at 90% target RD for RPCC/RAP samples (NCHRP 598)

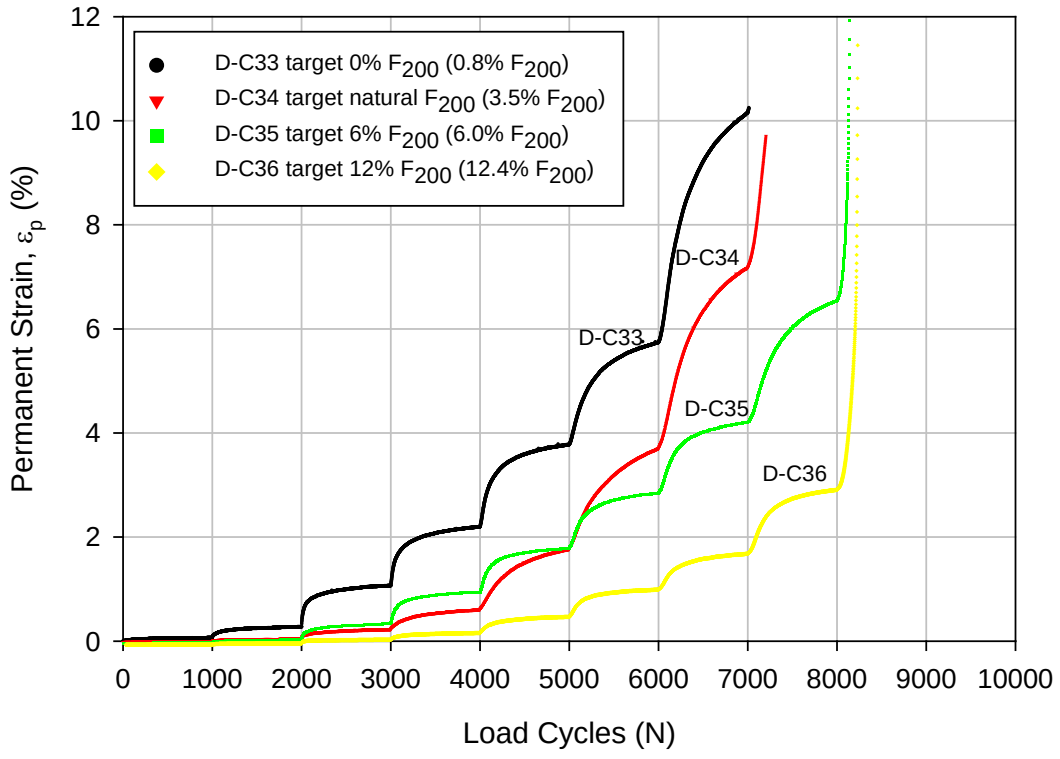

Figure 50. ε_p at 95% target RD for RPCC/RAP samples (NCHRP 598)

Results presented above were analyzed to assess the statistical significance of applied deviator stress, fines content, and relative density on the measured permanent deformation values. Statistical significance was assessed using F-test, and the results are summarized in Table 13. For the materials and the testing conditions in this study, based on the probability values (*p*-values = Probability > F), deviator stress and fines content were found to have statistically significant influence on the permanent deformation behavior. RD was not found to be a statistically significant parameter.

Table 13. Statistical analysis of significance of factors affecting ε_p of RPCC/RAP samples

Factor	Degree of Freedom	Sum of Squares	F Ratio	Probability >F	Significant?
Deviator Stress	5	27.88	26.67	<0.0001	Yes
RD	2	0.91	2.08	0.1343	No
F_{200}	3	6.86	10.53	<0.0001	Yes
RD*F_{200}	6	0.24	0.19	0.9797	No

Note: * means interaction between two factors.

Particle Degradation

Particle degradation due to cyclic loading was assessed by conducting particle-size analysis before and after NCHRP 598 testing on RPCC/RAP samples. The particle-size analysis test results were used to determining breakage index (BI). An example of the particle size analysis test results before and after testing is shown in Figure 51, which showed very minimal particle degradation (BI calculated as 1.4%). Results of BI values calculated for each test are summarized in Table 14. Results indicated that the BI values varied between 0 and 5%, which is not considered significant. Example calculations and particle size analysis test results for all samples are provided in Appendix B.

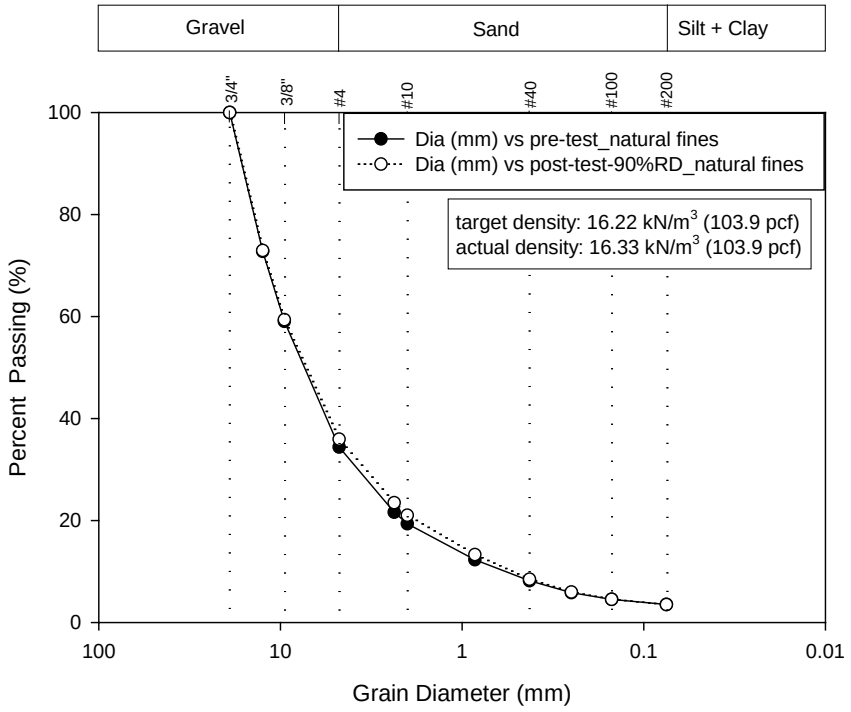

Figure 51. Gradation curves used for calculating BI for a RPCC/RAP sample

Table 14. BI summary for all NCHRP 598 ε_p test RPCC/RAP samples

	Fines content (%)			
Test No.	**Target**	**Pre-test**	**Post-test**	**BI (%)**
D-C25	0.0	0.8	1.4	4.8
D-C26	natural	3.5	3.7	1.4
D-C27	6.0	6.0	6.3	3.1
D-C28	12.0	12.4	12.2	2.3
D-C29	0.0	0.8	1.4	1.1
D-C30	natural	3.5	3.5	1.1
D-C31	6.0	6.0	6.7	2.1
D-C32	12.0	12.4	13.2	4.1
D-C33	0.0	0.8	1.4	0.1
D-C34	natural	3.5	3.5	2.4
D-C35	6.0	6.0	6.1	0.0
D-C36	12.0	12.4	13.3	4.3

Resilient Modulus and Shear Strength Tests Results

M_r Test Results

Mr tests were conducted on a total of 12 RPCC/RAP modified subbase material samples compacted to relative densities ranging from 85 to 95% and at fines contents varying between 0 and 12%. The moisture content of the sample was kept constant (6%). Test sample parameters are summarized in Table 15. The average M_r value of last five cycles in each load sequence was calculated for all load sequences and plotted with load sequence number for all M_r tests in Figure 52.

Table 15. Target and actual characteristics of M_r tests of RPCC/RAP samples

Test	**F_{200} (%)**		**ω (%)**		**RD (%)**		**γ_d (kN/m^3)**	
No.	**Target**	**Actual**	**Target**	**Actual**	**Target**	**Actual**	**Target**	**Actual**
M25	0.0	0.8	6.0	6.0	85.0	86.8	15.26	15.31
M26	natural	3.5		6.2		87.3	16.12	16.17
M27	6.0	6.0		6.5		84.3	16.77	16.73
M28	12.0	12.4		6.2		85.5	17.54	17.56
M29	0.0	0.8		5.9	90.0	92.5	15.41	15.48
M30	natural	3.5		7.7		79.1	16.22	16.01
M31	6.0	6.0		5.9		91.7	16.96	17.03
M32	12.0	12.4		6.0		91.2	17.74	17.79
M33	0.0	0.8		5.8	95.0	99.1	15.56	15.69
M34	natural	3.5		5.7		102.5	16.32	16.47
M35	6.0	6.0		6.2		95.6	17.17	17.19
M36	12.0	12.4		6.2		95.2	17.95	17.96

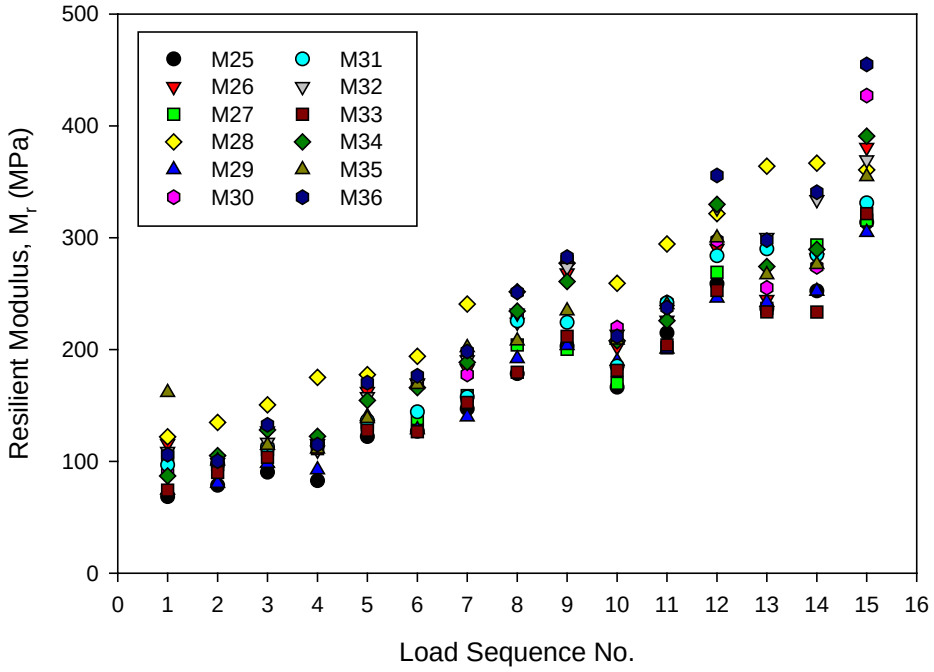

Figure 52. Summary of M_r results for RPCC/RAP samples

The data was analyzed to assess the statistical significance of applied stress level, RD, and fines content on the M_r values. Statistical significance was assessed using F-test and the results are summarized in Table 14. For the materials and the testing conditions in this study, based on the probability values (*p*-values = Probability > F), applied stress level and fines content were found to have statistically significant influence on the M_r values. RD was not found to be a statistically significant parameter.

Table 16. Statistical analysis of significance of factors affecting M_r of RPCC/RAP samples

Factor	Degree of Freedom	Sum of Squares	F Ratio	Probability >F	Significant?
Stress Level	14	1082720.5	248.67	<0.0001	Yes
F_{200}	2	81183.1	87.01	<0.0001	Yes
RD	3	1390.1	2.23	0.1105	No
RD*F_{200}	6	9553.6	5.12	<0.0001	Yes

Note: * indicates interaction between two factors.

The M_r test results are plotted against bulk stress for samples compacted to three different RD's in Figure 53. As indicated in the statistical analysis, no significant difference or trend in the data was observed between RD and M_r values. A similar observation was confirmed on recycled materials by Thom and Brown (1989) and Wolfe (2011).

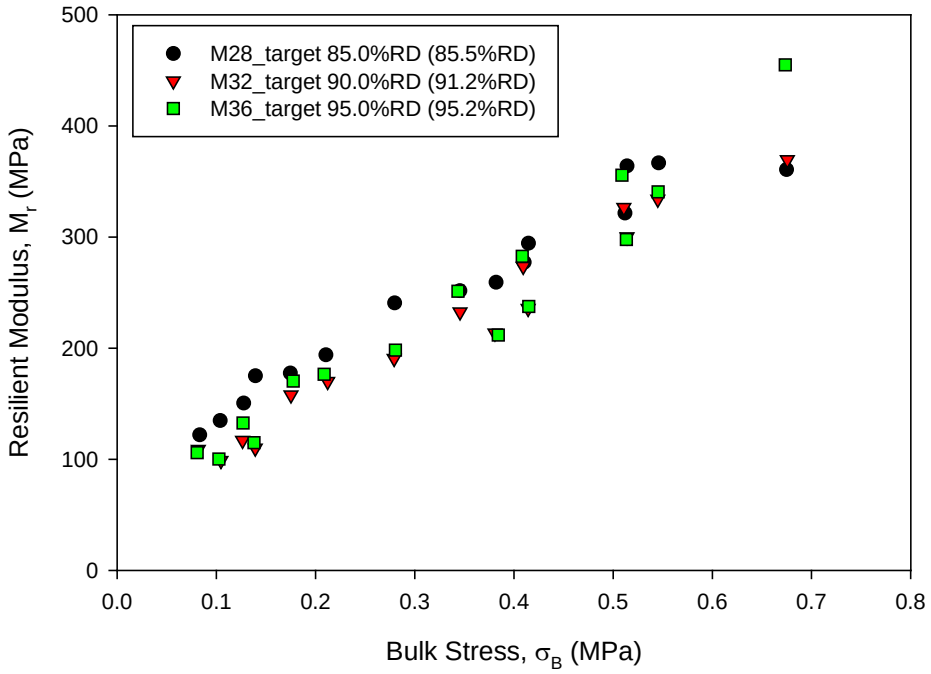

Figure 53. M_r results at 12.4% F_{200} for RPCC/RAP samples

The M_r test results are plotted against bulk stress for samples prepared with different fines content and compacted to 85 to 95% RD in Figure 54 to Figure 56, respectively. Samples with about 12.4% fines content showed the largest M_r values. Except samples with natural fines content (about 5%), M_r values generally increased with increasing fines content at all relative densities. This finding is in conflict with the conclusion reported by Thom and Brown (1987), Kamal et al. (1993), and Kancherla (2004) that the resilient modulus generally decreases with increasing fines content. However, Hicks and Monismith (1971) observed some increase in resilient modulus with increasing fines content for fully crushed aggregates.

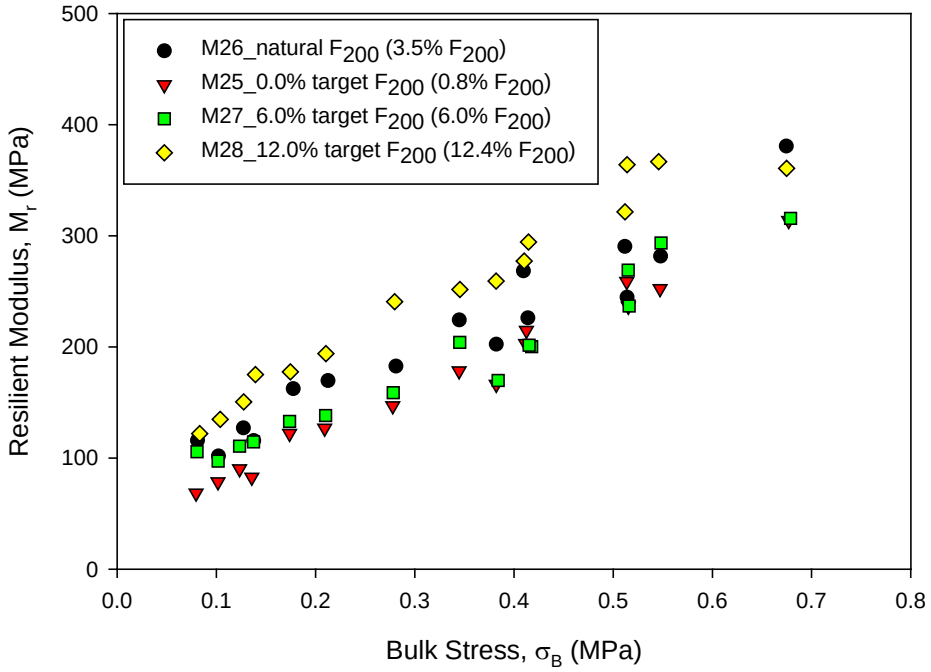

Figure 54. M_r for RPCC/RAP samples at 85% RD

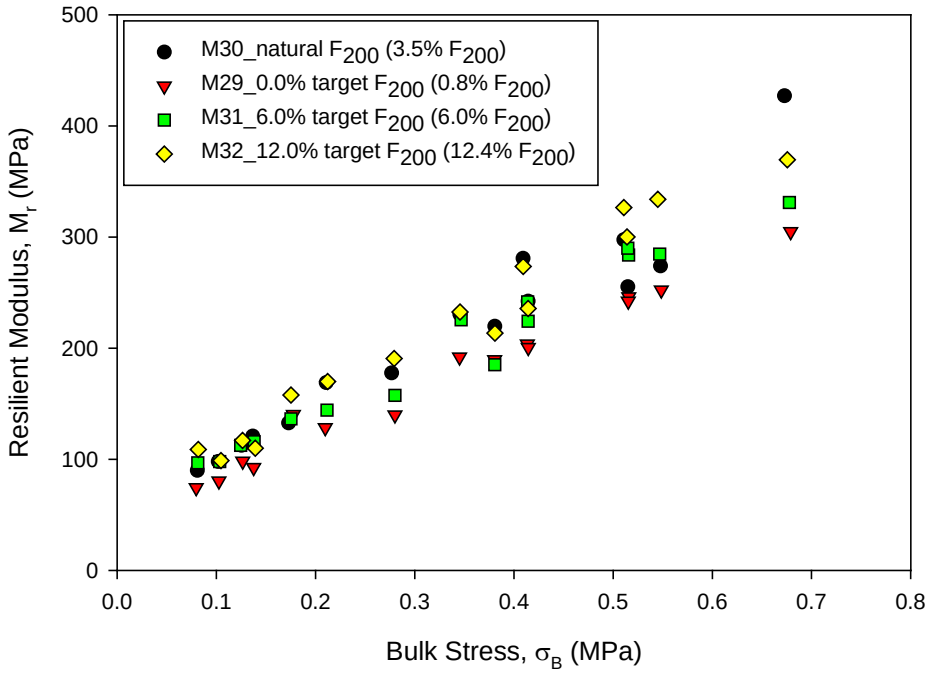

Figure 55. M_r of RPCC/RAP samples at 90% RD

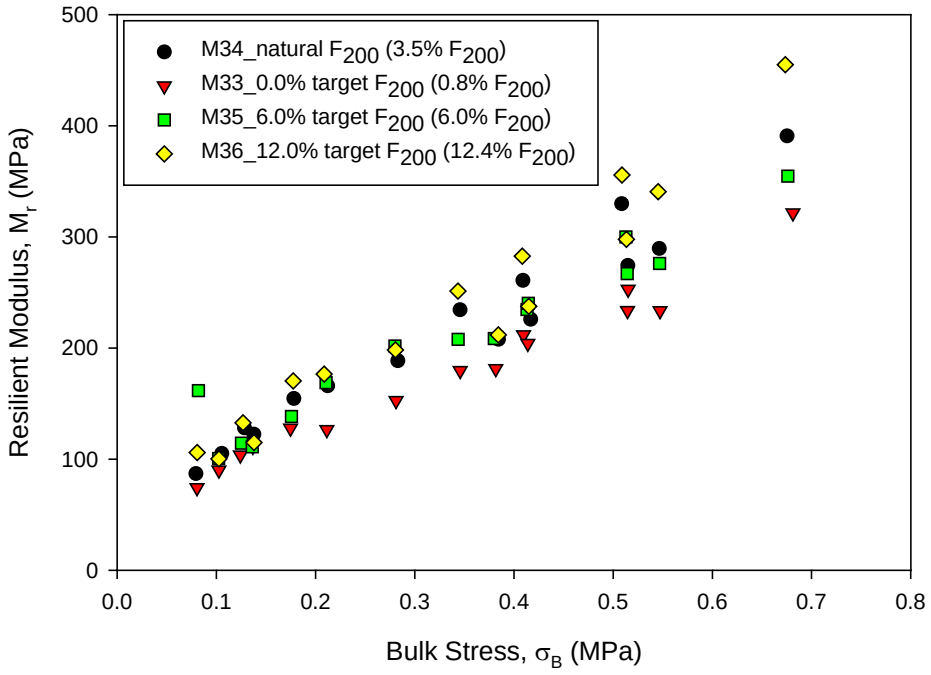

Figure 56. Comparison of M_r at 95% RD for RPCC/RAP samples

The M_r test results were analyzed to fit the stress-dependent constitutive model shown in Equation 1, to determine the k_1, $k2$, and $k3$ regression coefficients. These regression coefficients are summarized for each test sample in Table 17. The probability (*p*-values) associated with each

regression coefficient are also summarized in Table 17, as a way to indicate whether they were statistically significant in the model or not. The k_1 values ranged between 706 and 1354 and was statistically significant for all samples. The k_2 values ranged between 0.4 and 0.7 and was also statistically significant for all samples. The k_3 values ranged between -0.3 to 0.8 and were not always significant.

Table 17. Statistical analysis of parameters in predicting M_r of RPCC/RAP samples

Test No.	k_1 Values	P-value	SIG ?	k_2 Values	P-value	SIG ?	k_3 Values	P-value	SIG ?	R^2
M25	702.68	<0.0001	Y	0.661	<0.0001	Y	0.280	0.0071	Y	0.9857
M26	958.92	<0.0001	Y	0.404	<0.0001	Y	0.716	<0.0001	Y	0.9874
M27	878.21	<0.0001	Y	0.541	<0.0001	Y	0.278	0.1589	N	0.9356
M28	1354.20	<0.0001	Y	0.632	<0.0001	Y	-0.270	0.0116	Y	0.9772
M29	777.77	<0.0001	Y	0.632	<0.0001	Y	0.168	0.1042	N	0.9836
M30	844.73	<0.0001	Y	0.490	0.0003	Y	0.790	<0.0001	Y	0.9862
M31	900.07	<0.0001	Y	0.633	<0.0001	Y	0.116	0.4430	N	0.9639
M32	955.19	<0.0001	Y	0.608	<0.0001	Y	0.281	0.0307	Y	0.9753
M33	787.74	<0.0001	Y	0.545	<0.0001	Y	0.393	<0.0001	Y	0.9865
M34	911.05	<0.0001	Y	0.501	<0.0001	Y	0.615	<0.0001	Y	0.9883
M35	1033.27	<0.0001	Y	0.490	<0.0001	Y	0.315	0.1340	N	0.9200
M36	905.33	<0.0001	Y	0.539	<0.0001	Y	0.708	<0.0001	Y	0.9795

Note: SIG = statistical significance; R^2 = coefficient of determination; Y = yes; and N = no.

Unconsolidated Undrained Shear Strength

A summary of UU shear strength (s_u) test results on RPCC/RAP samples is provided in Table 18. The s_u values ranged between 70 and 140 kPa. Samples that contained 6.0% fines showed the lowest s_u and the samples with natural F_{200} 3.5% have the highest s_u.

Difference in s_u among samples with varied RD is small compared to difference among samples with different fines content. The Tukey HSD test was conducted to further analyze differences in the means of s_u values at different F_{200} levels (Table 19). This statistical analysis results confirmed the preliminary study on the s_u values summarized in Table 16. Samples that contains natural F_{200} (3.5%) have the largest mean s_u and samples with 6.0% F_{200} have the smallest mean s_u. In addition, the mean s_u values of samples contains natural and 6.0% F_{200} are statistically significantly different.

Table 18. Undrained shear strength results for RPCC/RAP samples

Test No.	$\sigma_{d\ max}$ (kPa)	ε_f (%)	s_u (kPa)
M25	153	1.35	76
M26	279	0.65	139
M27	146	0.83	73
M28	217	0.65	108
M29	250	3.94	125
M30	279	1.15	139
M31	170	2.56	85
M33	236	3.24	118
M34	251	3.57	126
M35	180	2.72	90
M36	237	0.46	118

Table 19. Least square fit analysis of the influence of fines content on s_u

Fines content	Letter		Least Square Mean
3.5%	A		134.67
12.4%	A	B	117.22
0.8%	A	B	106.33
6.0%		B	82.67

Note: Levels that are not connected by the same letter are significantly different.

Frost Heave and Thaw Weakening Test Results

Frost heave testing was conducted on four replicate samples for each material: clayey sand subgrade, RPCC/RAP modified subbase, and RPCC subbase. In addition, frost heave testing was also conducted RPCC material after removing about half and all of its fines passing the No. 200 sieve. Original RPCC sample contained about 5% fines. The objective of this additional testing with no fines content was to assess the influence of fines content in the RPCC material on its frost-heave and thaw-weakening susceptibility. Two samples each were tested with half of the fines removed and all the fines removed. The fines were removed by dry sieving the material.

Samples were compacted at their optimum moisture contents using standard Proctor compaction effort. After frost heave testing, the moisture content of the material was obtained by carefully slicing the sample into 6 layers and comparing the moisture contents of the layers with the initial batched moisture content. Thaw weakening susceptibility was evaluated by conducting CBR testing on one standard sample without subjecting it to freeze-thaw cycles and on four samples after subjecting them to freeze thaw cycles. Results are presented below separately for each material type.

Clayey Sand Subgrade

Moisture and dry density of the samples are shown on the standard Proctor curve of the material in Figure 57.

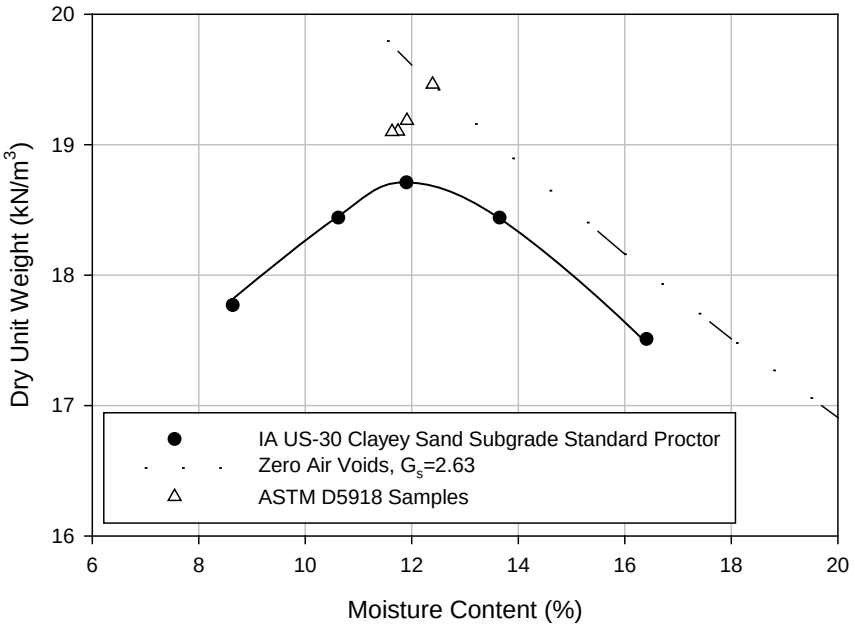

Figure 57. Standard Proctor test results and ASTM D5918 samples for clayey sand subgrade

The frost-heave versus time plots for the clayey sand subgrade are presented in Figure 58. All four subgrade samples heaved more during the second freeze compared to the first freeze, which also increased the slope of the heave versus time line. The temperature profiles for samples 1, 2, and 3 are similar; however sample 4 reached lower temperatures. The height of the samples slightly increased after the first freeze-thaw cycle, but increased more after the second freeze-thaw cycle.

The moisture content profiles are presented in Figure 59. Results showed that the moisture contents after testing were about 0 to 2% higher in the material after the freeze-thaw cycles, compared to its initial moisture content.

A summary of the frost-heave and thaw-weakening test results with CBR testing before and after freeze-thaw cycles is provided in Table 20. Based on the test results, the clayey subgrade material is rated as medium for frost-heave susceptibility and as high for thaw-weakening susceptibility.

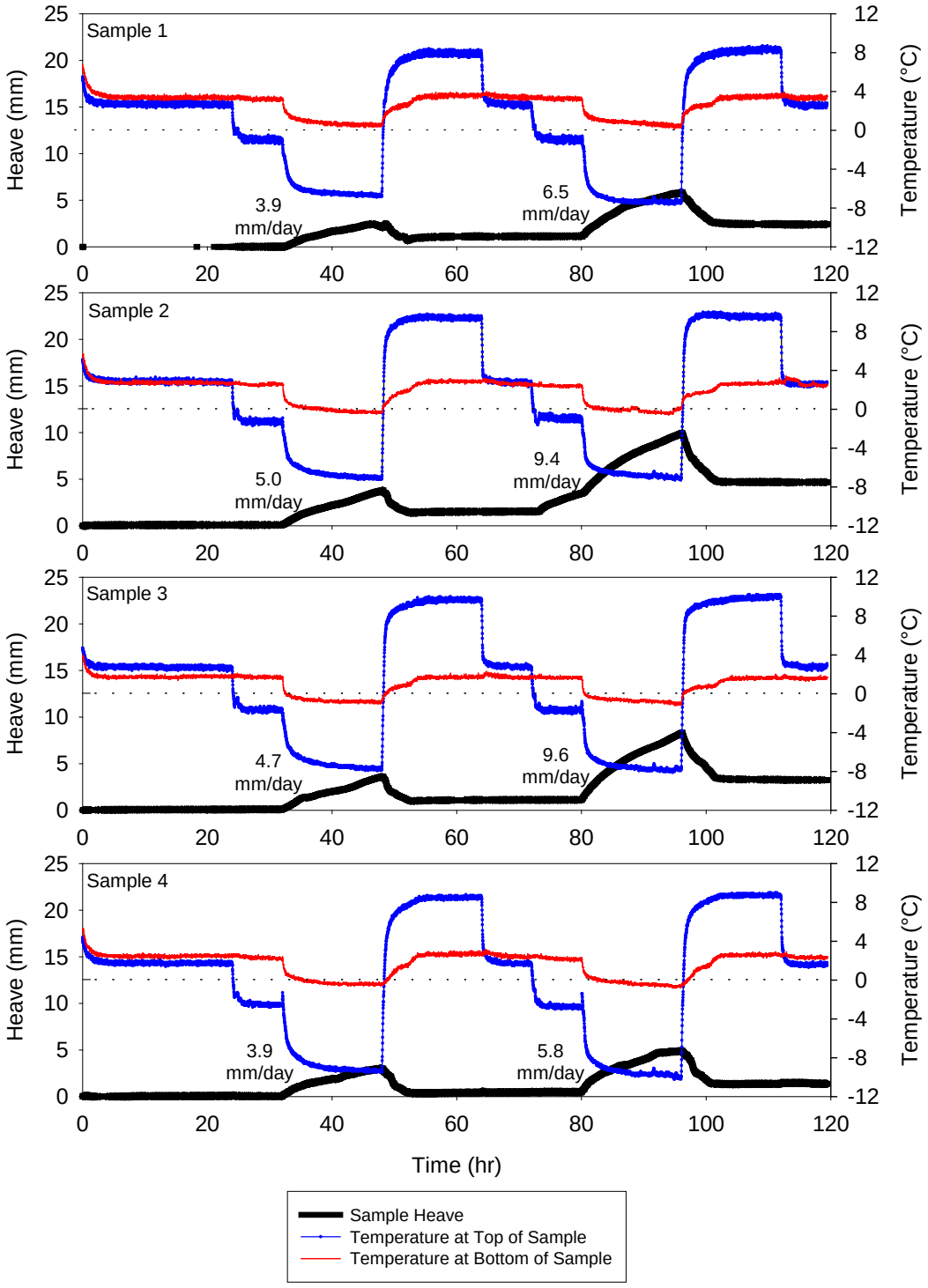

Figure 58. Frost heave and temperature versus time plots for clayey sand subgrade samples

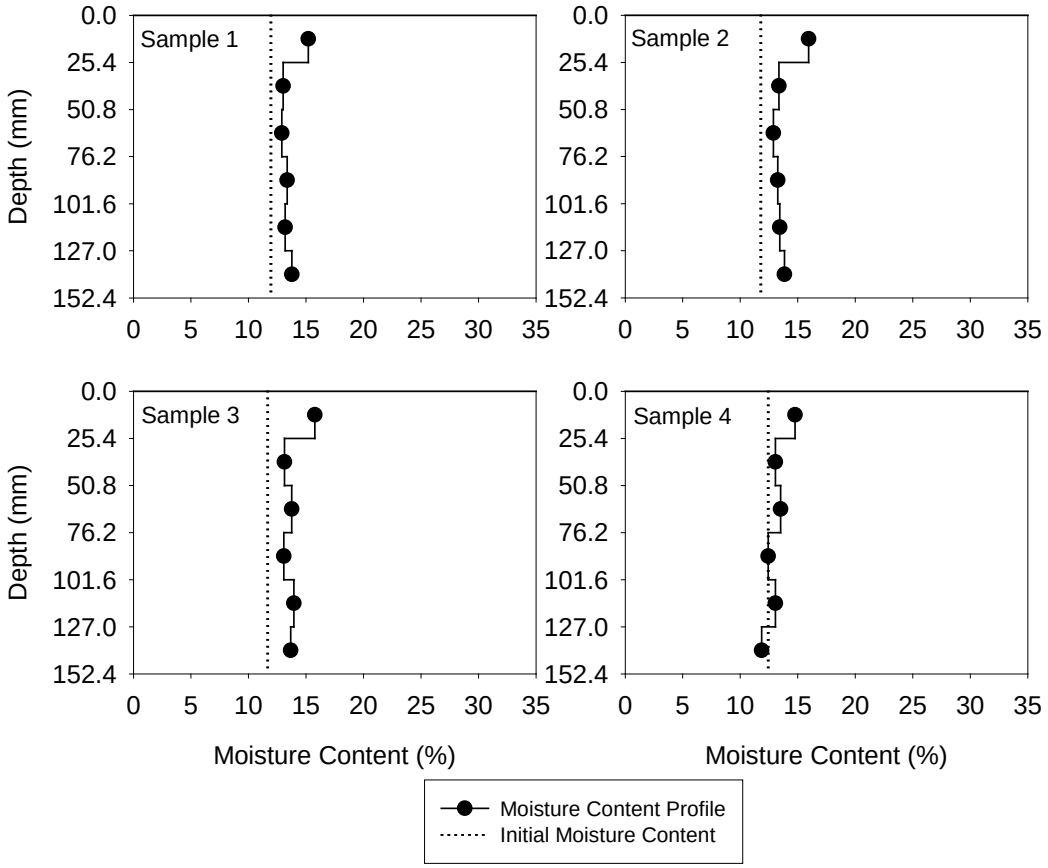

Figure 59. Moisture content profiles of clayey sand subgrade samples after F/T testing

Table 20. Frost-heave and thaw-weakening test results on clayey sand subgrade

Parameter	**μ**	**σ**	**COV (%)**	**no. of samples**
CBR (%) (standard test)		8.4		1
CBR (%) (after frost-susceptibility test)	2.7	0.4	14.7	4
1st Frost-heave rate (mm/day)	4.4	0.5	11.5	
2nd Frost-heave rate (mm/day)	7.8	2.0	25.2	
1st Frost-heave susceptibility rating		Medium		
2nd Frost-heave susceptibility rating		Medium		
Thaw-weakening susceptibility rating		High		

RPCC/RAP Modified Subbase

Moisture and dry density of the RPCC/RAP modified subbase samples are shown on the standard Proctor curve of the material in Figure 60.

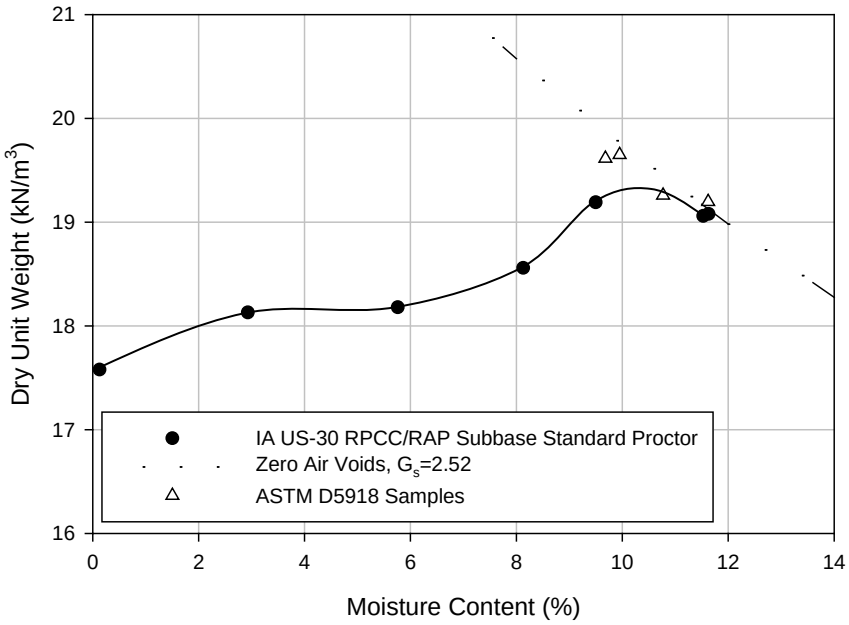

Figure 60. Standard Proctor test results and ASTM D5918 samples for RPCC/RAP modified subbase samples

The frost-heave versus time plots for the RPCC/RAP modified subbase samples are presented in Figure 61. The frost heave time plots for all four samples are very similar. The slope of the heave versus time lines decreased during the second freeze even though the total heave is nearly the same for the first and second freeze. The height of the samples slightly increased after the first and second freeze-thaw cycles.

The moisture content profiles are presented in Figure 62. Results showed that the moisture contents after testing were about the same as before testing for samples 1, 2, and 3, while sample 4 showed slightly lower moisture content after testing.

A summary of the frost-heave and thaw-weakening test results with CBR testing before and after freeze-thaw cycles is provided in Table 21. Based on the test results, the material is rated as medium for frost-heave susceptibility and negligible for thaw-weakening susceptibility.

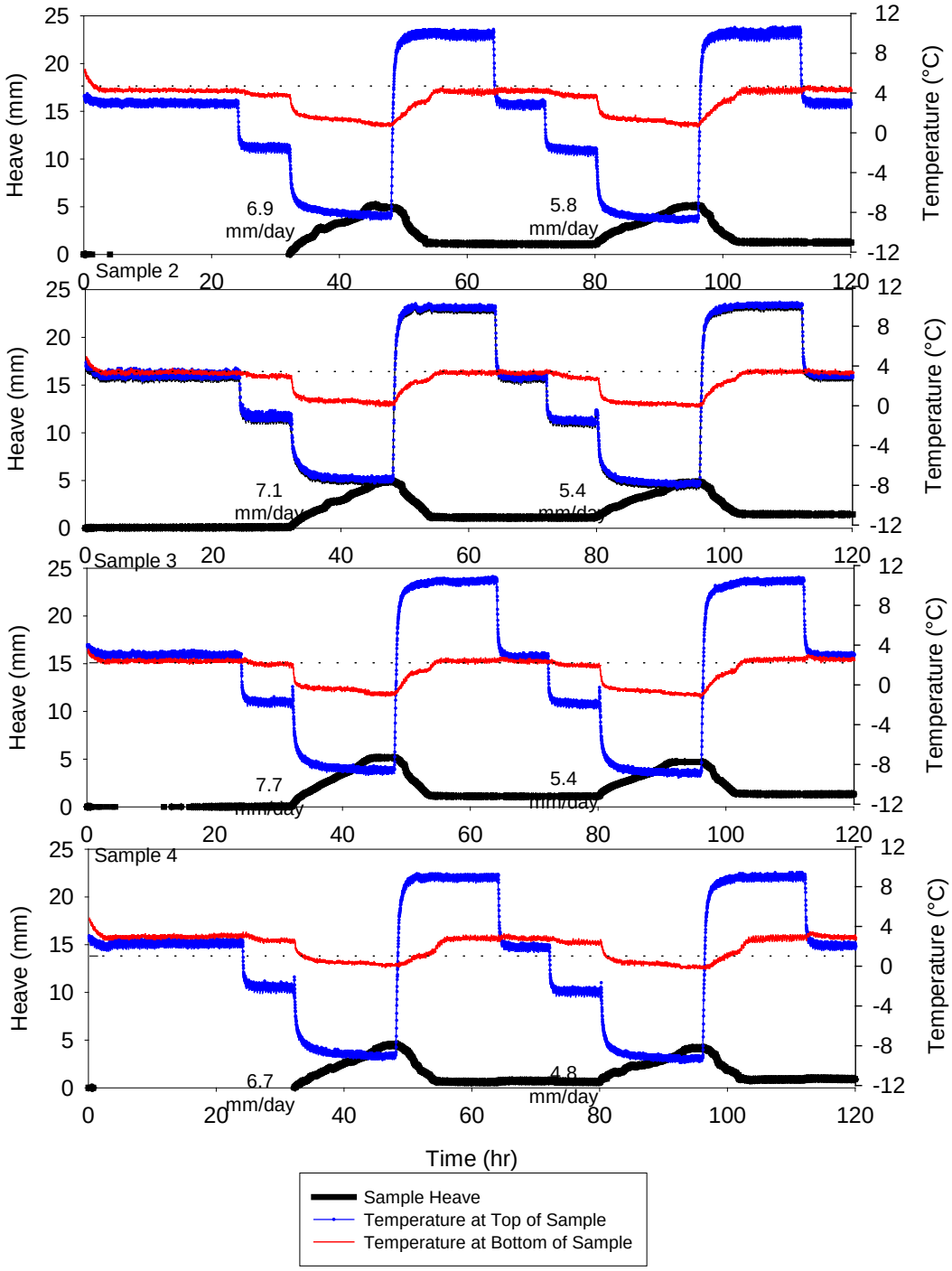

Figure 61. Frost heave and temperature versus time plots for RPCC/RAP modified subbase material

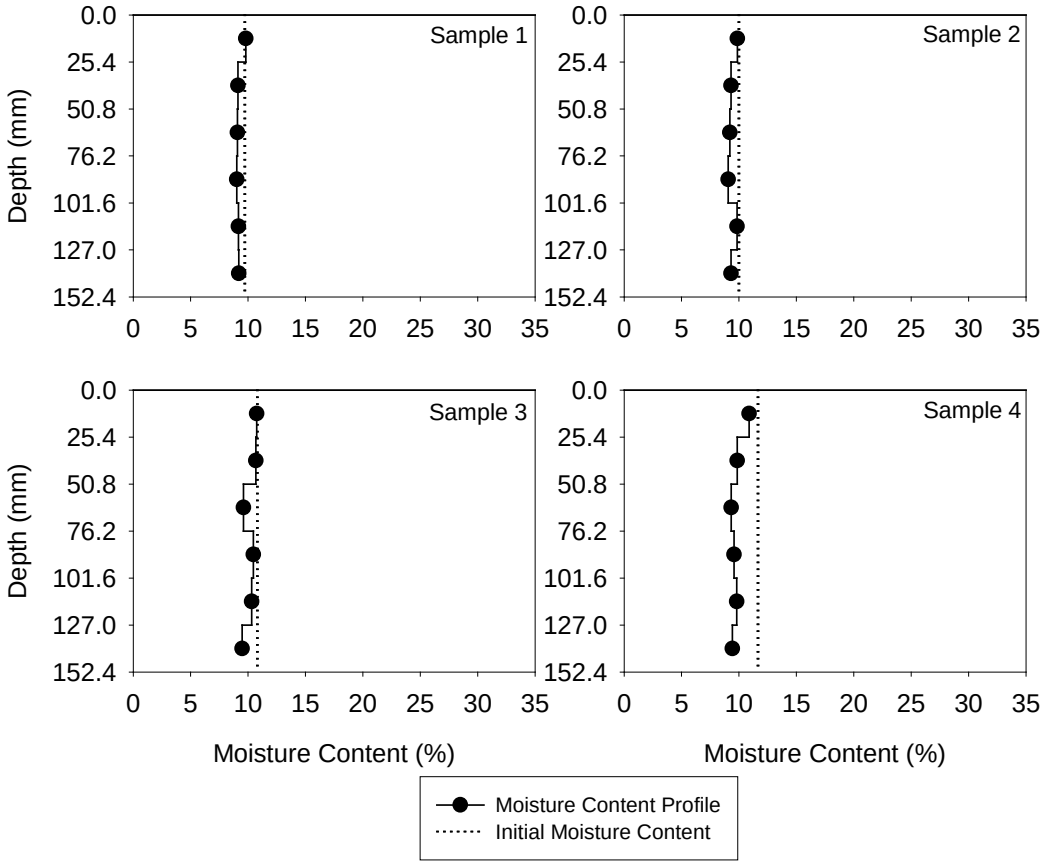

Figure 62. Moisture content profiles for RPCC/RAP modified subbase material

Table 21. Frost-heave and thaw-weakening test results for RPCC/RAP modified subbase material

Parameter	μ	σ	COV (%)	# of samples
CBR (%) (standard test)		40.6		1
CBR (%) (after frost-susceptibility test)	37.6	10.3	27.5	
1st Frost-heave rate (mm/day)	7.1	0.4	5.3	
2nd Frost-heave rate (mm/day)	5.4	0.4	7.5	4
1st Frost-heave susceptibility rating		Medium		
2nd Frost-heave susceptibility rating		Medium		
Thaw-weakening susceptibility rating		Negligible		

RPCC Modified Subbase

Moisture and dry density of the RPCC modified subbase samples are shown on the standard Proctor curve of the material in Figure 63.

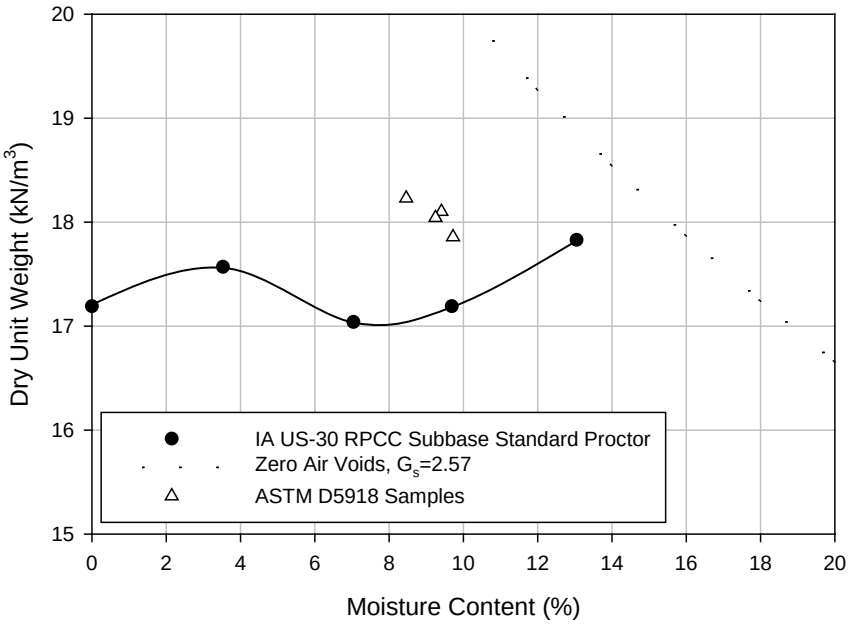

Figure 63. Standard Proctor test results and ASTM D5918 samples for RPCC modified subbase sample

The frost-heave versus time plots for the RPCC modified subbase samples are presented in Figure 66. The frost heave time plots for all four samples are very similar. The slope of the heave versus time line and the total heave decreases during the second freeze compared to the first freeze. The height of the samples increased after the first freeze, but remained nearly the same after the second freeze.

The moisture content profiles are presented in Figure 67. Results showed that the moisture contents after testing increased by 2 to 6% in all the samples compared to its initial moisture content.

A summary of the frost-heave and thaw-weakening test results with CBR testing before and after freeze-thaw cycles is provided in Table 22. Based on the test results, the material is rated as medium for frost-heave susceptibility and as negligible for thaw-weakening susceptibility.

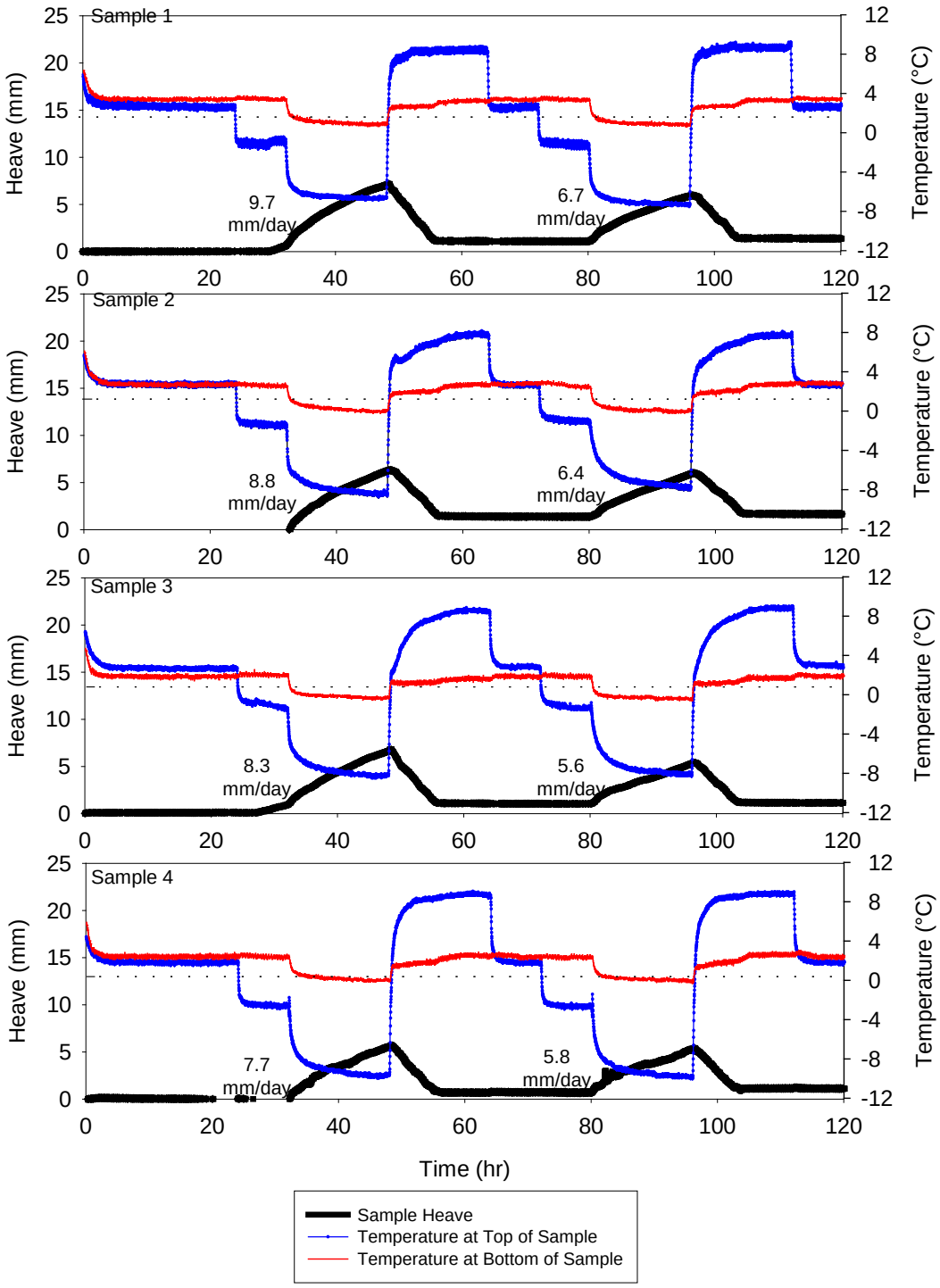

Figure 64. Frost heave and temperature versus time plots for RPCC modified subbase material

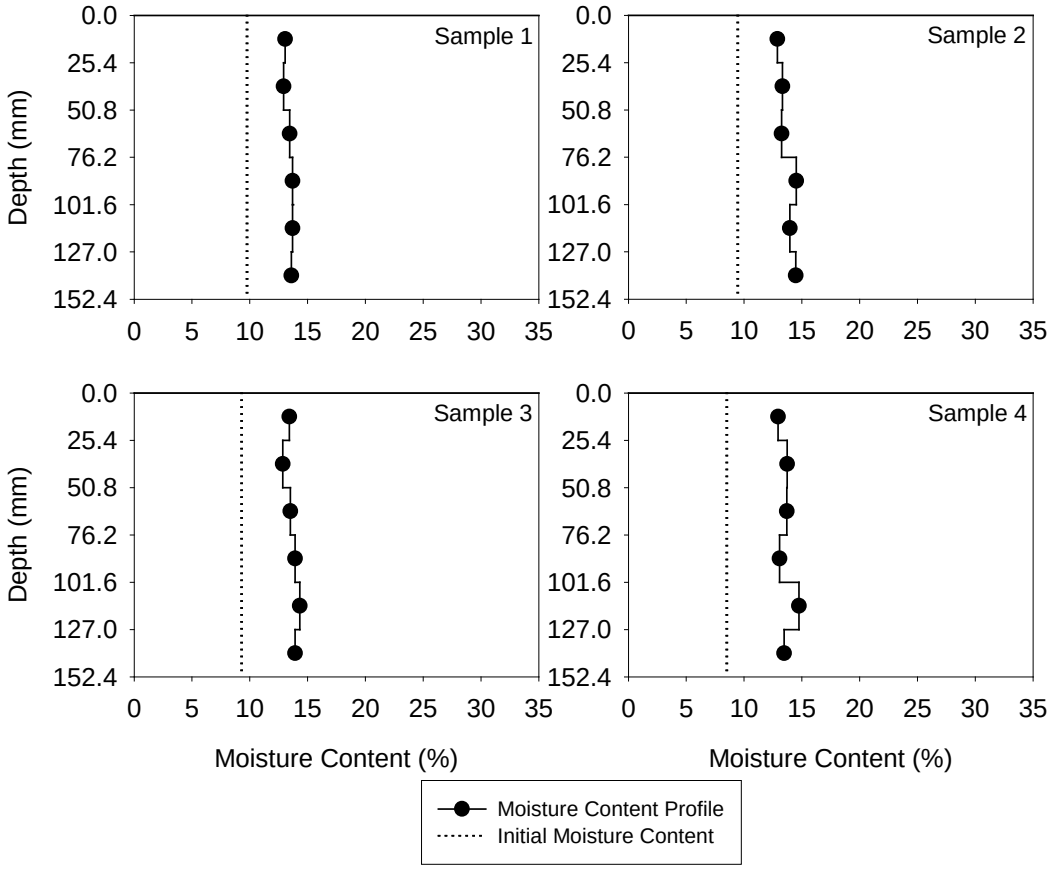

Figure 65. Moisture content profiles for RPCC modified subbase material

Table 22. Frost-heave and thaw-weakening test results for RPCC modified subbase material

Parameter	μ	σ	COV (%)	# of samples
CBR (%) (standard test)		70.3		1
CBR (%) (after frost-susceptibility test)	33.3	4.3	12.8	
1st Frost-heave rate (mm/day)	8.6	0.7	8.4	
2nd Frost-heave rate (mm/day)	6.1	0.5	8.0	4
1st Frost-heave susceptibility rating		High		
2nd Frost-heave susceptibility rating		Medium		
Thaw-weakening susceptibility rating		Negligible		

RPCC Modified Subbase after Removing Fines

The frost-heave versus time plots for the RPCC modified subbase samples with about half of the fines removed are shown in Figure 66. The first and second heaves versus time plots are very similar. The samples returned to their original height after the first and second freeze-thaw

cycles. The moisture content profiles are presented in Figure 67. Results showed that the moisture contents after testing increased by 2 to 3% in both samples.

The frost-heave versus time plots for the RPCC modified subbase samples with all of the fines removed are shown in Figure 68. The frost heave versus time plots for the two samples are very similar and behaved the same as the samples with its original fines content and half of the fines content. The moisture content profiles are presented in Figure 69. Results showed that the moisture contents after testing increased by 2 to 3% in both samples.

A summary of the frost-heave and thaw-weakening test results with CBR testing after freeze-thaw cycles is provided in Table 23 for samples with half fines removed and Table 24 with all fines removed, respectively. Based on the test results, the material is rated as medium for frost-heave susceptibility and as negligible for thaw-weakening susceptibility.

Based on the results from the modified gradations of RPCC with half and all of the fines removed, the frost-heave rate for the first and second freeze cycles was not affected by the fines content. The post freeze-thaw CBR values were also not affected by the fines content. The frost-heave and thaw-weakening susceptibility ratings are the same for all three gradations.

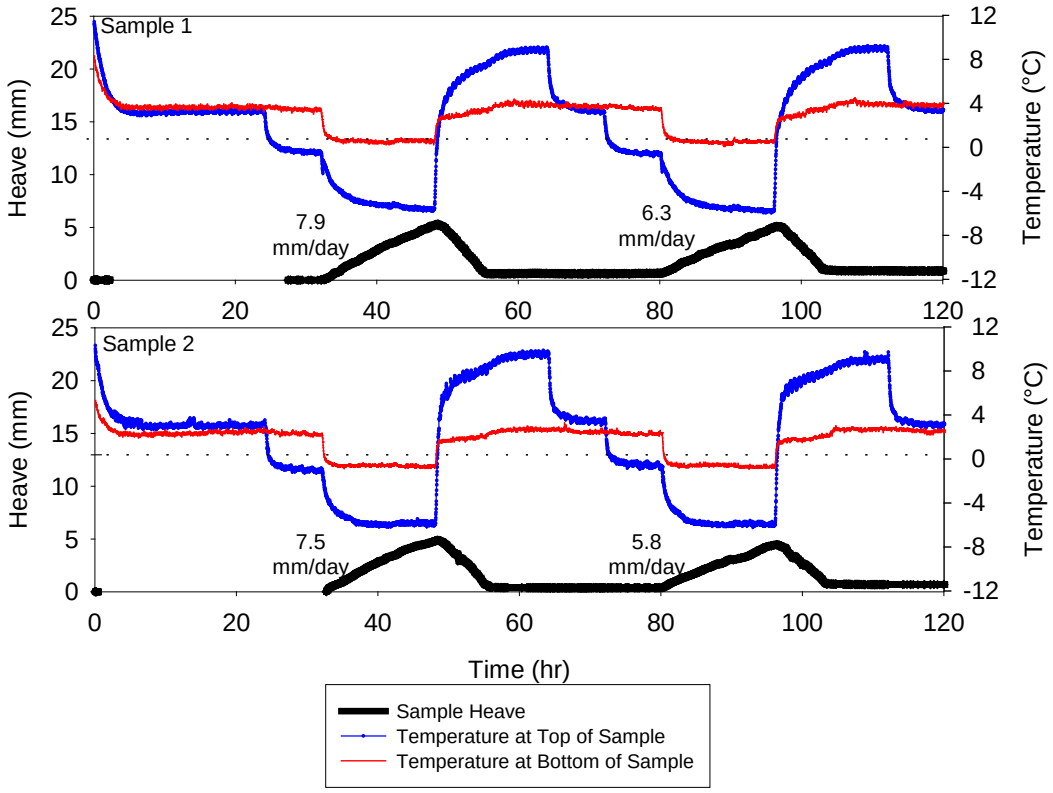

Figure 66. Frost heave and temperature versus time plots for RPCC modified subbase material with about half of the fines removed

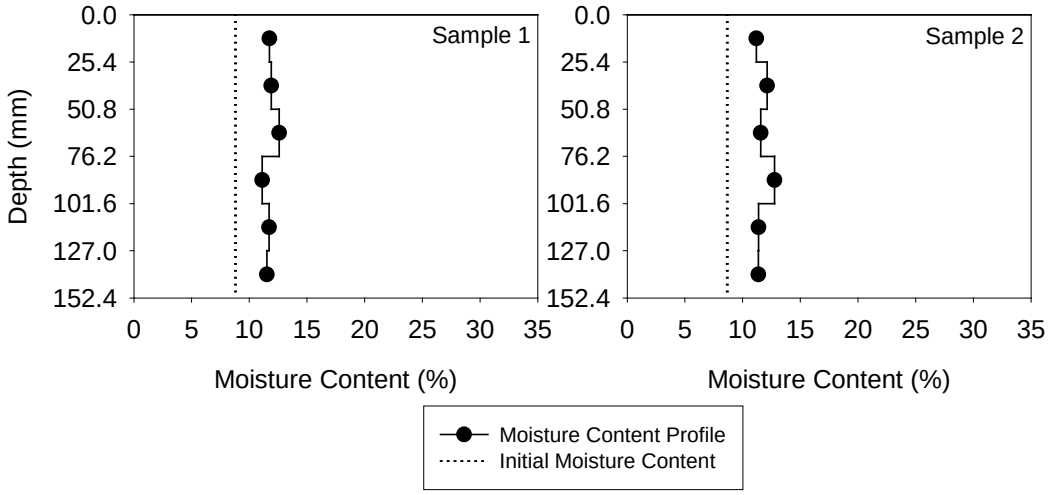

Figure 67. Moisture content profiles for RPCC modified subbase material with about half of the fines removed

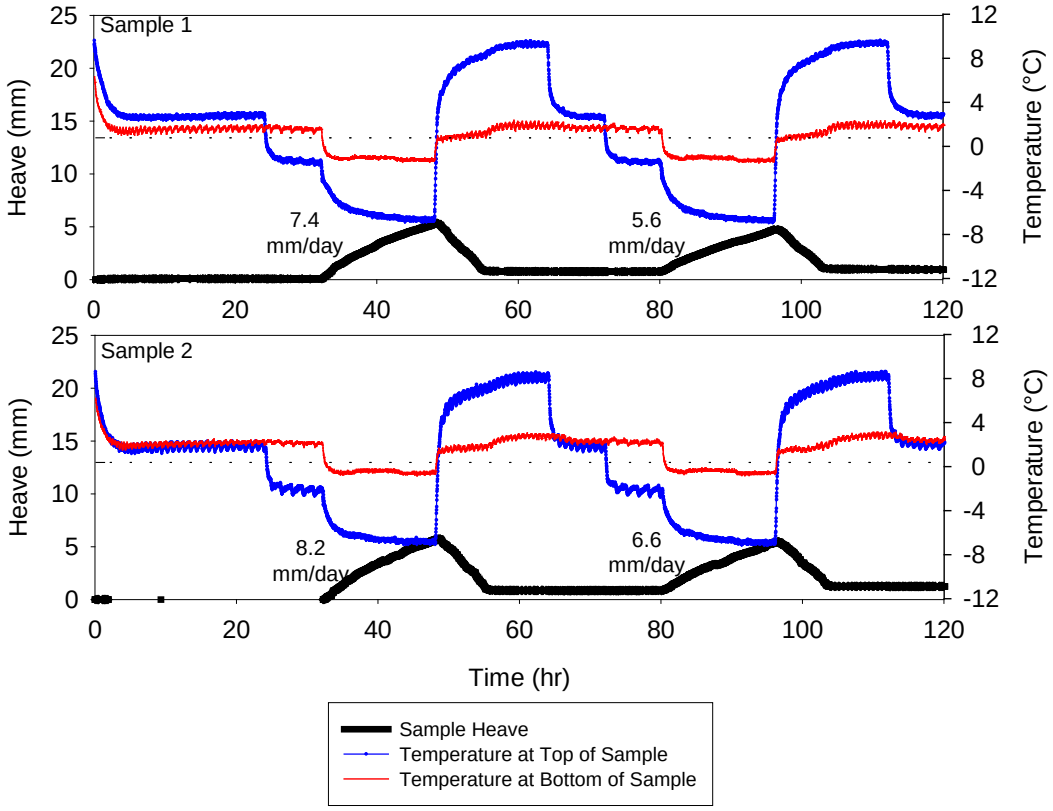

Figure 68. Frost heave and temperature versus time plots for RPCC modified subbase material with no fines

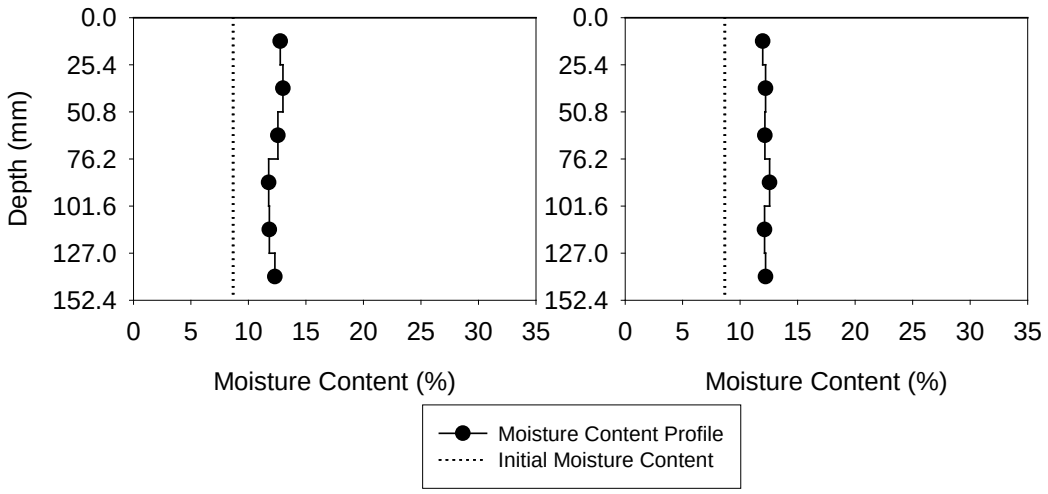

Figure 69. Moisture content profiles for RPCC modified subbase material with no fines

Table 23. Frost-heave and thaw-weakening test results for RPCC modified subbase material with about half of the fines removed

Parameter	μ	σ	COV (%)	# of samples
CBR (%) (standard test)		—		0
CBR (%) (after frost-susceptibility test)	39.2	8.3	21.1	2
1st Frost-heave rate (mm/day)	7.7	0.2	2.7	
2nd Frost-heave rate (mm/day)	6.1	0.3	5.7	
1st Frost-heave susceptibility rating		Medium		
2nd Frost-heave susceptibility rating		Medium		
Thaw-weakening susceptibility rating		Negligible		

Note: — = no test conducted

Table 24. Frost-heave and thaw-weakening test results for RPCC modified subbase material with no fines

Parameter	μ	σ	COV (%)	# of samples
CBR (%) (standard test)		—		0
CBR (%) (after frost-susceptibility test)	35.5	4.0	11.3	2
1st Frost-heave rate (mm/day)	7.8	0.4	5.4	
2nd Frost-heave rate (mm/day)	6.1	0.7	10.8	
1st Frost-heave susceptibility rating		Medium		
2nd Frost-heave susceptibility rating		Medium		
Thaw-weakening susceptibility rating		Negligible		

Note: — = no test conducted

CHAPTER 5. FIELD TESTING RESULTS

This chapter presents overview of the project in terms of its condition before reconstruction and design details of the new construction, field investigations performed before the reconstruction on the old pavement, and results from field testing conducted after pavement foundation layer and pavement layer construction. The FWD and DCP test results obtained on the new pavement and foundation layers were compared with the assumed design input parameters.

Project Overview and Field Investigations

This project is located on US 30 in Boone County in Iowa and involved removal of the existing old pavement, which showed severe pavement distresses, between mileposts 139.0 and 147.27. According to the historical as-built records provided by Iowa DOT (2009), the existing pavement consisted of nominal 76 mm (3 in.) thick asphalt concrete (AC) overlay on nominal 229 mm (9 in.) thick portland cement concrete (PCC). The pavement layers were underlain by nominal 102 mm (4 in.) thick asphalt treated base (ATB). The PCC layer was placed in 1973 over the ATB layer and the section was resurfaced with the AC overlay in 1992.

A field investigation was conducted by the ISU research team on the existing pavement in February and March 2010 (in winter/frozen condition) prior to the reconstruction work. The existing pavement showed severe surface distresses with reflective cracking and vertical upheave near joints, especially during winter (Figure 70). The Iowa DOT also reported incidents of damage to vehicle tires and problems with snowplow blade contact. Initial field investigations by the Iowa DOT rated the ride quality of the pavement section as “poor” based on pavement condition index (PCI) ranging between 54 and 56 on a 0-100 scale (100 being good and 0 being failed condition). ISU field investigations involved obtaining core samples of the existing pavement near joints using 254 mm (10 in.) and 100 mm (4 in.) diameter diamond rotary bits. This investigation was performed between milepost 140.79 and 140.80 on US 30 EB and between mileposts 143.53 and 143.61 on US 30 WB. The core samples were visually inspected, and then were sealed and sent to the laboratory for additional testing. Visual inspections were conducted to evaluate the joint deterioration and vertical heave profiles were measured longitudinally across the joints.

As part of the reconstruction work that began in summer of 2011, the existing pavement and the ATB layers were removed and the subgrade was undercut during the reconstruction process to place a nominal 410 mm (16 in.) thick modified subbase over the natural existing subgrade. The modified subbase layer consisted of 150 mm (6 in.) thick RPCC material at the surface underlain by 260 mm (10 in.) thick mixture of RPCC/RAP material. A nominal 254 mm (10 in.) thick JPCP was placed on the newly constructed foundation layer. Thickness design of the new pavement was conducted by the Iowa DOT according to the PCA (1984) method, by assuming a modulus of subgrade reaction (k) value of 41 kPa/mm (150 pci) for the foundation layer. The new pavement and foundation layer cross-section is shown in Figure 71.

The ISU research team was present on the project site after the foundation layer construction was completed in June and August 2011. During June 2011 field testing, the pavement foundation

layers were instrumented with thermocouple temperature sensors to monitor seasonal temperature variations in the foundation layer with depth as well as temperature variations across the pavement width. The vertical temperature variations were monitored to assess frost depth and freezing/thawing periods, and the temperature variations across the pavement width were monitor to assess the influence of snow cover on the shoulder on the mainline pavements. During August 2011 field testing, LWD and DCP tests were conducted on the foundation layers. In June 2012, about a year after the pavement construction was completed, falling weight deflectometer (FWD) tests were conducted on the pavement near mid-panel and joints at locations where foundation layer testing had been conducted.

Figure 70. The existing pavement on US 30 EB showing severe surface distresses

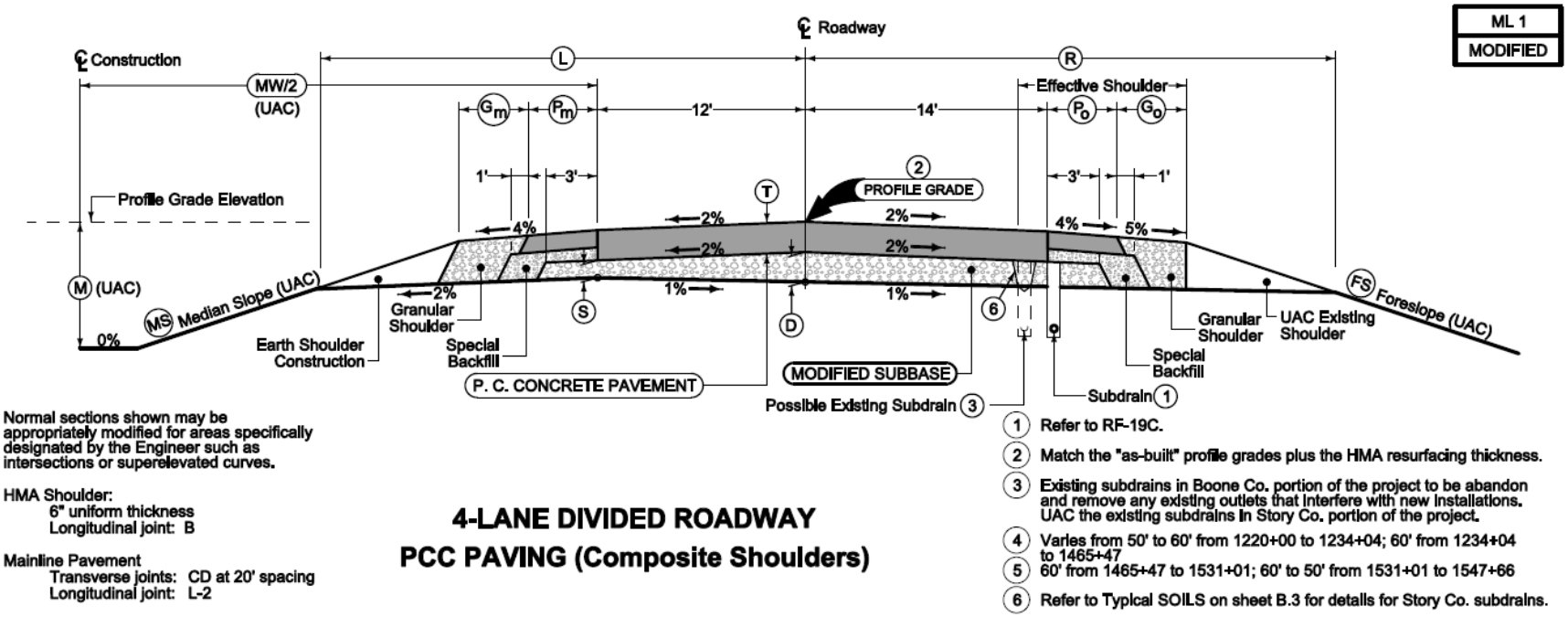

Figure 71. Cross-section of the new construction on US 30 (provided by Iowa DOT)

Field Testing on Old Pavement

Field testing on the old pavement involved obtaining core samples and vertical heave measurements near joints. Testing was conducted on February 26, 2010 and March 4, 2010. Core samples were extracted using diamond rotary bits of 254 mm (10 in.) and 102 mm (4 in.) diameters. Water lubrication was not used during coring in order to preserve in situ moisture content of the cored samples. Air was used as a drilling medium where needed. Cores were inspected in situ and sent to the laboratory for moisture content testing. Results from core extraction, inspection, and laboratory testing, and vertical heave measurements are presented separately in the following sections.

Core Sample Extraction and Testing

Two joints in the westbound lane at mile posts 143.53 and 143.61 were cored on February 26, 2010 (Figure 72). In addition, coring was also performed at the middle of the slab panel between mile posts 143.53 and 143.52.

Figure 72. US 30 at mile 143.55 looking west (a) and east (b) (02/26/2010)

A 102 mm (4 in.) diameter core was drilled at the joint at mile post 143.53 (Figure 73). The top AC layer was first extracted and then the coring was extended into the underlying PCC layer. Some ice lenses were noticed at the AC/PCC interface (Figure 74). The PCC layer sample could not be obtained due to weak and deteriorated structure of the concrete. Standing water was observed in the cored 102 mm (4 in.) diameter cavity.

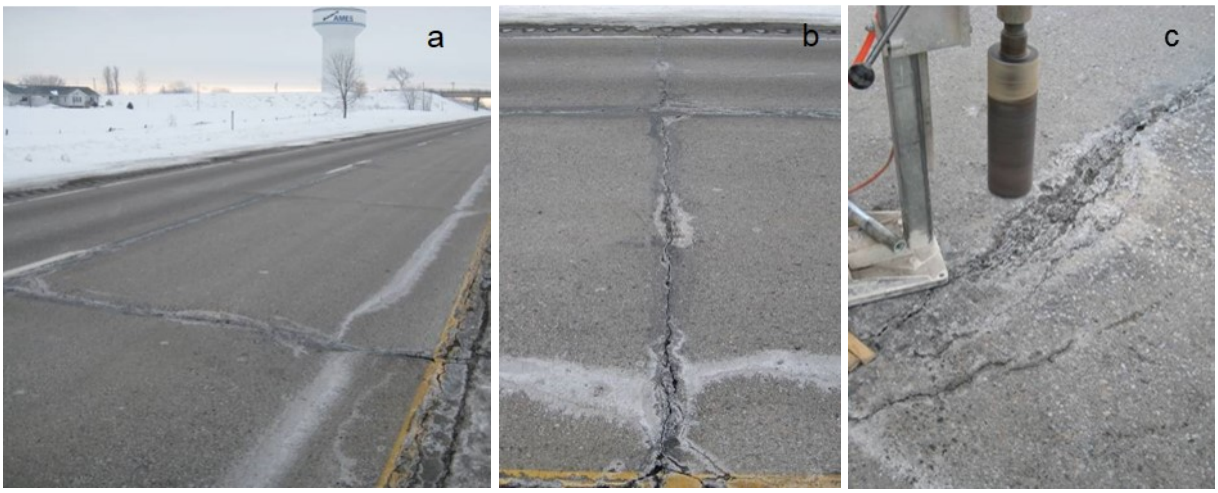

Figure 73. Three views of the joint at mile 143.53: isometric view (a); side view north direction (b); and coring a 4 in. diameter sample at the joint (c) (02/26/2010)

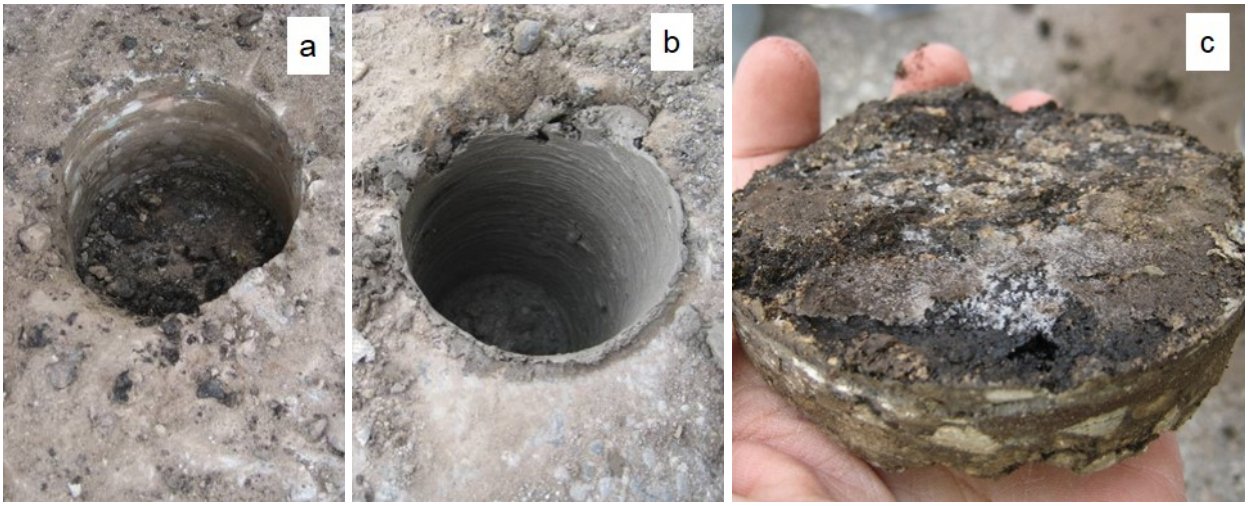

Figure 74. Four-inch diameter coring at joint at mile 143.53: cavity at top of PCC layer (a); cavity drilled 4 in. deep (b); extracted 4 in. diameter PCC sample with ice lenses at the PCC/AC interface (c) (02/26/2010)

A 254 mm (10 in.) diameter core was drilled at joint at milepost 143.61 (Figure 75). The AC layer was first extracted and then drilled into the PCC layer. An intact sample of the AC layer could not be obtained (Figure 75).

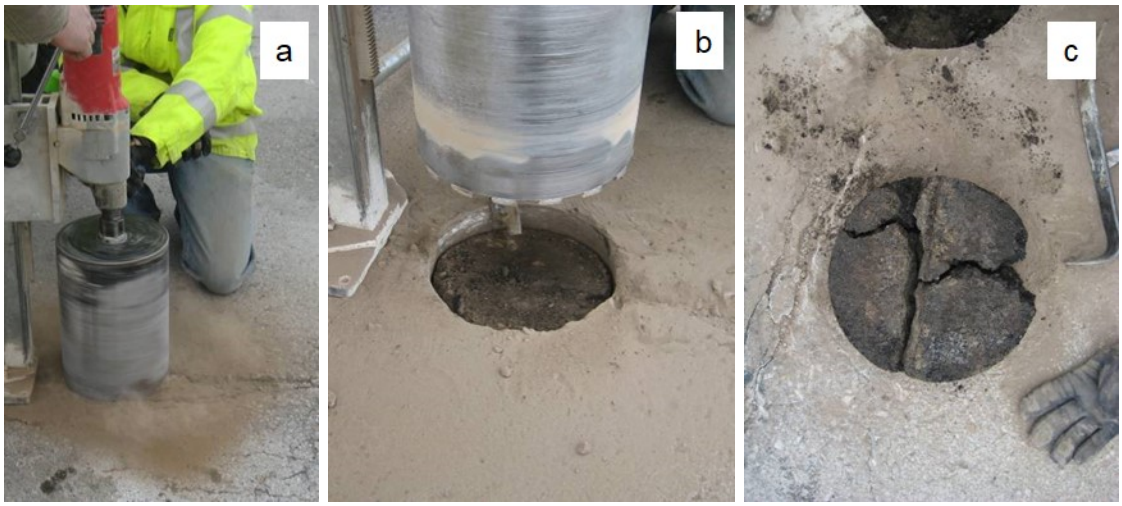

Figure 75. Ten-inch diameter coring at joint at mile 143.61: coring in progress (a); cavity at top of PCC layer (b); extracted AC core sample (c) (02/26/2010)

A 254 mm (10 in.) diameter core was drilled at the middle of the slab panel between miles 143.53 and 143.52 (Figure 76). The AC layer was first extracted. The extraction of the rest of the PCC core was unsuccessful, so a 102 mm (4 in.) diameter drill bit was used to extract a 102 mm (4 in.) diameter sample in two pieces (Figure 76). The second (smaller) piece showed evidence of ATB base. The PCC core was extracted in sound structural condition, and no evidence of free water was observed in the core.

It was observed that the coring process did result in thawing of the ice lenses in the pavement layers due to heat created by friction.

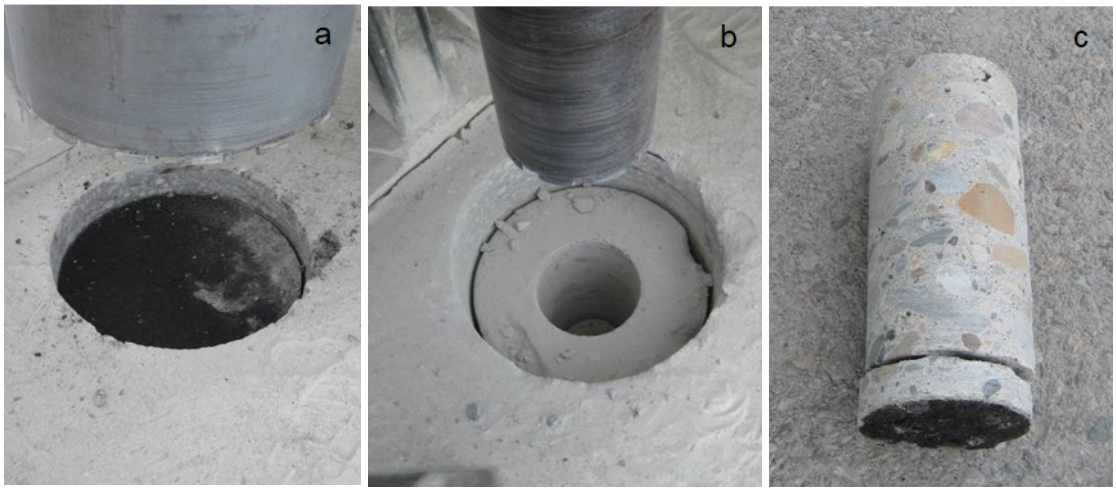

Figure 76. Middle of slab panel between mile 143.53 and 143.54: 10 in. diameter cavity at top of PCC layer (a); 4 in. diameter cavity drilled in predrilled 10 in. cavity (b); extracted 4 in. diameter two PCC cores with smaller indicating ATB (c) (02/26/2010)

Two joints located in the eastbound lane at mile posts 140.79 and 140.80 were cored on March 4, 2010. A 254 mm (10 in.) diameter core was drilled at the joint at mile post 140.79 (Figure 77). The drilling was done into the PCC layer, but an intact sample was not obtained due to weak and deteriorated structure of concrete. Standing water was observed in the cored 254 mm (10 in.) diameter cavity (Figure 79). A reinforcing dowel was observed in the cavity and was removed. While surface corrosion existed, the structural integrity of the dowel was intact. A 102 mm (4 in.) diameter core was obtained on the PCC pavement and ATB interface (Figure 79). Standing water was also observed on the ATB layer.

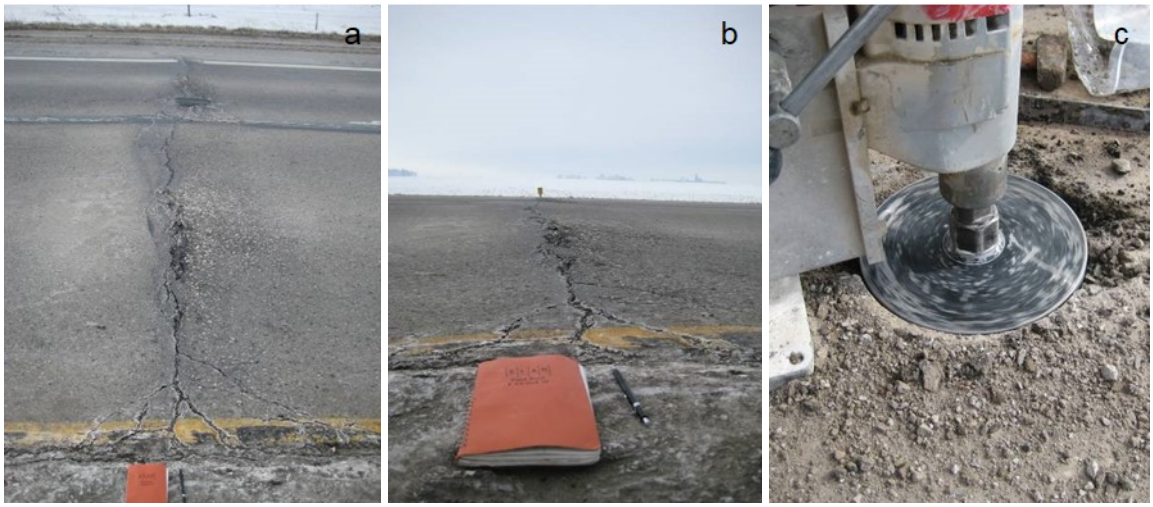

Figure 77. Joint at mile 140.79: Isometric view (a); profile view looking south (b); coring a 10 in. diameter sample (c) (03/04/2010)

Figure 78. Joint at mile 140.80: Isometric view (a); profile view looking south (b); top view of joint section (c) (03/04/2010)

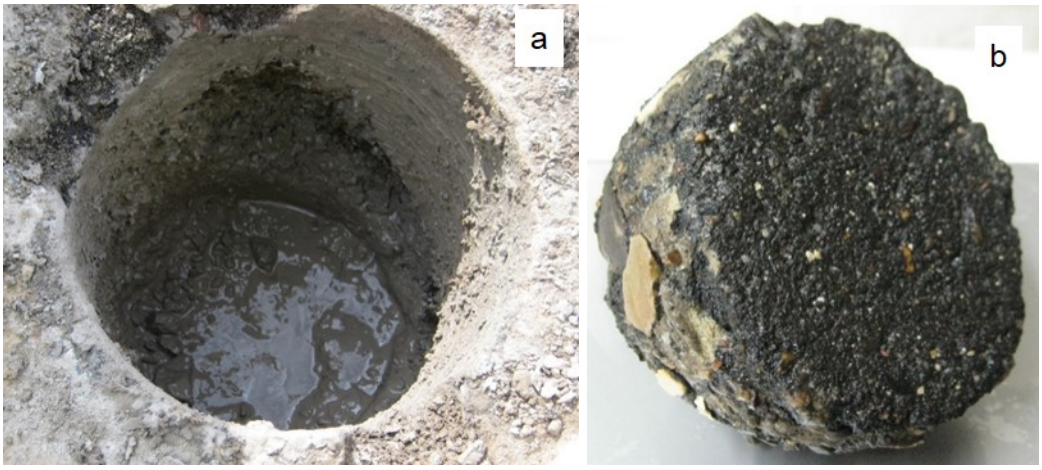

Figure 79. Joint at mile 140.79: View down the 10 in. diameter cored hole (a) and 4 in. ATB sample (03/04/2010)

Oven-dried gravimetric moisture contents of the extracted samples and a brief description of the samples are provided in Table 25. The gravimetric moisture contents of PCC samples ranged between 12.5% and 20.4%. The PCC layer samples obtained from joints showed very little structural integrity.

Table 25. Sample characteristics

Lane and mile post	Date	Depth (in.)	Description	w (%)
Westbound 143.55	2/26/2010	2 to 4	PCC/AAC interface	9.2
Westbound 143.55	2/26/2010	4 to 8	PCC. Sample has no structure; appears granular as removed	20.4
Westbound 143.55	2/26/2010	9	Cuttings from core	14.5
Eastbound 140.85	3/4/2010	0 to 2	AAC top lift	2.0
Eastbound 140.85	3/4/2010	2 to 4	AAC lower lift	8.7
Eastbound 140.85	3/4/2010	4 to 6	PCC. Sample has no structure; appears granular as removed	15.2
Eastbound 140.85	3/4/2010	6 to 8	PCC. Sample has no structure; appears granular as removed	16.3
Eastbound 140.85	3/4/2010	8 to 10	PCC. Sample has no structure; appears granular as removed; contains reinforcing steel	18.8
Eastbound 140.85	3/4/2010	10 to 13	PCC. Sample has some structural integrity and was removed in larger pieces	12.5
Eastbound 140.85	3/4/2010	13 to 17	ATB. Fine grained material does not appear highly permeable	6.9

Vertical Heave Measurement

Vertical heave profiles were measured longitudinally along four transverse joints. Locations were marked about 305 mm (12 in.) apart starting at painted edge line as an initial measurement point and extending up to 2.4 m (96 in.) longitudinally in the travel direction (Figure 80). Once

the locations on the selected joints were identified, a marked steel rod was mounted above the marked joint location of interest with ends of the rod extending away from the joint. The rod was mounted on wooden blocks located at each end of the rod to provide a support (Figure 81). The rod was used to establish a reference elevation for making vertical profile measurements between the rod and the pavement. The profile measurements were taken at 25 mm (1 in.) and 50 mm (2 in.) increments. The measurements were taken using calipers where the distances from the rod down to the point of interest on the pavement were recorded. Collected measurements were normalized with a reference to the lowest measured point identified as a zero level elevation.

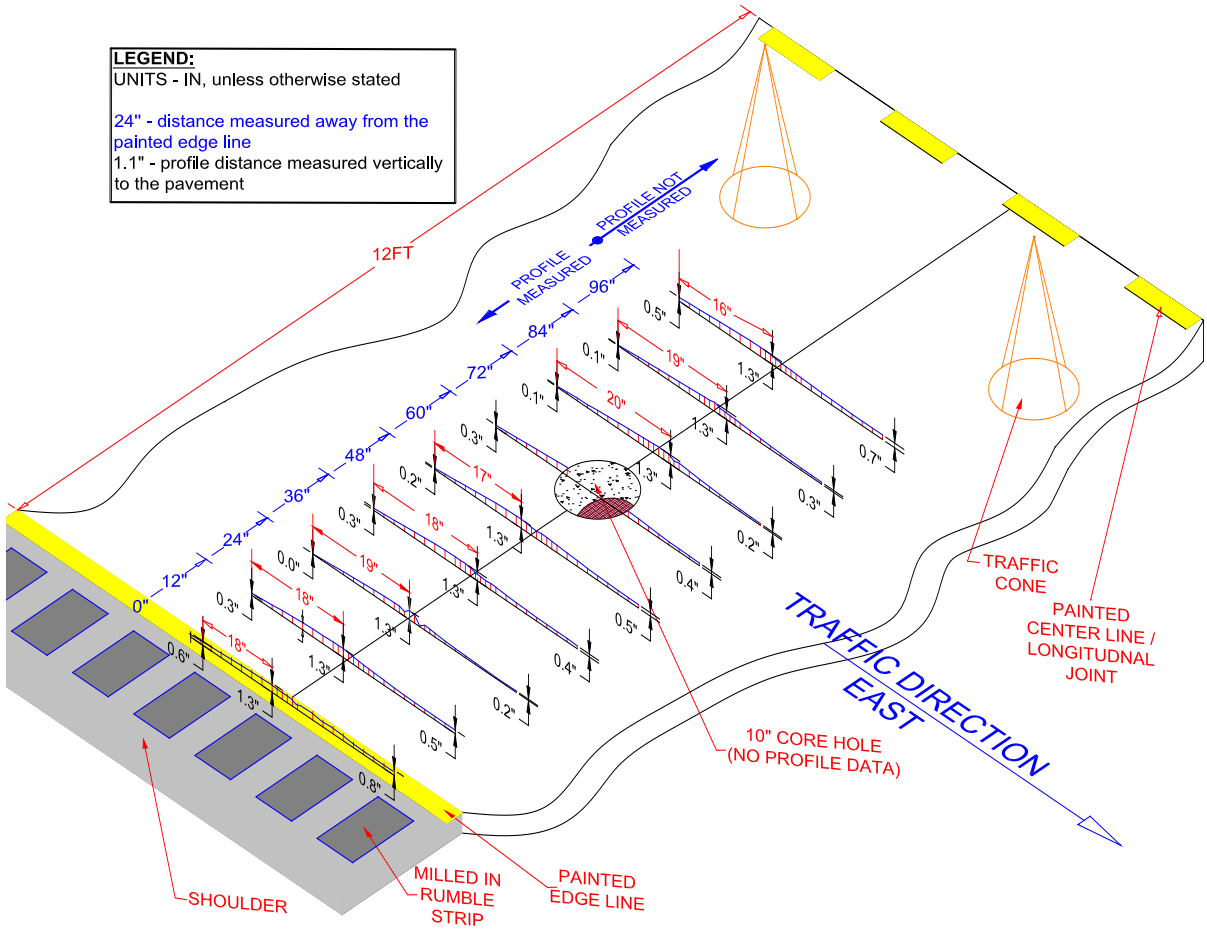

Figure 80. Isometric AutoCAD sketch of vertical profile measurements at joint 4

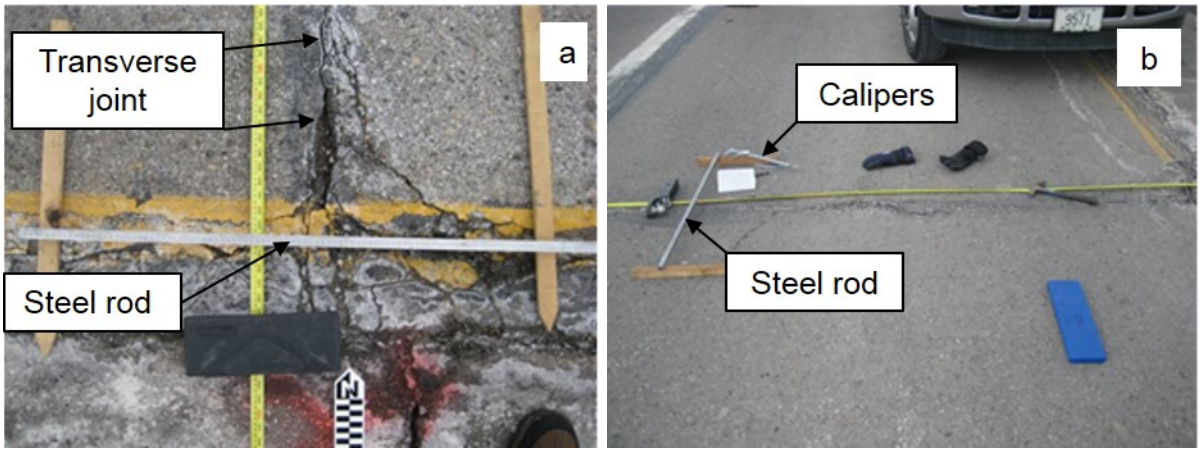

Figure 81. Setup for measuring the vertical heave profiles with calipers at a joint using a mounted steel rod as a point of reference: top view (a) and side view (b)

At joint 1 (milepost 143.55 on the westbound lane) vertical heaves ranging between 18 mm (0.7 in.) to 25 mm (1.0 in.) were measured (Figure 82). At joint 2 (milepost 143.61 on the westbound lane) vertical heaves ranging between 15 mm (0.6 in.) to 30 mm (1.2 in.) were measured (Figure 83).

At joint 3 (milepost 140.79 on the eastbound lane) vertical heaves ranging between 13 mm (0.5 in.) and 23 mm (0.9 in.) were measured near (Figure 84). At joint 4 (milepost 140.89 on the eastbound lane) vertical heaves ranging between 25 mm (1.0 in.) to 38 mm (1.5 in.) were measured (Figure 85).

Kriged spatial contour maps of vertical heave measurements are presented in Figure 86 and Figure 87.

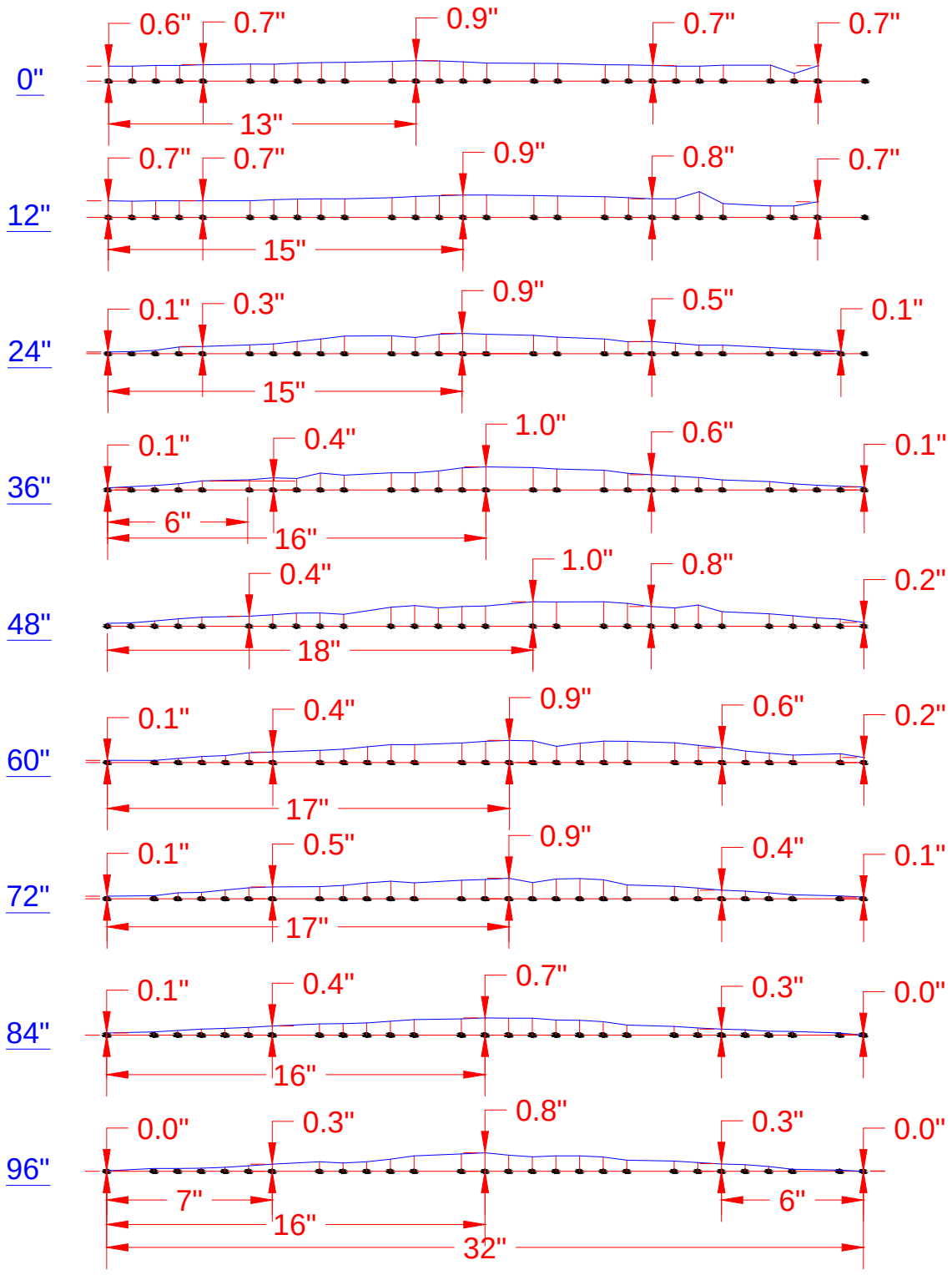

Figure 82. Joint 1: Transverse joint longitudinal profile at mile 143.53 (02/26/2010)

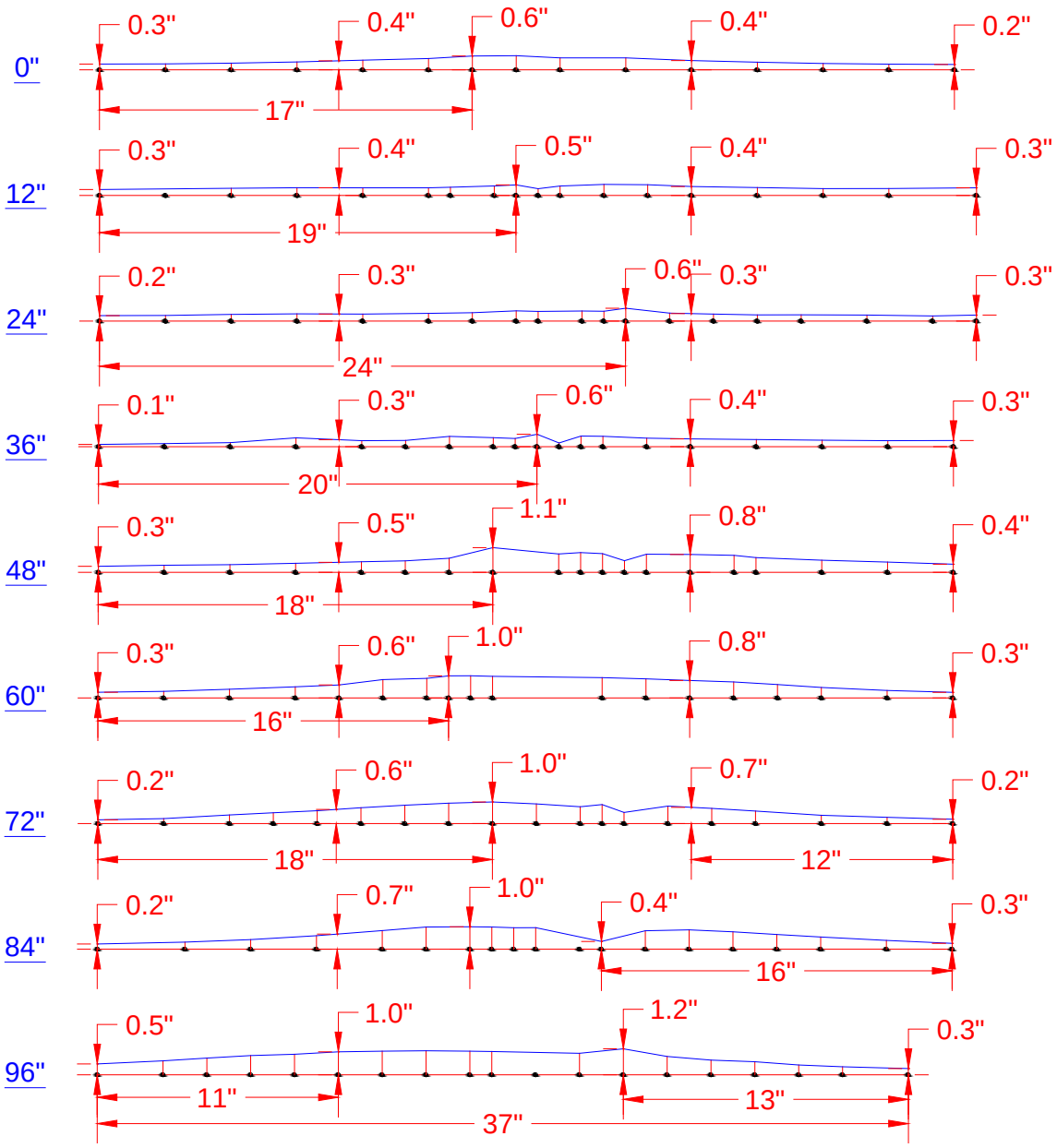

Figure 83. Joint 2: Transverse joint longitudinal profile at mile 143.61 (02/26/2010)

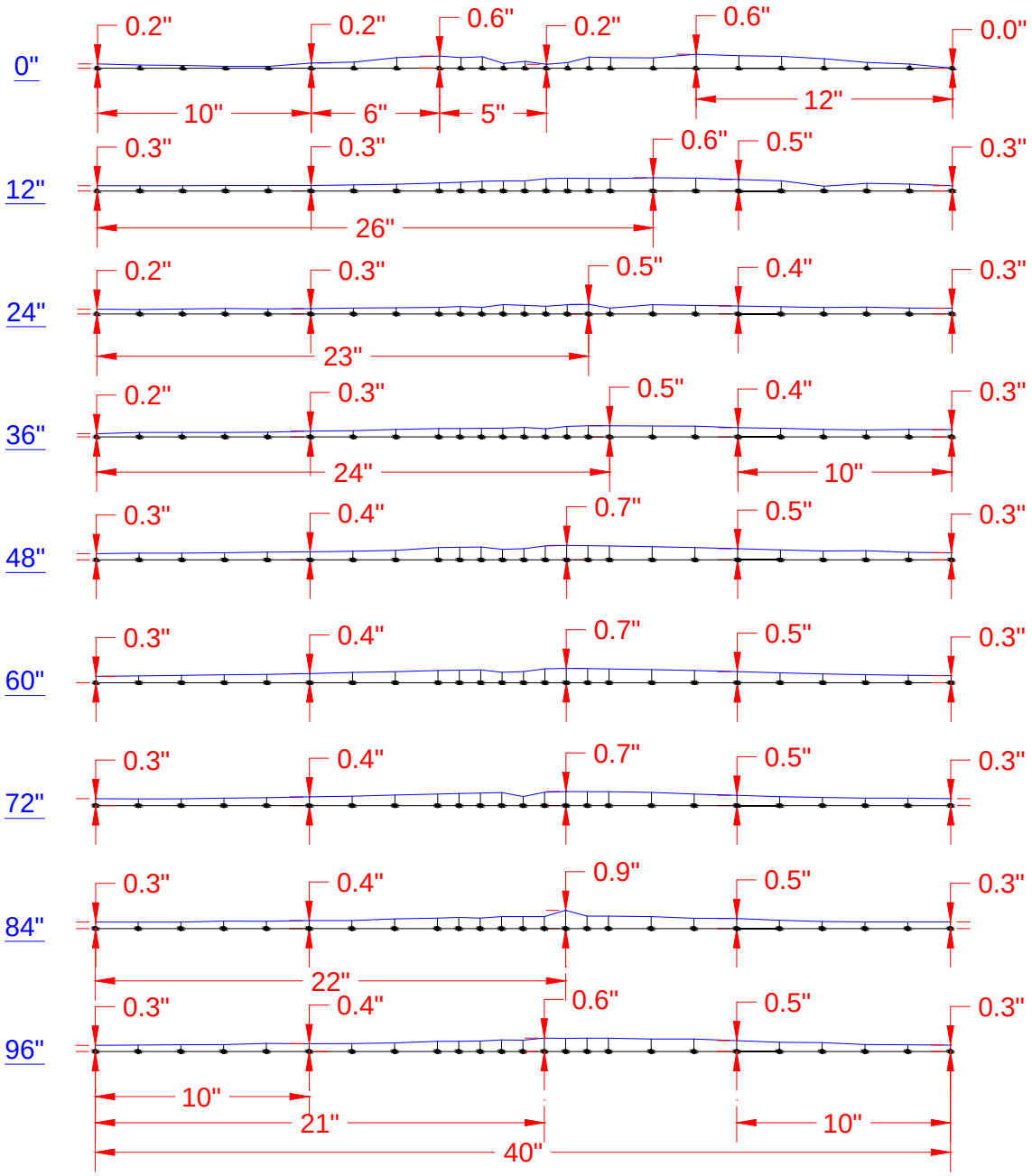

Figure 84. Joint 3: Transverse joint longitudinal profile at mile 140.79 (03/04/2010)

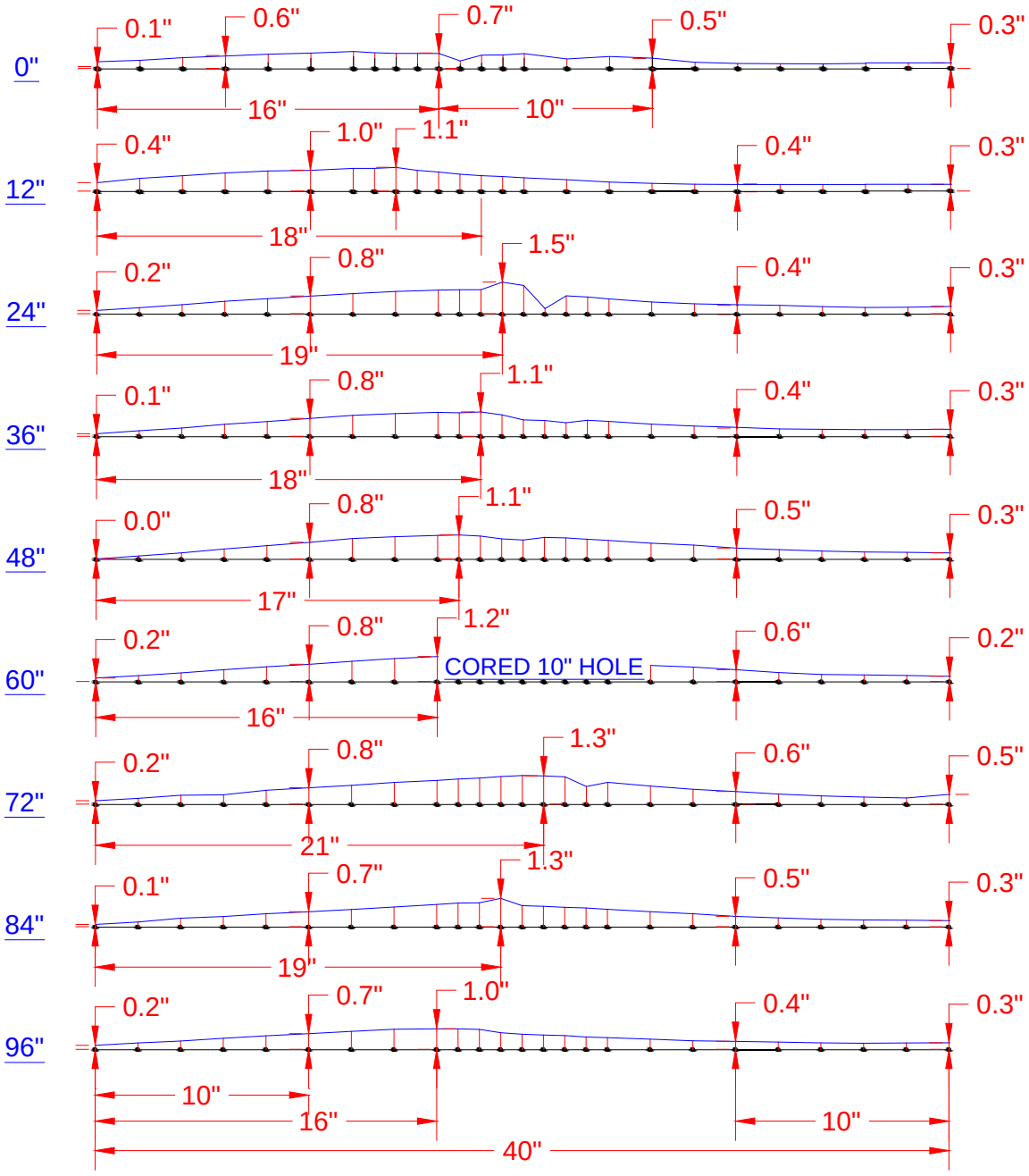

Figure 85. Joint 4: Transverse joint longitudinal profile at mile 140.80 (03/04/2010)

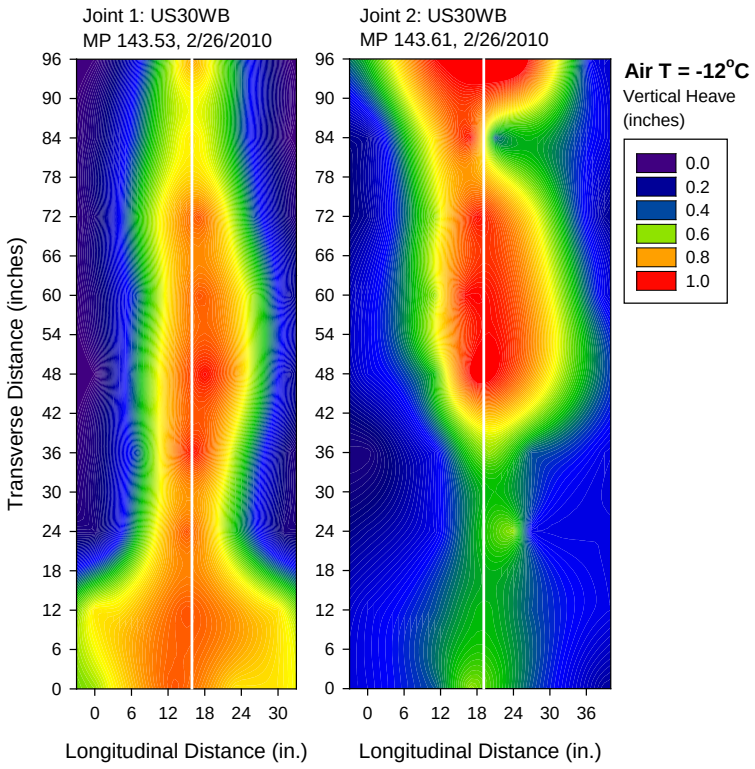

Figure 86. Joints 1 and 2: Spatial contour plots of vertical heave

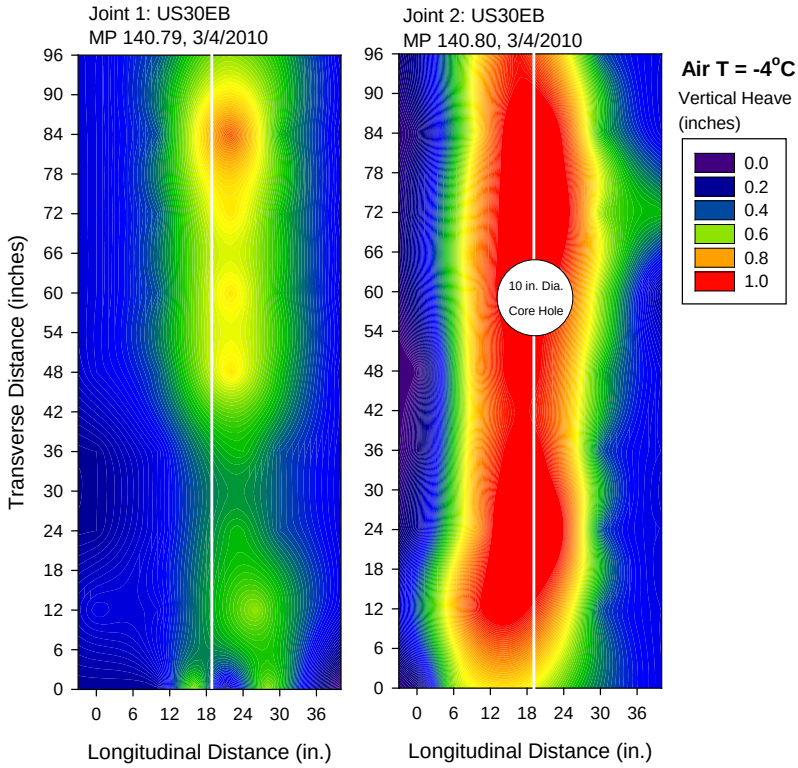

Figure 87. Joints 3 and 4: Spatial contour plots of vertical heave

Field Testing on New Foundation Layers

In situ DCP and LWD tests were conducted on the foundation layers and FWD tests were conducted on the pavement layer. Air temperatures were monitored during field testing, and temperature probes were installed at depth and transversely in the pavement foundation at one location. All testing was conducted on US30 EB lane near between Sta. 1394+00 and 1396+00. Pictures during testing on the RPCC modified subbase layer and the PCC surface layer are shown in Figure 88 and Figure 89.

Figure 88. Field testing on finished RPCC modified subbase layer (June 8, 2011)

Figure 89. Field testing on finished pavement surface (June 6, 2012)

DCP and LWD Testing

DCP and LWD tests were conducted on the RPCC modified subbase layer on August 8, 2011. Tests were conducted after compaction and trimming operations are completed and just prior to paving operations.

DCP tests were conducted at 20 test locations, with 10 locations each in the left and right lanes over a 100 m distance along the center lane. The DCP-CBR and cumulative blows with depth profiles for left and right lanes are presented in Figure 90. CBR values of each layer at each test location are plotted with distance in Figure 91.

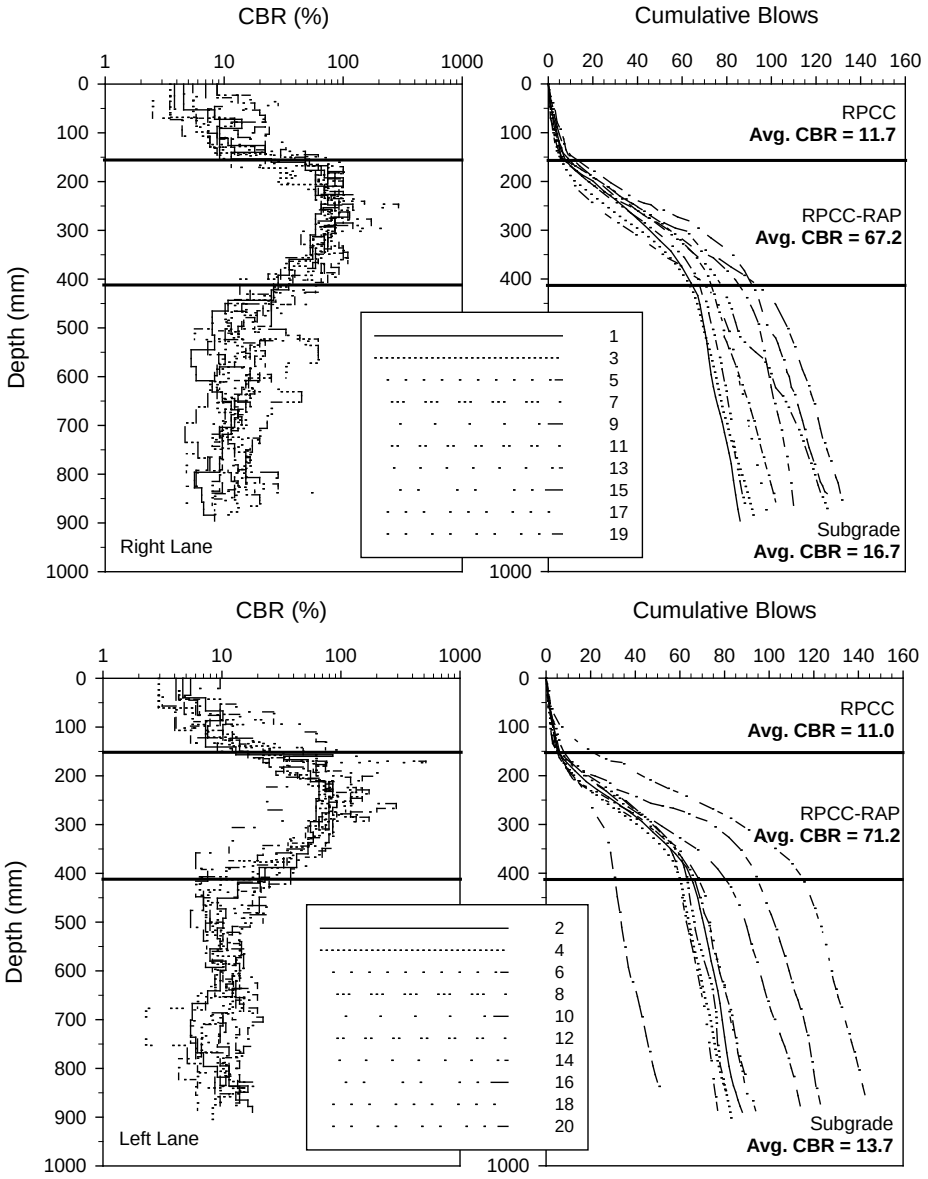

Figure 90. DCP-CBR profiles

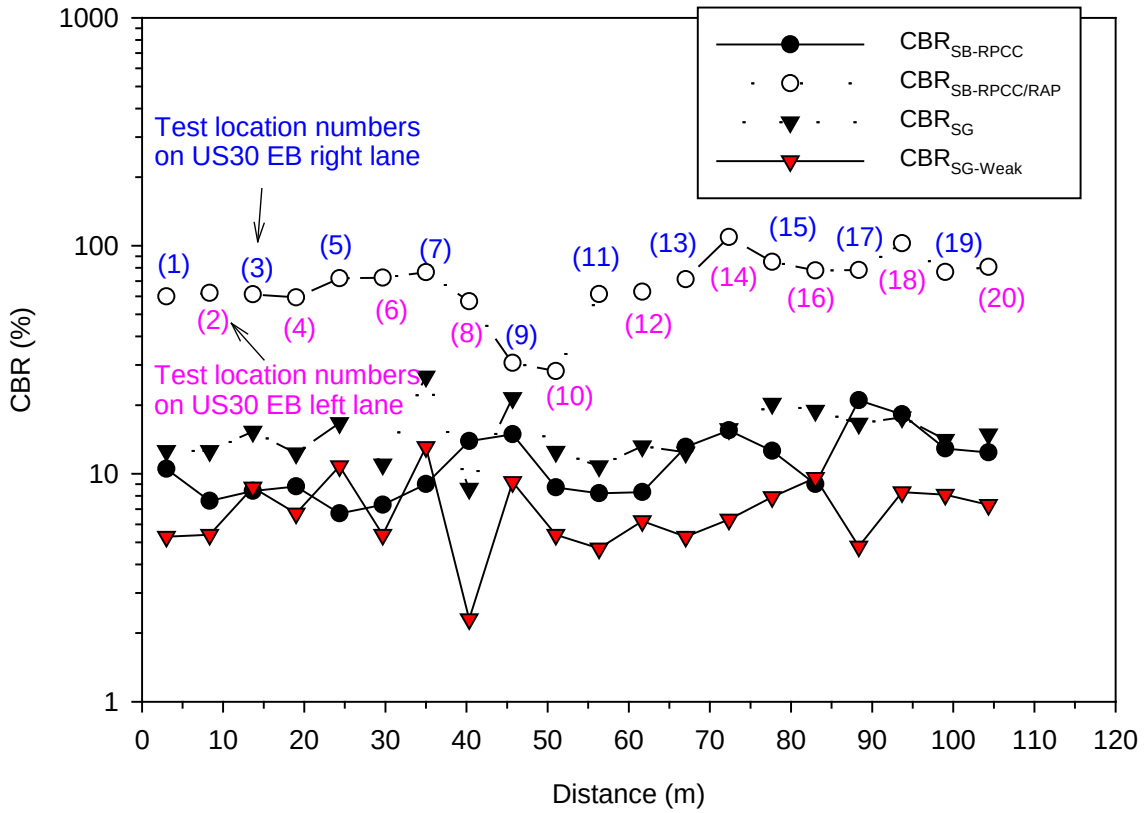

Figure 91. Average CBR values of pavement layers at each test location where 0 m is Sta. 1394+20

Histograms of CBR values of each layer are provided in Figure 92 along with statistical mean (μ), standard deviation (σ), and coefficient of variation (COV) of the CBR of each layer.. CBR values were lower in the top 150 mm (6 in.) RPCC modified subbase layer, that the bottom 10 in. of RPCC/RAP modified subbase layer, and that the subgrade was very variable. The average CBR of the RPCC modified subbase layer was about 11, the average CBR of the RPCC/RAP layer was about 69, and the subgrade CBR (for the top 300 mm) was about 14. The CBR of the weakest layers in the subgrade was about 7.0.

Figure 93 shows the E_{LWD} values of 40 longitudinal test points starting at Sta. 1394+20 with 20 test locations in each of the left and right lanes over a 105 m distance along the center of each lane. In addition, 32 tests were conducted at Sta. 1394.60 transversely across the full pavement width. Results indicated the E_{LWD} varied between 11 and 79 MPa in the longitudinal direction and between 19 and 100 MPa in the transverse direction.

LWD tests were conducted transversely to capture the variability observed at the surface with aggregate segregation as shown in Figure 94 and Figure 95. E_{LWD} values on the right lane were comparatively higher than in the left lane. As can be seen in the figures, higher moduli values were in areas with more fines content. Figure 96 is a histogram of E_{LWD} values along with μ, σ, and COV statistics.

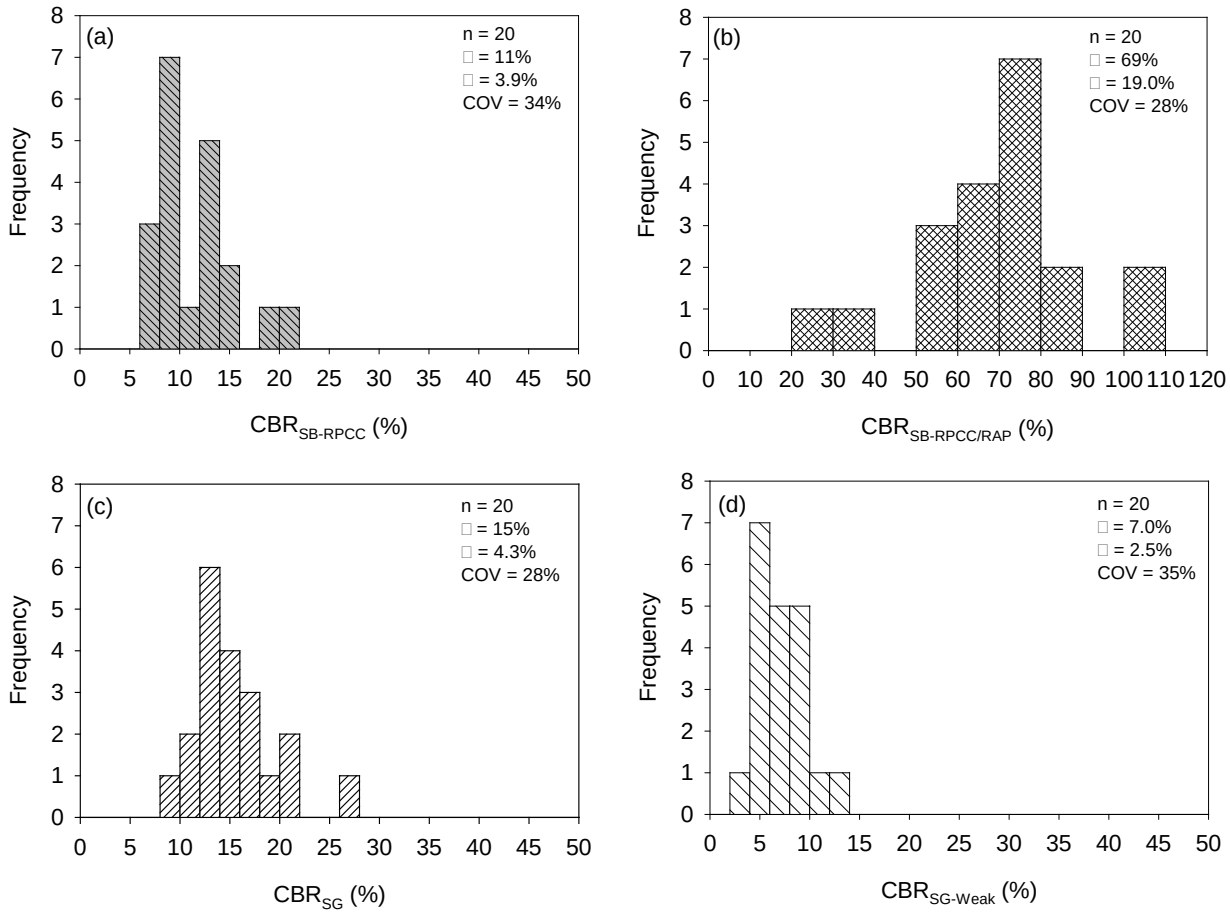

Figure 92. Histograms of DCP-CBR values of RPCC modified subbase (a); RPCC/RAP modified subbase (b); subgrade (c); and weakest subgrade layer (d)

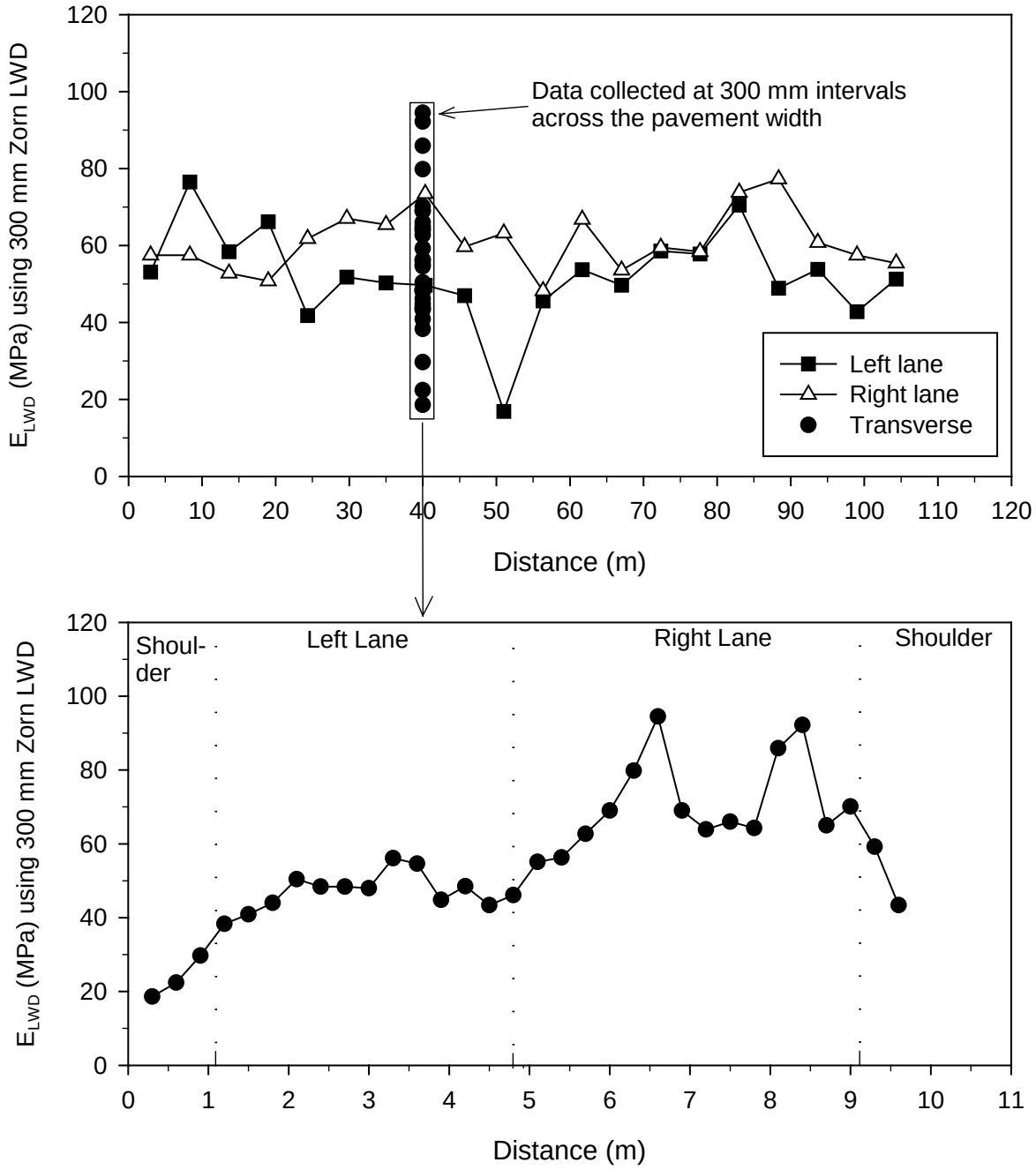

Figure 93. E_{LWD} at each longitudinal test location where 0 m = Sta. 1394+20 (top) and from locations across the lane at Sta. 1394+60 (bottom)

Figure 94. RPCC modified subbase layer surface

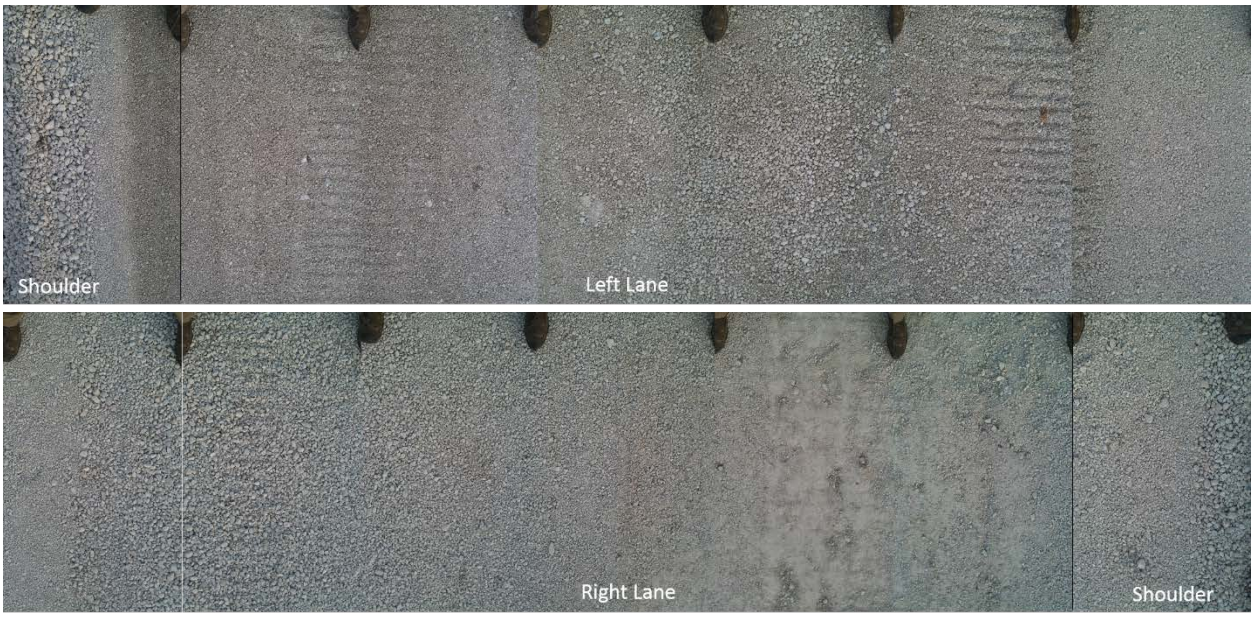

Figure 95. RPCC modified subbase layer surface from left lane shoulder (top) to right lane shoulder (bottom)

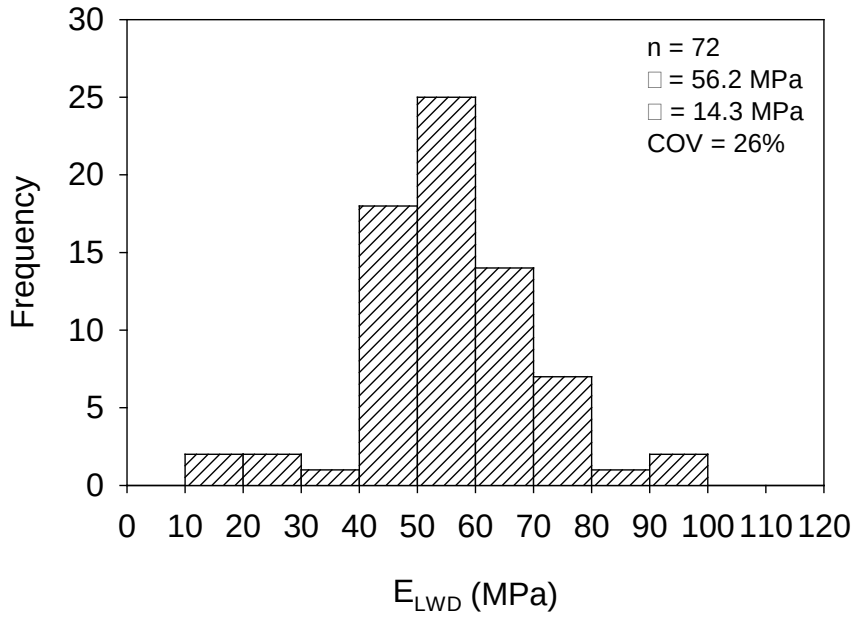

Figure 96. Histogram of E_{LWD} on the subbase layer

Field Testing on New Pavement

Kuab Falling Weight Deflectometer Tests

FWD tests were conducted on the pavement layer on June 6, 2012. Tests were conducted near the mid-panel and at joints (Figure 97). FWD D_0, I, $k_{FWD\text{-}Static\text{-}Corr}$ values for tests conducted near mid panel, and D_0, I, and LTE for tests conducted near joint are presented in Figure 98. A histogram of $k_{FWD\text{-}Static\text{-}Corr}$ values is provided in Figure 99, which shows that the average k was about 37.1 kPa/mm with a COV of about 7%.

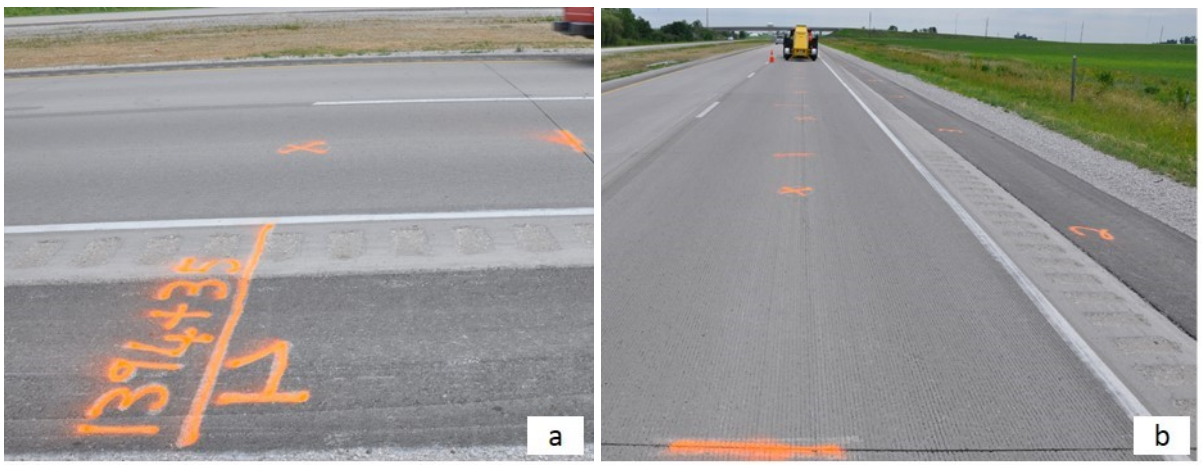

Figure 97. Start point for FWD tests at 1394+35 (a) and a view from the start point (b)

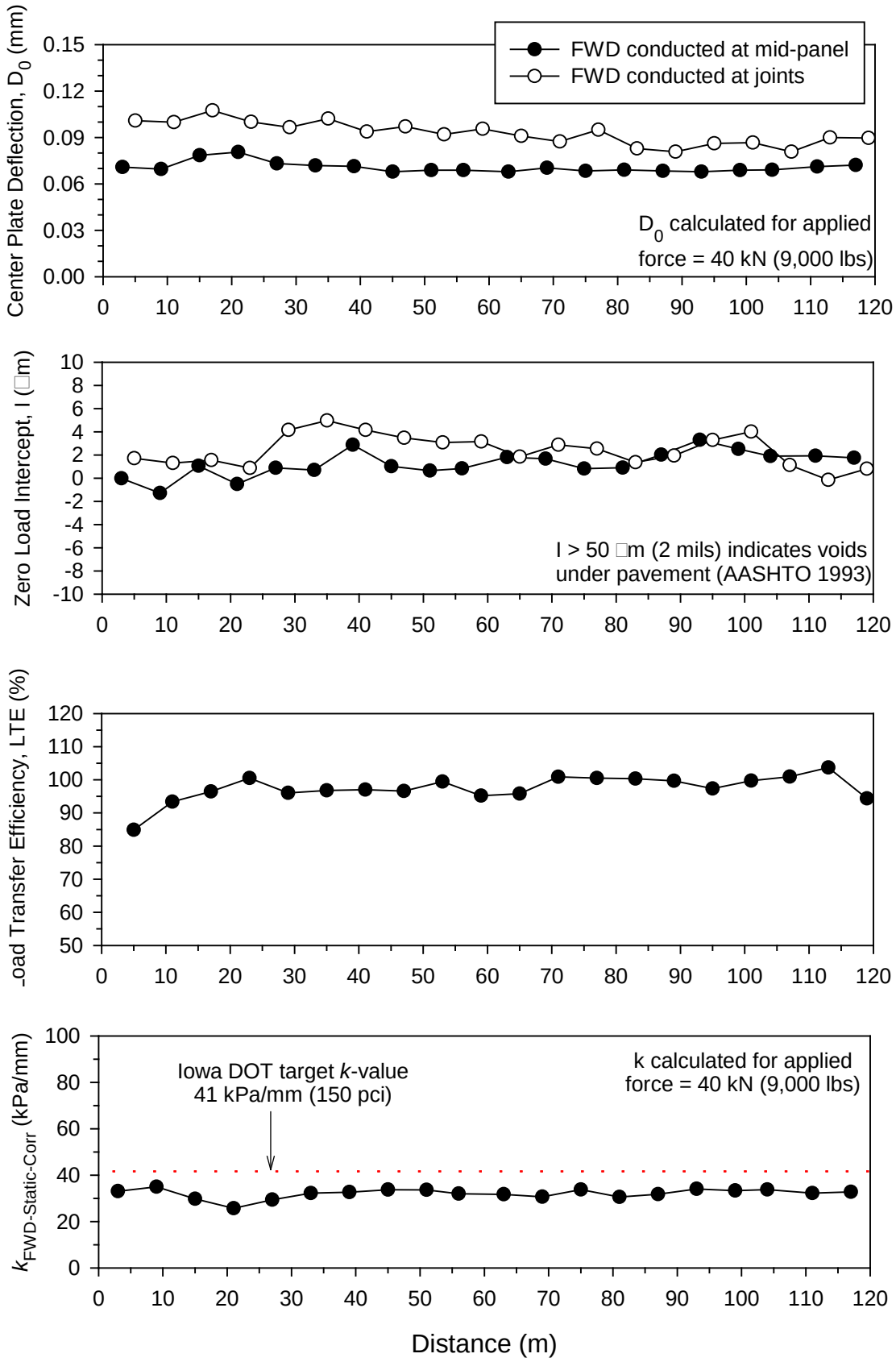
Center Plate Deflection, D_0 (mm)
FWD conducted at mid-panel
FWD conducted at joints
D_0 calculated for applied force = 40 kN (9,000 lbs)
Zero Load Intercept, I (□m)
I > 50 □m (2 mils) indicates voids under pavement (AASHTO 1993)
-oad Transfer Efficiency, LTE (%)
$k_{FWD\text{-}Static\text{-}Corr}$ (kPa/mm)
Iowa DOT target *k*-value 41 kPa/mm (150 pci)
k calculated for applied force = 40 kN (9,000 lbs)
Distance (m)

Figure 98. FWD test results where 0 m = Sta. 1394+20

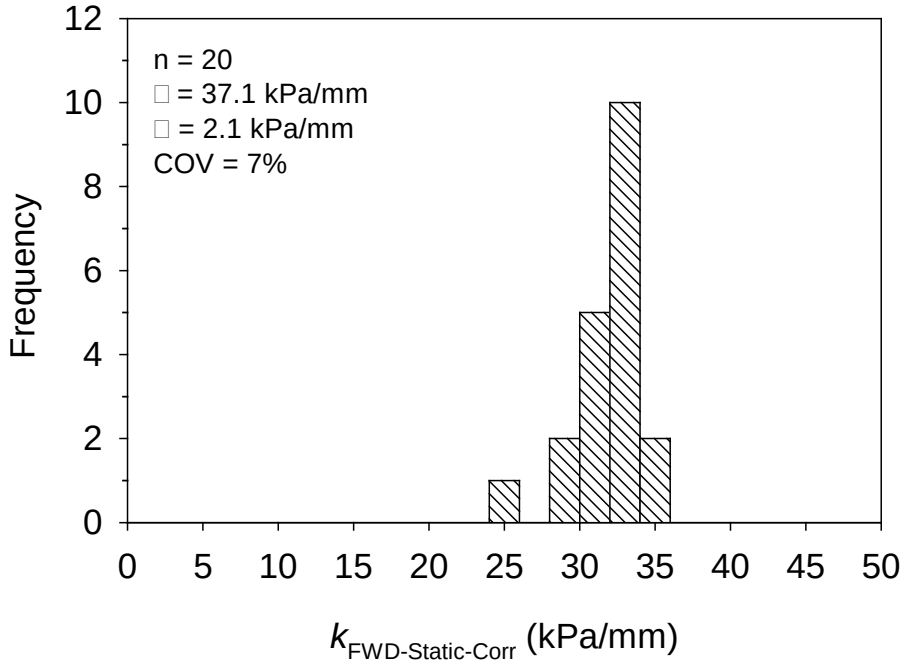

Figure 99. Histogram of $k_{FWD\text{-}Static\text{-}Corr}$

Comparison of FWD-k Values with Design Assumed Values

The *k* values obtained from FWD test, and using the PCA and AASHTO procedures using CBR-*k* correlations are summarized in Figure 100. Both CBR_{SG} and $CBR_{SG\text{-}Weak}$ were used in calculating the *k* values using the PCA and AASHTO procedures.

The average *k* values determined from the three procedures are presented as bar charts in Figure 115. The results showed the following:

- The *k* values determined from the FWD test showed the lowest values, and were closer to the assumed design *k* value. On average, the average $k_{FWD\text{-}Static\text{-}Corr}$ value was about 0.95 times the design *k* value.

- The $k_{PCA(1984)}$ calculated based on $CBR_{SG\text{-}Weak}$ were also closer to the assumed design *k* value. The average $k_{PCA(1984)}$ calculated based on CBR_{SG} was about 1.4 times higher than the design *k* value.

- The *k* values calculated using the empirical relationships between CBR and *k* from AASHTO (1993) produced the highest values. The average $k_{AASHTO(1993)}$ was about 2 to 4 times higher than the design *k* value.

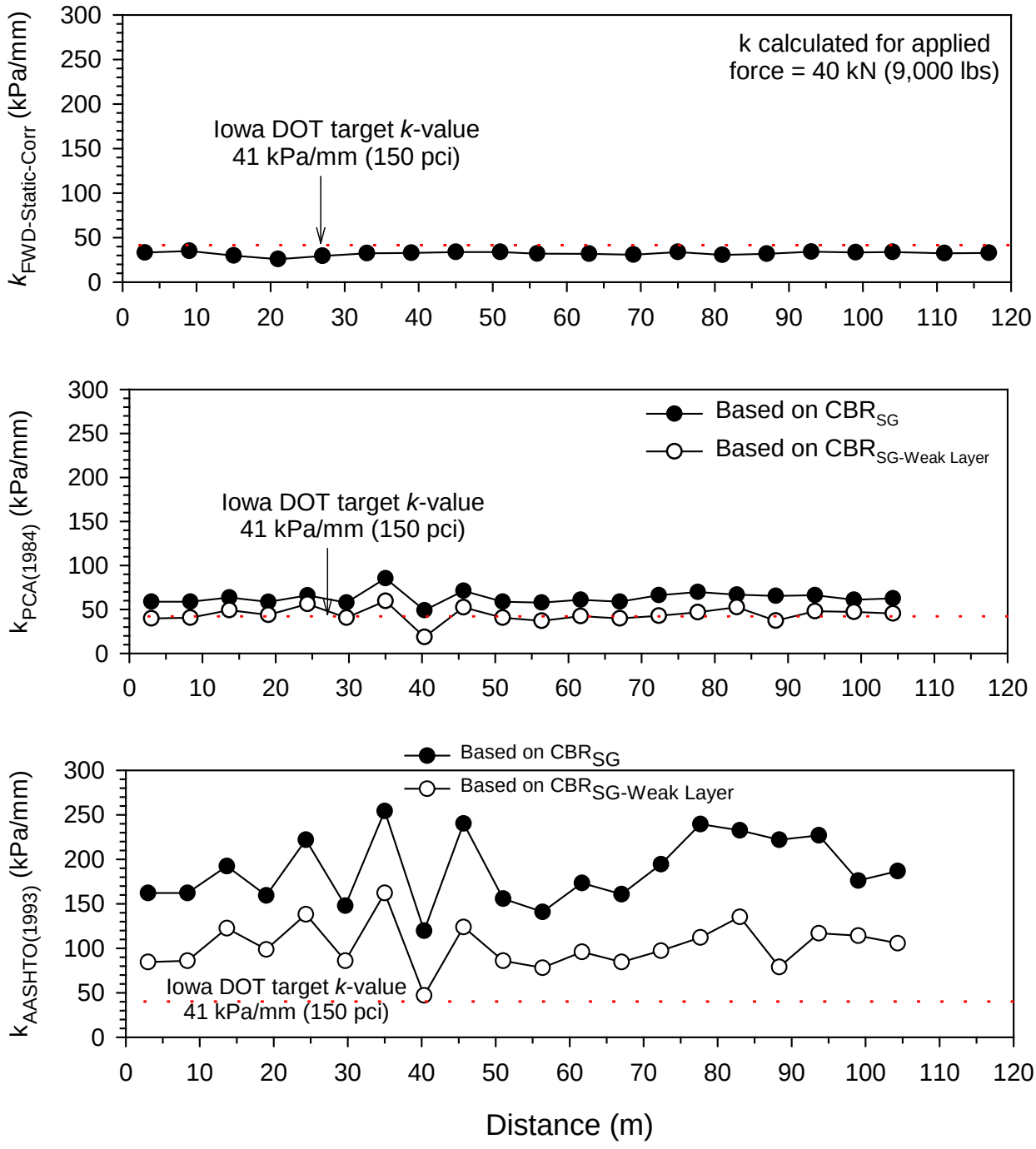

Figure 100. Calculated *k* values based on different methods

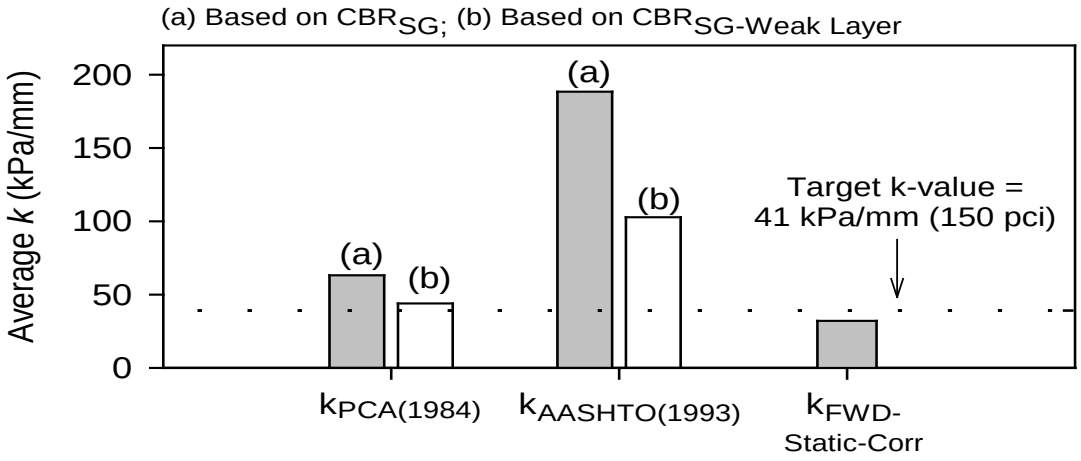

Figure 101. Bar chart comparing the design target *k* value with measured and estimated *k* values from field measurements

Comparison of DCP-CBR and k Values

Relationships and data published in the literature are compared with $k_{FWD\text{-}Static\text{-}Corr}$ and CBR_{SG} values in Figure 102 and with $CBR_{SG\text{-}Weak}$ values in Figure 103. $CBR_{SG\text{-}Weak}$ values are in line with published relationships, but CBR_{SG} values are not. Nevertheless, CBR versus *k* relationships show significant scatter and present significant uncertainty in the predictions.

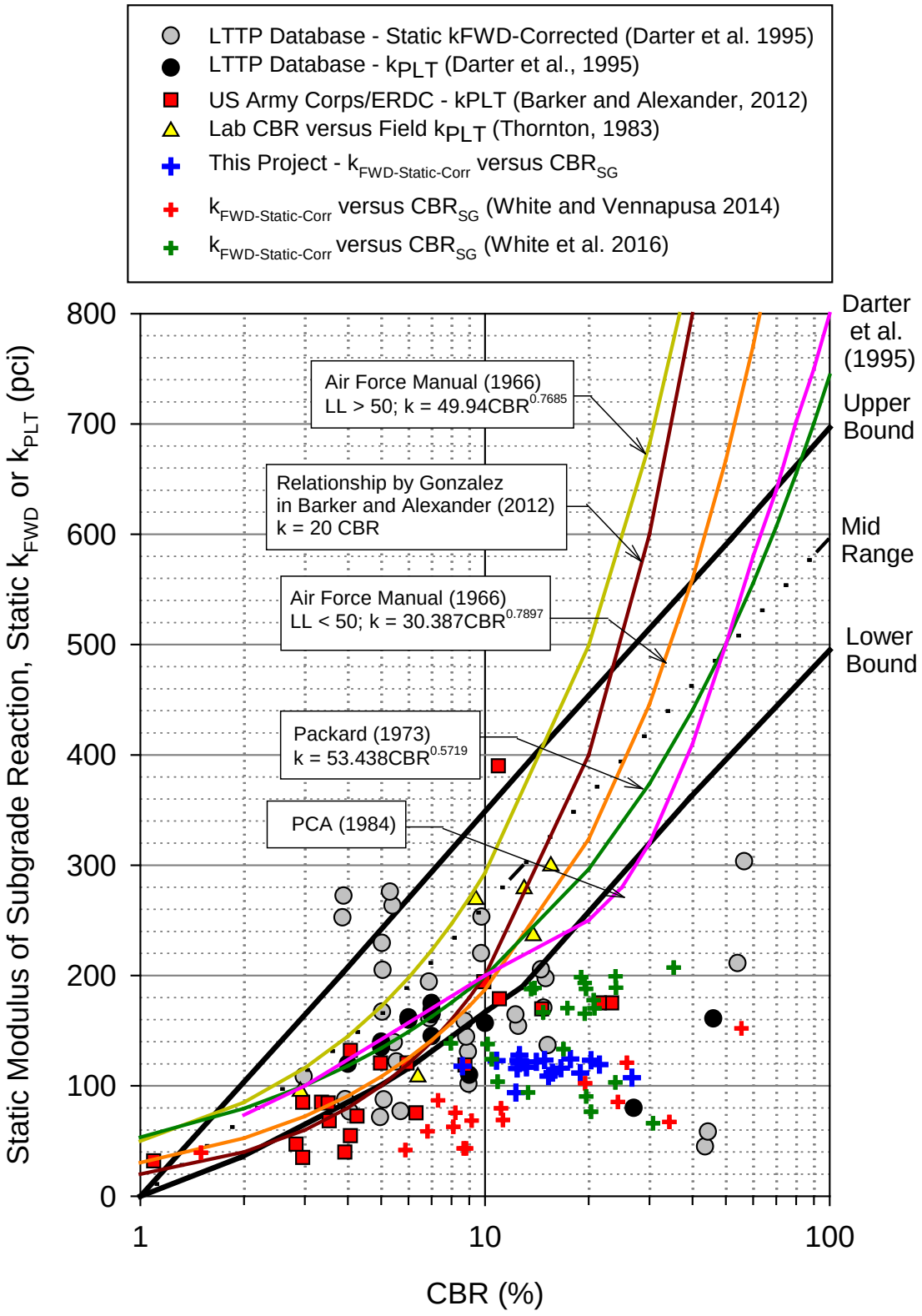

Figure 102. Average $k_{FWD\text{-}Static\text{-}Corr}$ versus average CBR_{SG} compared with relationships published in the literature (1 pci = 0.27 kPa/mm)

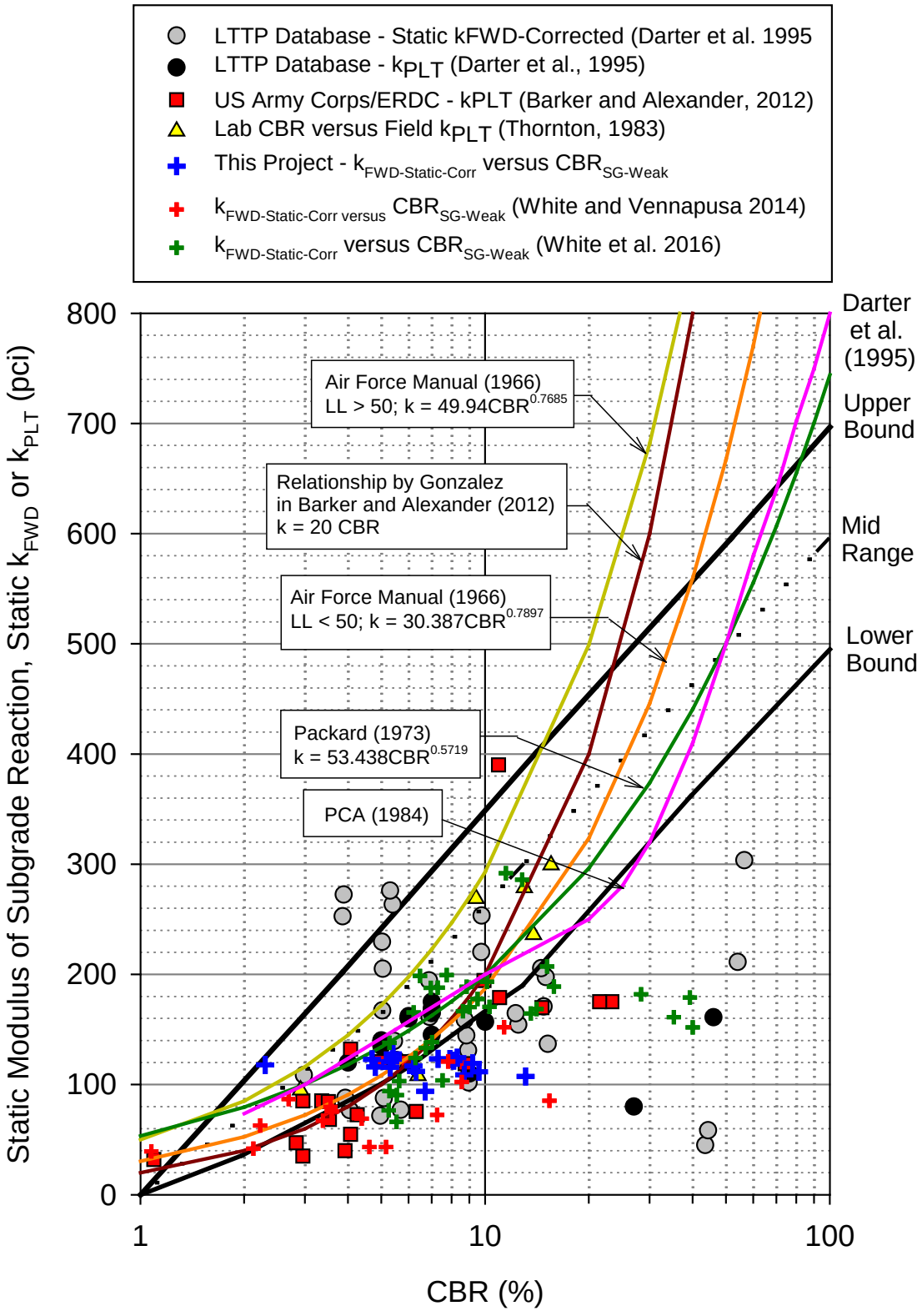

Figure 103. Average $k_{FWD\text{-}Static\text{-}Corr}$ versus average $CBR_{SG\text{-}Weak\ Layer}$ compared with relationships published in the literature (1 pci = 0.27 kPa/mm)

Pavement Temperature Monitoring

The number of freeze-thaw cycles with depth calculated for each year from 2011 to 2015 from the temperature monitoring data near mile 143.68 are presented in Figure 104. The cycles were determined using ±1°C as boundary values. The zero degree isotherms or frozen zones during the four winters are presented in Figure 106.

Figure 105 shows a pavement snow cover situation from Iowa DOT road cameras. The snow fall history based on snow depth is presented in Figure 107. The peak snow date of each winter was selected to assess temperature variations across the pavement width. The temperature changes. The average temperature data (over 6 hour periods) on the day before, during, and after the snow day are plotted in Figure 108 to Figure 111.

Key findings from the temperature monitoring results are as follows:

- Freeze-thaw cycles decreased with depth as expected. The number of freeze-thaw cycles at the surface ranged between 60 and 82 cycles and decreased to about 5 to 10 cycles near the bottom of the pavement. The number of cycles decreased to less than 3 at 0.7 m depth and no freeze-thaw cycles were observed at depths greater than 1.1 m during the monitoring period.
- Frost penetration depth reached around 0.6 to 0.8 m for three winters, while the maximum frost depth of 1.1 m was observed during 2012–2013 winter.
- The annual peak snow depth ranged from around 100 to 280 mm. The transverse temperature results did not show significant temperature differences (less than 1°C) between the areas beneath the driving lanes and effective shoulders, which suggests that no snow cover insulation effects were observed at this site.

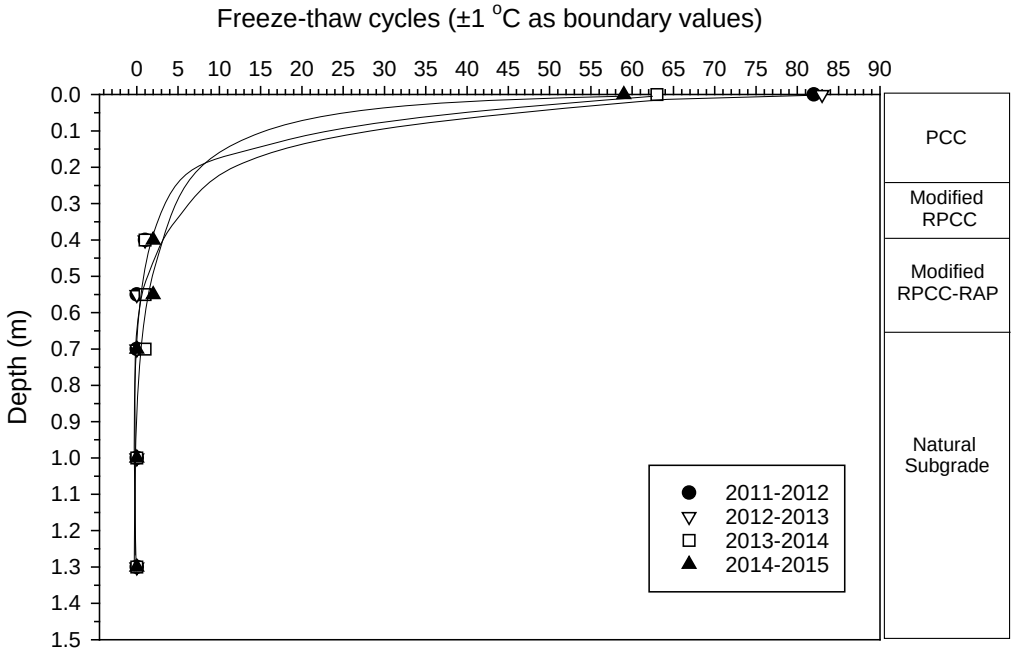

Figure 104. Freeze-thaw cycles of winters at depth from 2011 to 2015 using ±1ºC as boundary values

Figure 105. Pavement shoulder under snow cover (Iowa DOT road cameras at the project site on 02/25/2015)

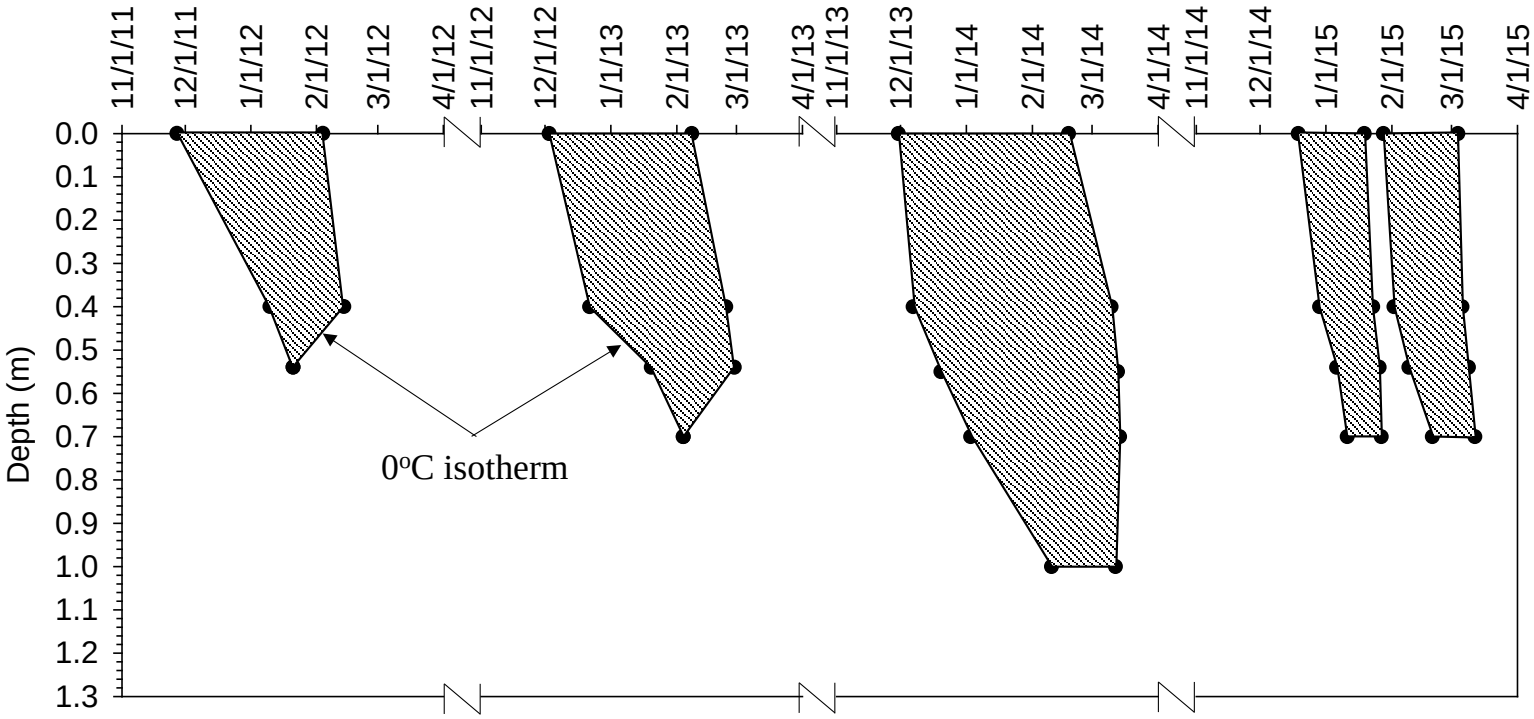

Figure 106. Estimated frozen zones (shaded areas) at mile 143.68 from 2011 to 2015

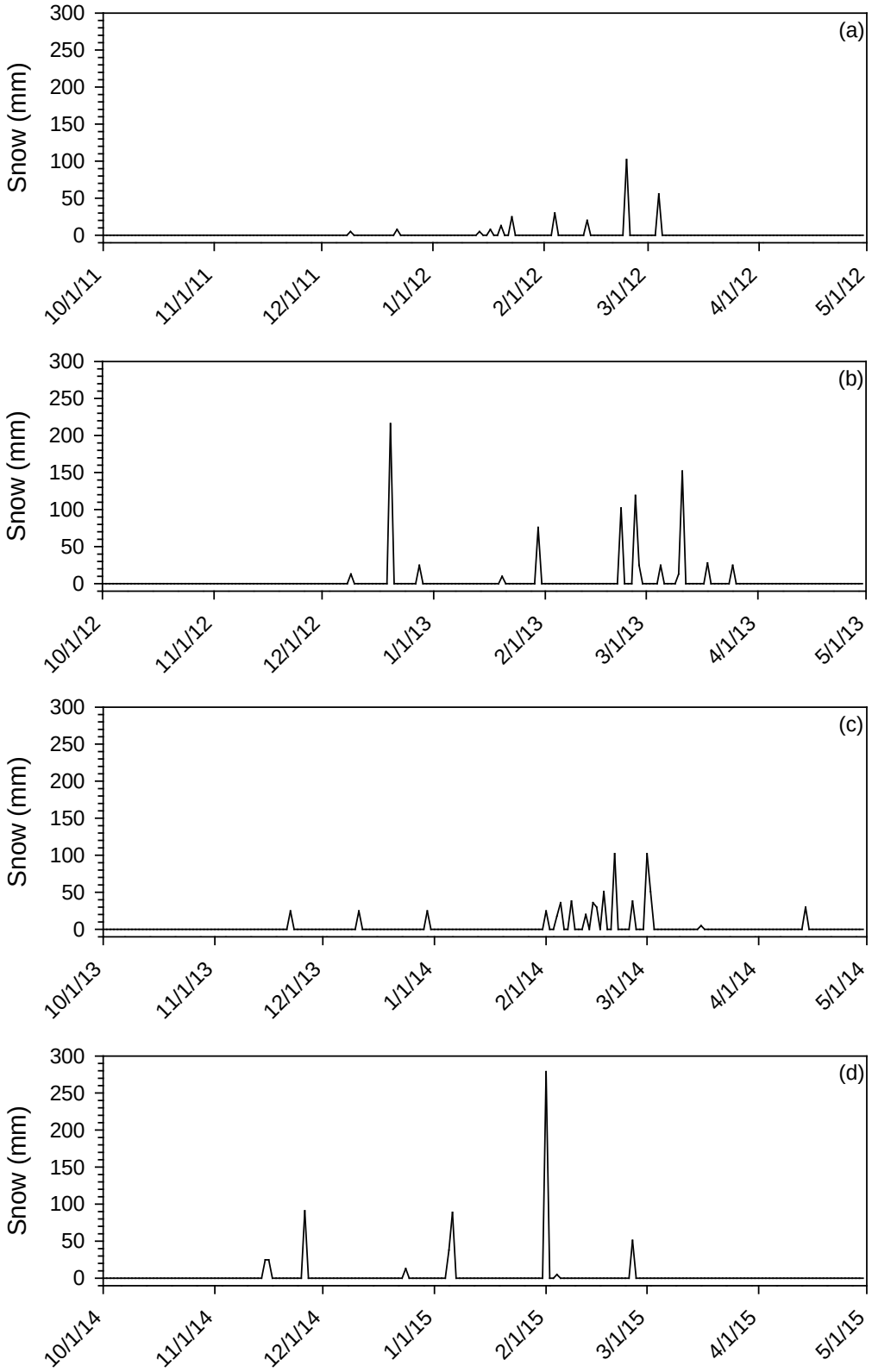

Figure 107. Seasonal snow depth histories for 2011–2012 (a); 2012–2013 (b); 2013–2014 (c), and 2014–2015 (d) (data from www.usclimatedata.com)

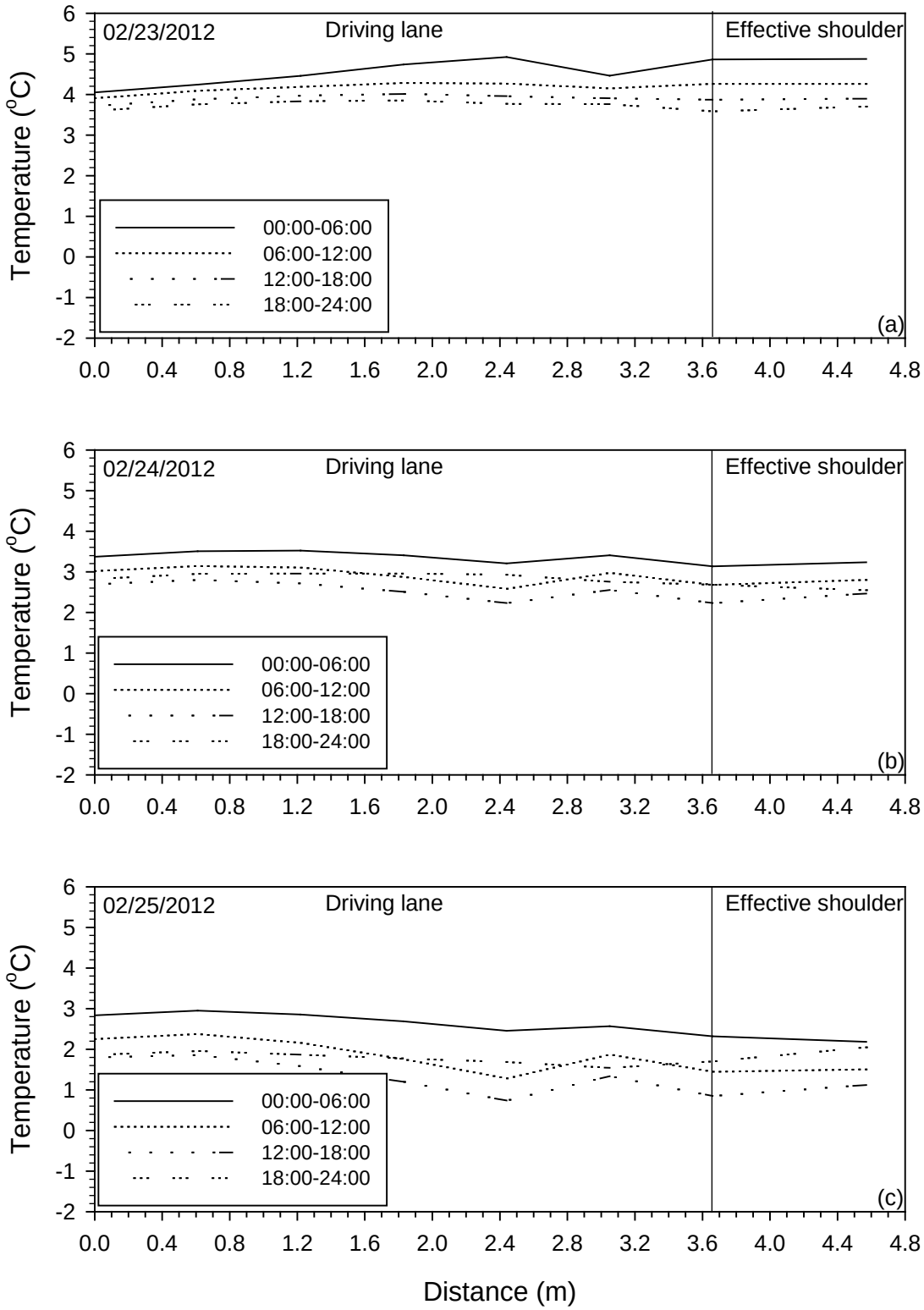

Figure 108. Transverse pavement temperature variation before (a), during (b), and after (c) the peak snow day in the 2011–2012 winter

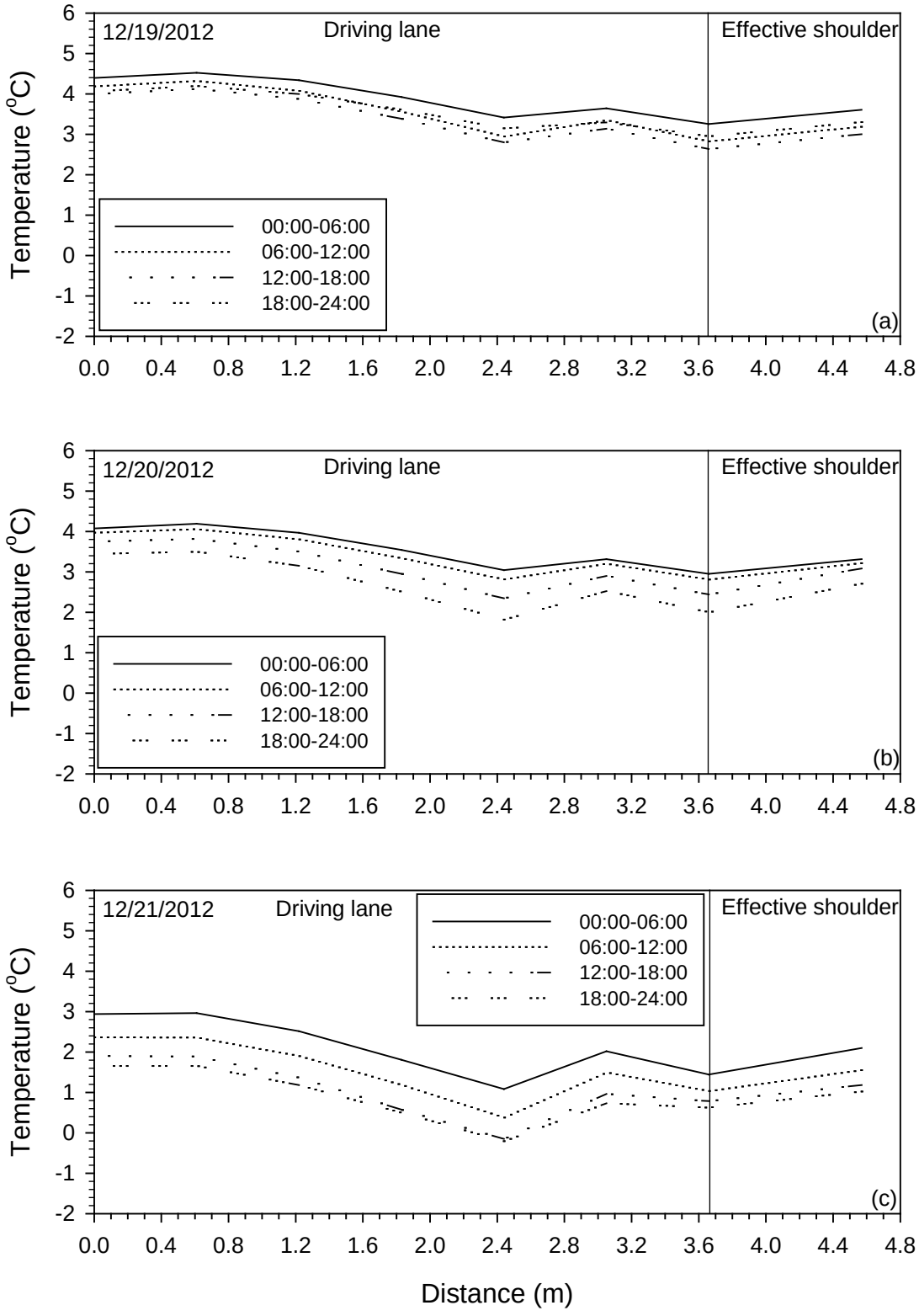

Figure 109. Transverse pavement temperature variation before (a), during (b), and after (c) the peak snow day in the 2012–2013 winter

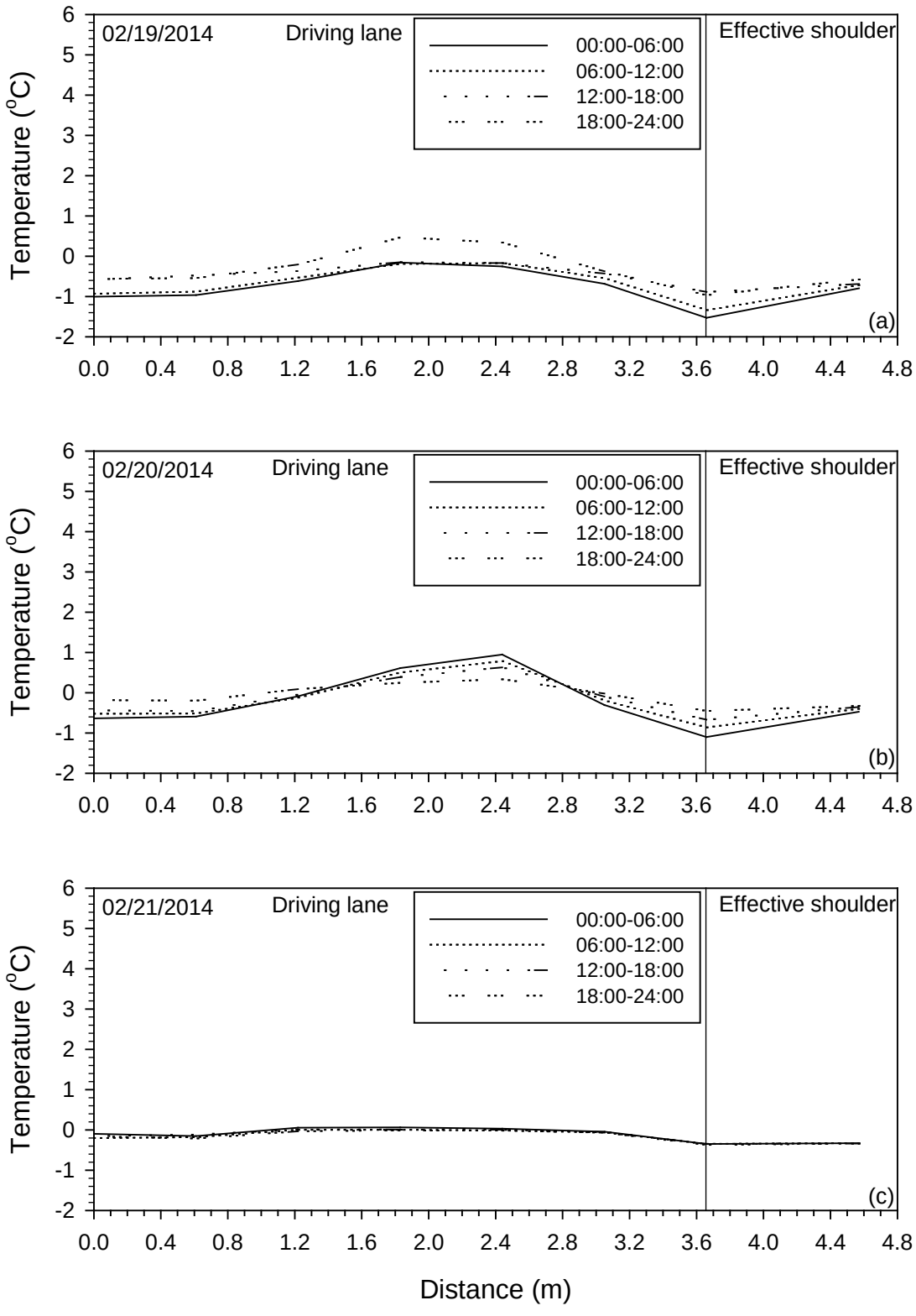

Figure 110. Transverse pavement temperature variation before (a), during (b), and after (c) the peak snow day in the 2013–2014 winter

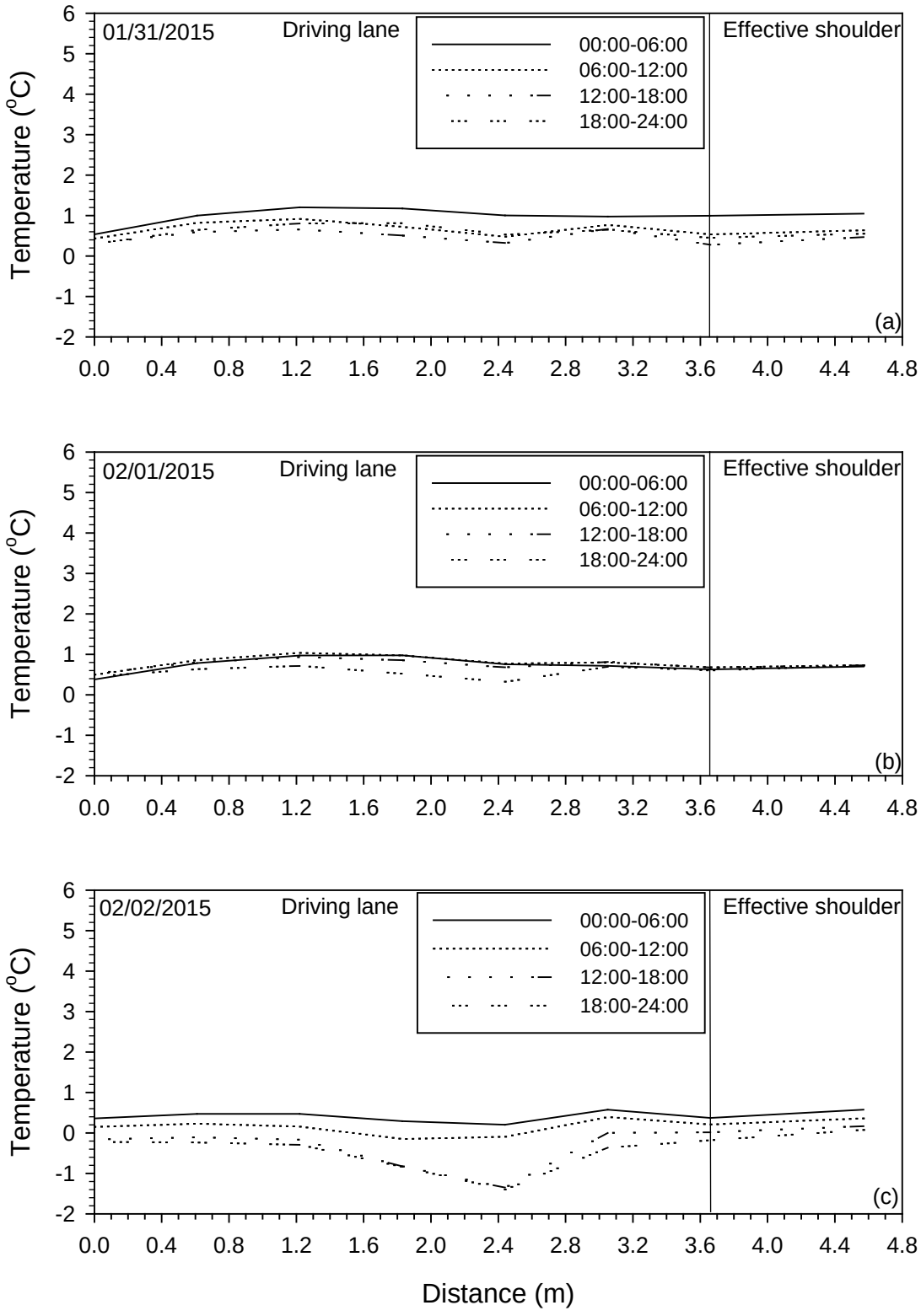

Figure 111. Transverse pavement temperature variation before (a), during (b), and after (c) the peak snow day in the 2014–2015 winter

CHAPTER 6. SUMMARY AND CONCLUSIONS

This report presents results and analysis of field and laboratory tests from a field study conducted on the US 30 reconstruction project in Boone County, Iowa. The project involved removal of the existing pavement which showed severe pavement distresses, reconstruction of the pavement foundation layers (base, subbase, and subgrade), and placement of a new jointed plain cement pavement (JPCC) on the east and west bound lanes of US 30 between mileposts 139.0 and 147.27. Field testing was conducted by the Iowa State University (ISU) research team on the existing pavement prior to the reconstruction work, and on the newly constructed pavement and the foundation layers.

The existing pavement consisted of nominal 76 mm (3 in.) thick asphalt concrete (AC) overlay on nominal 229 mm (9 in.) thick portland cement concrete (PCC). The pavement layers were underlain by nominal 102 mm (4 in.) thick asphalt treated base (ATB). The existing pavement and the ATB layers were removed and the subgrade was undercut during the reconstruction process to place a nominal 410 mm (16 in.) thick modified subbase over the natural existing subgrade. The modified subbase layer consisted of 150 mm (6 in.) thick recycled portland cement concrete (RPCC) material or crushed limestone at the surface underlain by 260 mm (10 in.) thick mixture of RPCC and recycled asphalt pavement (RAP) material. A nominal 254 mm (10 in.) thick JPCP was placed on the newly constructed foundation layer.

Following is a summary of key findings from testing on the existing pavement:

- The existing pavement showed severe pavement distresses with reflective cracking and vertical upheave near joints, especially during winter. The Iowa DOT also reported incidents of damage to vehicle tires and problems with snowplow blade contact.
- Initial field investigations by the Iowa DOT rated the ride quality of the pavement section as “poor” based on pavement condition index (PCI) ranging between 54 and 56 on a 0-100 scale (100 being good and 0 being failed condition).
- Core samples of the existing pavement were obtained near joints using 254 mm (10 in.) and 100 mm (4 in.) diameter diamond rotary bits. These core samples showed that the PCC and the ATB layers were severely deteriorated. Ice lenses and trapped water were presented at the interface of the HMA overlay and PCC, and PCC and ATB layers.
- The gravimetric moisture contents of PCC layer samples ranged between 12.5% and 20.4%. The PCC layer samples obtained from joints showed very little structural integrity.
- Vertical heaves ranging between 15 mm (0.6 in.) to 38 mm (1.5 in.) were measured at two four joints tested.

A detailed laboratory testing plan was executed on bulk samples of RPCC, RPCC/RAP, and subgrade layers. Laboratory testing included characterizing soil index properties, moisture-dry unit weight relationships, resilient modulus (M_r), permanent deformation and particle degradation behavior under cyclic triaxial loading, and frost-heave and thaw-weakening susceptibility. Following are some key findings from the laboratory study:

- Cyclic triaxial testing on RPCC/RAP material indicated that deviator stress and fines content have statistically significant influence on the permanent deformation behavior of the material. Relative density of the material was not found to be a statistically significant parameter for the range testing (85% to 95% relative density).
- Particle degradation due to cyclic loading was assessed by conducting particle-size analysis before and after cyclic triaxial loading on RPCC/RAP material samples. The particle-size analysis test results were used to determining breakage index (BI). Results indicated that the BI values varied between 0 and 5%, which is not considered significant.
- No significant difference or trend in the data was observed between relative density and M_r values on RPCC/RAP material samples. A similar observation was confirmed on recycled materials by other researchers.
- M_r test results on RPCC/RAP material showed that samples with about 12% fines content showed the largest M_r values and M_r values generally increased with increasing fines content at all relative densities.
- Based on M_r testing on the RPCC/RAP materials at 85 to 95% relative density, the k_1 regression coefficient values ranged between 706 and 1354 and was statistically significant for all samples, and the k_2 values ranged between 0.4 and 0.7 and was also statistically significant for all samples. The k_3 values ranged between -0.3 to 0.8 and were not always statistically significant.
- Undrained shear strength (s_u) testing on RPCC/RAP materials varied between 70 and 140 kPa. Samples that contained 6% fines showed the lowest s_u and the samples with natural 3.5% fines content showed the highest s_u. Difference in s_u among samples with varied relative density was small compared to difference among samples with different fines content.
- Freeze thaw testing on the subgrade material showed that moisture contents after testing were about 0 to 2% higher in the material after the freeze-thaw cycles, compared to its initial moisture content. The clayey subgrade material tested was rated as medium for frost-heave susceptibility and as high for thaw-weakening susceptibility.
- Freeze that testing on the RPCC material showed that the moisture contents after testing increased by 2 to 6% in all the samples compared to its initial moisture content. The material was rated as medium for frost-heave susceptibility and as negligible for thaw-weakening susceptibility.

In situ LWD and DCP tests were conducted on the newly constructed foundation layers to determine the mechanistic properties of the foundation layers for comparison with the assumed design values. FWD tests were conducted after the pavement was placed. A summary of the field test results are as follows:

- The CBR values were lower in the top 150 mm (6 in.) RPCC modified subbase layer than the bottom 10 in. of RPCC/RAP modified subbase layer, and the subgrade was very variable. The average CBR of the RPCC modified subbase layer was about 11, the average CBR of the RPCC/RAP layer was about 69, and the subgrade CBR (for the top 300 mm) was about 14. The CBR of the weakest layers within the subgrade was about 7.0.
- LWD test results indicated the elastic modulus varied between 11 and 79 MPa in the longitudinal direction, it varied between 19 and 100 MPa in the transverse direction. The

tests were conducted transversely across the pavement width to capture the variability observed at the surface with aggregate segregation. The higher moduli values corresponded well with areas where more fines were present at the surface.

- The *k* values determined from the FWD test ($k_{FWD\text{-}Static\text{-}Corr}$) showed the lowest values, and were closer to the assumed design *k* value. On average, the average $k_{FWD\text{-}Static\text{-}Corr}$ value was about 0.95 times the design *k* value.
- The *k* values determined from $CBR_{SG\text{-}Weak}$ (i.e., CBR of the weakest layer in the subgrade) using the correlations shown in PCA (1984) ($k_{PCA(1984)}$) were also closer to the assumed design *k* value. The average $k_{PCA(1984)}$ calculated based on CBR_{SG} (i.e., average CBR of the top 300 mm of the subgrade) was about 1.4 times higher than the design *k* value.
- The *k* values calculated using the empirical relationships between CBR and *k* from AASHTO (1993) ($k_{AASHTO(1993)}$) produced values that were about 2 to 4 times higher than the design *k* value.
- Comparison between the $k_{FWD\text{-}Static\text{-}Corr}$ and CBR_{SG} in comparison with published relationships are presented in this report. A similar comparison was provided with $CBR_{SG\text{-}Weak}$ values. These comparisons suggest that the relationships are generally in line with the published data in the literature when $CBR_{SG\text{-}Weak}$ are considered, but not with CBR_{SG}. Nevertheless, the CBR versus *k* relationships show significant scatter and present significant uncertainty in the predictions. Designers must use caution when using such correlations. Developing site-wide or local correlations can provide better confidence in the empirical relationships.

Key findings from the temperature monitoring results are as follows:

- Freeze-thaw cycles decreased with depth as expected. The number of freeze-thaw cycles at the surface ranged between 60 and 82 cycles and decreased to about 5 to 10 cycles near the bottom of the pavement. The number of cycles decreased to less than 3 at 0.7 m depth and no freeze-thaw cycles were observed at depths greater than 1.1 m during the monitoring period.
- The maximum frost depth of 1.1 m was observed during 2012–2013 winter, and in the remaining three winters of the monitoring period (2011–2015), the frost penetration depth reached around 0.6 to 0.8 m.
- The temperature measurements obtained across the pavement width did not show significant temperature differences ($< 1^{o}C$) between the areas beneath the driving lanes and the shoulders, which suggests that no snow cover insulation effects were observed at this site.

REFERENCES

AASHTO. (1993). *AASHTO design guide for design of pavement structures*. American Association of State Highway and Transportation Officials, Washington D.C.

AASHTO T307-99. (2007). "Standard method of test for determining the resilient modulus of soils and aggregate materials." American Association of State Highway and Transportation Officials (AASHTO), Washington, D.C.

AASHTO (2008). Mechanistic-Empirical Pavement Design Guide: A Manual of Practice. 2nd Edition. American Association of State Highway and Transportation Officials, Washington, D.C.

Andersland, O.B., and Ladanyi, B. (2004). *Frozen ground engineering*, 2nd Ed., John Wiley and Sons, Inc., New Jersey.

Andrei, D., M. W. Witczak, C. W. Schwartz, and J. Uzan. 2004. Harmonized resilient modulus test method for unbound pavement materials. *Transportation Research Record*, 1874. Transportation Research Board, Washington, DC, 29–37.

ASTM C127-07. "Standard test method for density, relative density (specific gravity), and absorption of coarse aggregate." American Standards for Testing Methods (ASTM), West Conshohocken, PA.

ASTM C136-06. 2010. "Standard test method for sieve analysis of fine and coarse aggregates." American Standards for Testing Methods (ASTM), West Conshohocken, PA.

ASTM D422-63. "Standard test method for particle-size analysis of soils." American Standards for Testing Methods (ASTM), West Conshohocken, PA.

ASTM D698-07. "Standard test method for laboratory compaction characteristics of soil using standard effort (12,400 ft-lbf/ft3 (600 kN-m/m3))." American Standards for Testing Methods (ASTM), West Conshohocken, PA.

ASTM D854-10. "Standard test methods for specific gravity of soil solids by water pycnometer." American Standards for Testing Methods (ASTM), West Conshohocken, PA.

ASTM D1557-07. "Standard test method for laboratory compaction characteristics of soil using modified effort 56,000 ft-lbf/ft^3 2,700 kN-m/m^3." American Standards for Testing Methods (ASTM), West Conshohocken, PA.

ASTM D2216-10. "Standard test methods for laboratory determination of water (moisture) content of soil and rock by mass." American Standards for Testing Methods (ASTM), West Conshohocken, PA.

ASTM D2487-10. "Standard test method for classification of soil for engineering purposes unified soil classification system." American Standards for Testing Methods (ASTM), West Conshohocken, PA

ASTM D3282-09. 2010. Standard test method for classification of soils and soil-aggregate mixtures for highway construction purposes. American Standards for Testing Methods (ASTM), West Conshohocken, PA

ASTM D4253-00. "Standard test methods for maximum index density and unit weight of soils using a vibratory table." American Standards for Testing Methods (ASTM), West Conshohocken, PA.

ASTM D4254-00. "Standard test methods for minimum index density and unit weight of soils and calculation of relative density." American Standards for Testing Methods (ASTM), West Conshohocken, PA.

ASTM D4318-10. “Standard test methods for liquid limit, plastic limit, and plasticity index of soils.” American Standards for Testing Methods (ASTM), West Conshohocken, PA.
ASTM D5918-06. (2010). “Standard test methods for frost heave and thaw weakening susceptibility of soils.” American Standards for Testing Methods (ASTM), West Conshohocken, PA.
ASTM D6951-03. (2010). “Standard test method for use of the dynamic cone penetrometer in shallow pavement applications.” American Standards for Testing Methods (ASTM), West Conshohocken, PA.
Baladi, G., Dawson, T., and Sessions, C. (2009). *Pavement Subgrade MR Design Values for Michigan’s Seasonal Changes*. Final Report, RC-1531. Michigan Department of Transportation.
Barksdale, R.D. (1972). “Laboratory evaluation of rutting in base course materials.” Proceedings of the Third International Conference on Structural Design of Asphalt Pavements, London, 1972, 161–174.
Becker, P. J., White, D. J., Vennapusa, P. K. R., and Dunn, M. J. (2014). “Freeze-Thaw Performance Assessment of Stabilized Pavement Foundations.” Transportation Research Board, 93rd Annual Meeting, January 12–16, 2014, Washington, D.C.
Darter, M.I., Hall, K.T., and Kuo, C-M. (1995). *Support under Portland Cement Concrete Pavements*, NCHRP Report 372, Transportation Research Board, Washington, D.C.
Drumm, E. C. and Meier, R.W. (2003) “LTPP Data Analysis: Daily and Seasonal Variations in In Situ Material Properties, Project 20-50(7&12)” Final Report to National Cooperative Highway Research Program, <http://trb.org/publications/nchrp/nchrp_w60.pdf>.
Hicks, R.G., and Monismith, C.L. (1971). “Factors influencing the resilient properties of granular materials.” Highway Research Board Record, 345, 15–31.
Hoover, J.M., Huffman, R.T., and Davidson, P.A. (1962). “Soil stabilization field trials, primary Highway 117, Jasper Country, Iowa.” The Forty First Annual Meeting of the Highway Research Board, NAS-NRC, Washington D.C., January 1962.
Iowa DOT. (2009). “Test Section by Milepost.” Primary Office of Materials, Highway Division. Special Investigations Office of Materials Highway Division Iowa Department of Transportation, Ames, IA
Indraratna, B., Lackenby, J., and Christie, D. (2005). “Effect of confining pressure on the degradation of ballast under cyclic loading.” *Géotechnique*, 55(4), 325–328.
Janssen, D. J., and Snyder, M. B. (2000). “Temperature-moment concept for evaluating pavement temperature data.” *Journal of Infrastructure Systems*, 6(2), 81–83.
Janoo, V.C., and Berg, R.L. (1996). PCC Airfield Pavement Response during Thaw-Weakening Periods – A Field Study. Special Report 96-12. CRREL, US Army Corps of Engineers.
Johnson, A. E. (2012). “Freeze-thaw performance of pavement foundation materials.” M.S. thesis. Iowa State University, Ames, IA.
Joint Departments of the Army and Air Force USA. (1985). Pavement Design for Seasonal Frost Conditions. Technical Manual TM 5–818–2/AFM 88–6, Chapter 4. Washington, D.C. U.S. Government Printing Office.
Jones, W., Farnam, Y., Imbrock, P., Spiro, J., Villani, C., Golias, M., Olek, J., and Weiss, W.J. (2013). *An overview of joint deterioration in concrete pavement. Mechanisms, Solution Properties, and Sealers*. Purdue University, West Lafayette, Indiana. 10.5703/1288284315339.

Jong, D., Bosscher, P.J., and Benson, C.H. (1998). “Field Assessment of Changes in Pavement Moduli Caused by Freezing and Thawing,” *Transportation Research Record*, No. 1615, Transportation Research Board, National Research Council, Washington, D.C., pp. 41–48.

Kamal, M.A., Dawson, A.R., Farouki, O.T., Hughes, D.A.B., and Sha‘at, A.A. (1993). “Field and Laboratory Evaluation of the Mechanical Behavior of Unbound Granular Materials in Pavements,” *Transportation Research Record* 1406, Transportation Research Board, Washington, D.C., pp. 88–97.

Kancherla, A. (2004). “Resilient modulus and permanent deformation testing of unbound granular materials.” M.S. thesis, Texas A&M University, College Station, TX.

Kolisoja, P. (1998). “Large scale dynamic triaxial tests.” III. Delprosjektrapport 20, Arbeidsfelleskapet KPG, Oslo, Norway.

Konrad, J-M, and Roy, M. (2000). “Flexible pavement in cold regions: a geotechnical perspective.” Can. Geotech. J. 37: 689–699 (2000).

Lary, J. A., Mahoney, J. P., and Sharma, J. (1984). Evaluation of Frost Related Effects on Pavements. Final Report, WA-RD 67.1. Washington State Transportation Research Center and the University of Washington.

Li, W., Pour-Ghaz, M., Castro, J., and Weiss, J. (2012). “Water absorption and critical degree of saturation relating to freeze-thaw damage in concrete pavement joints.” *Journal of Materials in Civil Engineering*. 2012.24:299-307.

Lukanen, E. O., Worel, B. J., and Clyne, T. (2006). “MnROAD Environmental Factors that Affect Ride.” Proceedings of the 13th International Conference on Cold Regions Engineering. Ed. M. Davies, J.E. Zufelt, July 23–26, Orono, Maine.

NDDOT. (2015). “Why there are Spring Load Restrictions.” North Dakota Department of Transportation. Accessed in December 10, 2015.

Newcomb, D. E., and Birgisson, B. (1999). NCHRP Synthesis of Highway Practice 278: Measuring In Situ Mechanical Properties of Pavement Subgrade Soils. Transportation Research Board, National Research Council, Washington D.C., 1999. 43–51.

Ovik, J. M., Siekmeier, J. A., and Van Deusen, D. A. (2000). Improved Spring Load Restriction Guidelines Using Mechanistic Analysis. Final Report. 2000-18. Minnesota Department of Transportation.

PCA (Portland Cement Association). (1984). *Thickness design for concrete highway and street pavements*, Portland Cement Association.

Saeed, A. (2008). “Performance-related tests of recycled aggregates for use in unbound pavement layers.” NCHRP report 598, Transportation Research Board, Washington, D.C.

Saarenketo, T., and Saara, A. (2005). *Managing spring thaw weakening on low volume roads – problem description, load restriction policies, monitoring and rehabilitation.* Final report 2_3 Roadex II Project. Roadscanners.

Schmalzer, P. N. (2006). *LTPP Manual for Falling Weight Deflectometer Measurements – Version 4.1*. Report No. FHWA-HRT-06-132, Federal Highway Administration, McLean, VA.

Simonsen, E., and Isacsson, U. (1999). “Thaw weakening of pavement structures in cold regions.” *Cold Regions Science and Technology*. 29(2), 135–151.

Taylor, P.C. (2011). “Preventing joint deterioration in concrete pavements a summary of current knowledge.” Map Brief 6-1, Moving Advancements into Practice. National Concrete Pavement Technology Center, Ames, IA. http://www.cproadmap.org/publications/MAPbrief6-1.pdf

Taylor, P.C., Sutter, L., and Weiss, J. (2012). *Investigation of deterioration of joints in concrete pavements*. Final report. Institute for Transportation, Iowa State University, Ames, IA.

Thom, N.H., and Brown, S.F. (1987). “Effect of moisture on the structural performance of a crushed-limestone road base.” *Transportation Research Record*, 1121. Transportation Research Board, Washington, D.C., 50–56.

Thom, N.H., and Brown, S.F. (1989). “The mechanical properties of unbound aggregates from various sources.” Unbound Aggregates in Roads: Proceedings of the Fifth International Symposium on Unbound Aggregates in Roads, Dawson, A. (ed.), UNBAR 5, Nottingham, United Kingdom, 130–142.

U.S. Climate Data. http://www.usclimatedata.com/climate/ames/iowa/united-states/usia0026 Accessed on August 1, 2015.

Vandenbossche, J. M. (2005). “Effects of slab temperature profiles on the use of falling weight deflectometer data to monitor joint performance and detect voids.” *Transportation Research Record*, 2005, Transportation Research Board, Washington, D.C., 75–85.

Von Quintus, H.L., and Simpson, A.L. (2002). *Back-Calculation of Layer Parameters for LTPP Test Sections, Volume II: Layered Elastic Analysis for Flexible and Rigid Pavements*. Final Report May 1997 – August 2001. FHWA-RD-01-113. Federal Highway Administration.

White, D.J., and Vennapusa, P. (2014). *Optimizing Pavement Base, Subbase, and Subgrade Layers for Cost and Performance of Local Roads – Field Data Report*. Concrete Pavement Technology Center and Center for Earthworks Engineering Research, Iowa State University, Ames, IA.

Witczak, M., and Uzan, J. (1988). “The universal airport design system, Report I of IV: Granular material characterization.” Department of Civil Engineering, University of Maryland, College Park, MD.

Wolfe, A.J. (2011). “Behavior of composite pavement foundation materials subjected to cyclic loading.” M.S. thesis, Iowa State University, Ames, IA.

Vennapusa, P., and D. J. White. (2009). “Comparison of light weight deflectometer measurements for pavement foundation materials.” *Geotechnical Testing Journal*, ASTM, 32(3), 239-251.

Zhang, J. (2013). “Investigation of deterioration of joints in concrete pavements.” Ph.D. Thesis. Iowa State University, Ames, IA.

Zhang, J., White, D.J., Taylor, P.C., and Shi, C. (2015). “A case study of evaluating joint performance in relation with subsurface permeability in cold weather region.” *Cold Regions Science and Technology*. 110(2015)19-25. 10.1016/j.coldregions.2014.11.003.

Zorn, G. (2003). *Operating manual: Light drop-weight tester ZFG2000*, Zorn Stendal, Germany.

APPENDIX A: AASHTO 1972, AASHTO (1993), AND PCA (1984) DESIGN CHARTS

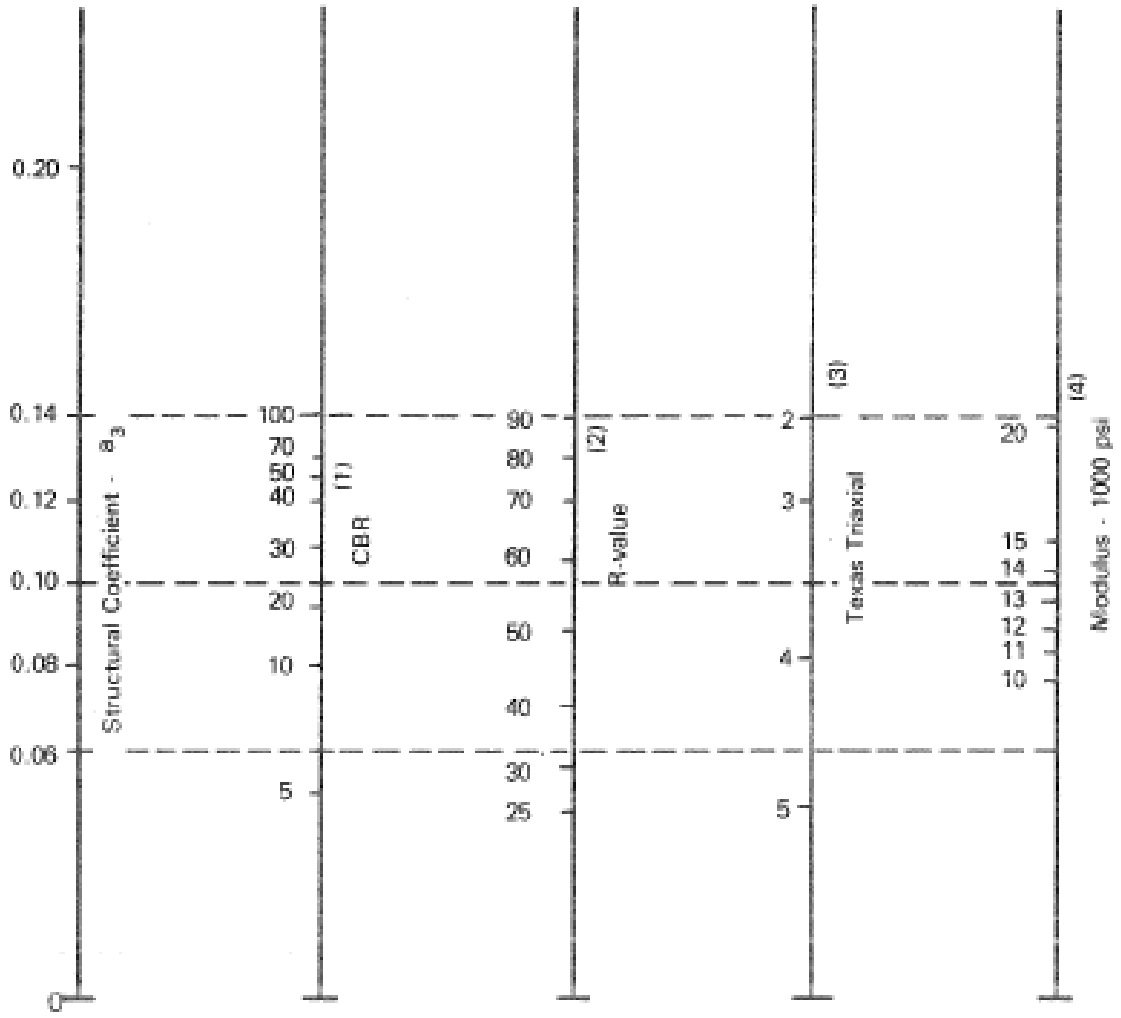

(1) Scale derived from correlations from Illinois.

(2) Scale derived from correlations obtained from The Asphalt Institute, California, New Mexico and Wyoming.

(3) Scale derived from correlations obtained from Texas.

(4) Scale derived on NCHRP project *(3)*.

Figure 112. Chart to estimate modulus of subbase layer (E_{SB}) from CBR (from AASHTO 1993 based on results from van Til et al. 1972)

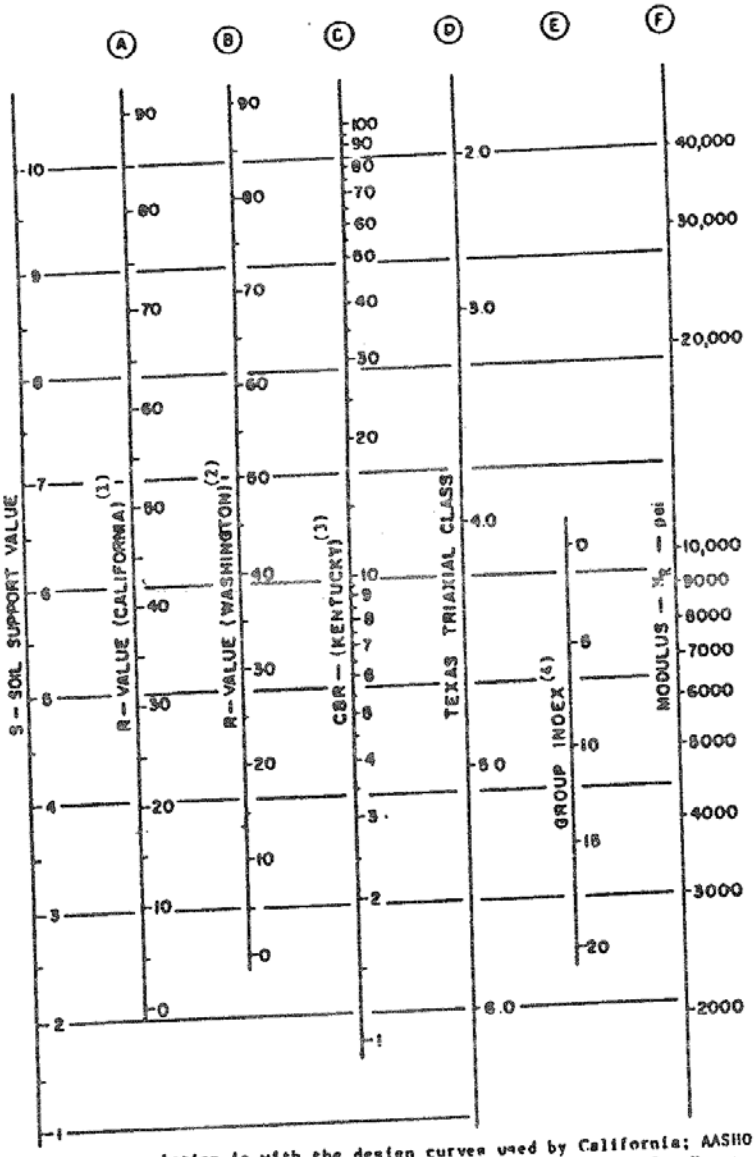

(1) The correlation is with the design curves used by California; AASHO designation is T-173-60, and exudation pressure is 240 psi. See Hveem, F.N., and Carmany, R.M., "The Factors Underlying the Rational Design of Pavements." Proc. HRB, Vol. 28 (1948) pp. 101-136.
(2) The correlation is with the design curves used by Washington Dept. of Highways; exudation pressure is 300 psi. See "Flexible Pavement Design Correlation Study." HRB Bull. 133 (1956).
(3) The correlation is with the CBR design curves developed by Kentucky. See Drake, W.B., and Havens, J.H., "Re-Evaluation of Kentucky Flexible Pavement Design Criterion." HRB Bull. 233 (1959) pp. 33-56. The following conditions apply to the laboratory-modified CBR: specimen is to be molded at or near the optimum moisture content as determined by AASHO T-99; dynamic compaction is to be used with a hammer weight of 10 lb dropped from a height of 18 in.; specimen is to be compacted in five equal layers with each layer receiving 10 blows; specimen is to be soaked for 4 days.
(4) This scale has been developed by comparison between the California R-value and the Group Index determined by the procedure in Proc. HRB Vol. 25 (1945) pp. 376-392.

Figure 113. Chart to estimate M_r of subgrade from CBR (from AASHTO 1993 Appendix FF)

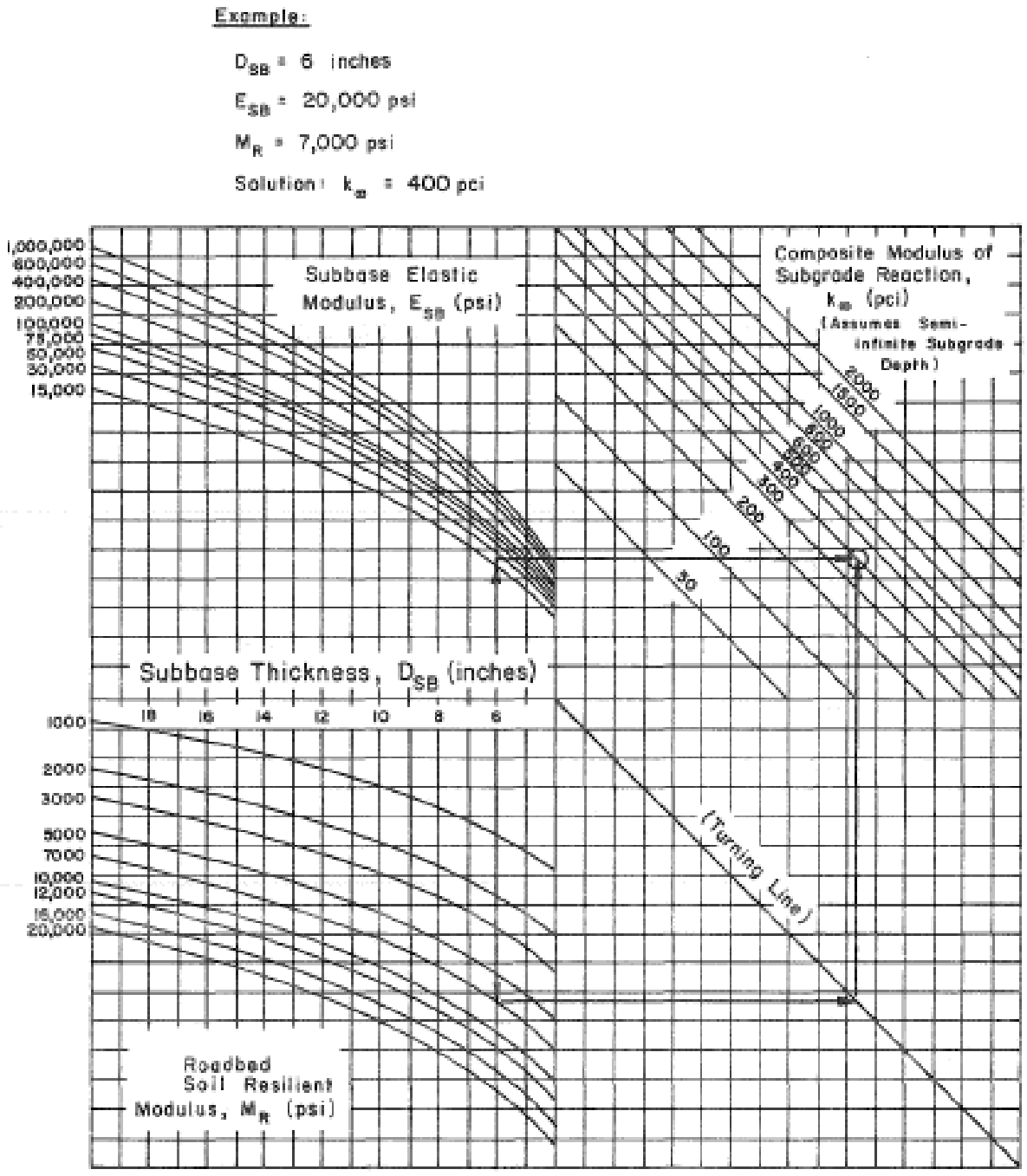

Figure 3.3. Chart for Estimating Composite Modulus of Subgrade Reaction, k_∞, Assuming a Semi-Infinite Subgrade Depth. (For practical purposes, a semi-infinite depth is considered to be greater than 10 feet below the surface of the subgrade.)

Figure 114. Chart for estimating composite modulus of subgrade reaction ($k_{comp\text{-}AASHTO(1993)}$) assuming a semi-infinite subgrade depth (from AASHTO 1993)

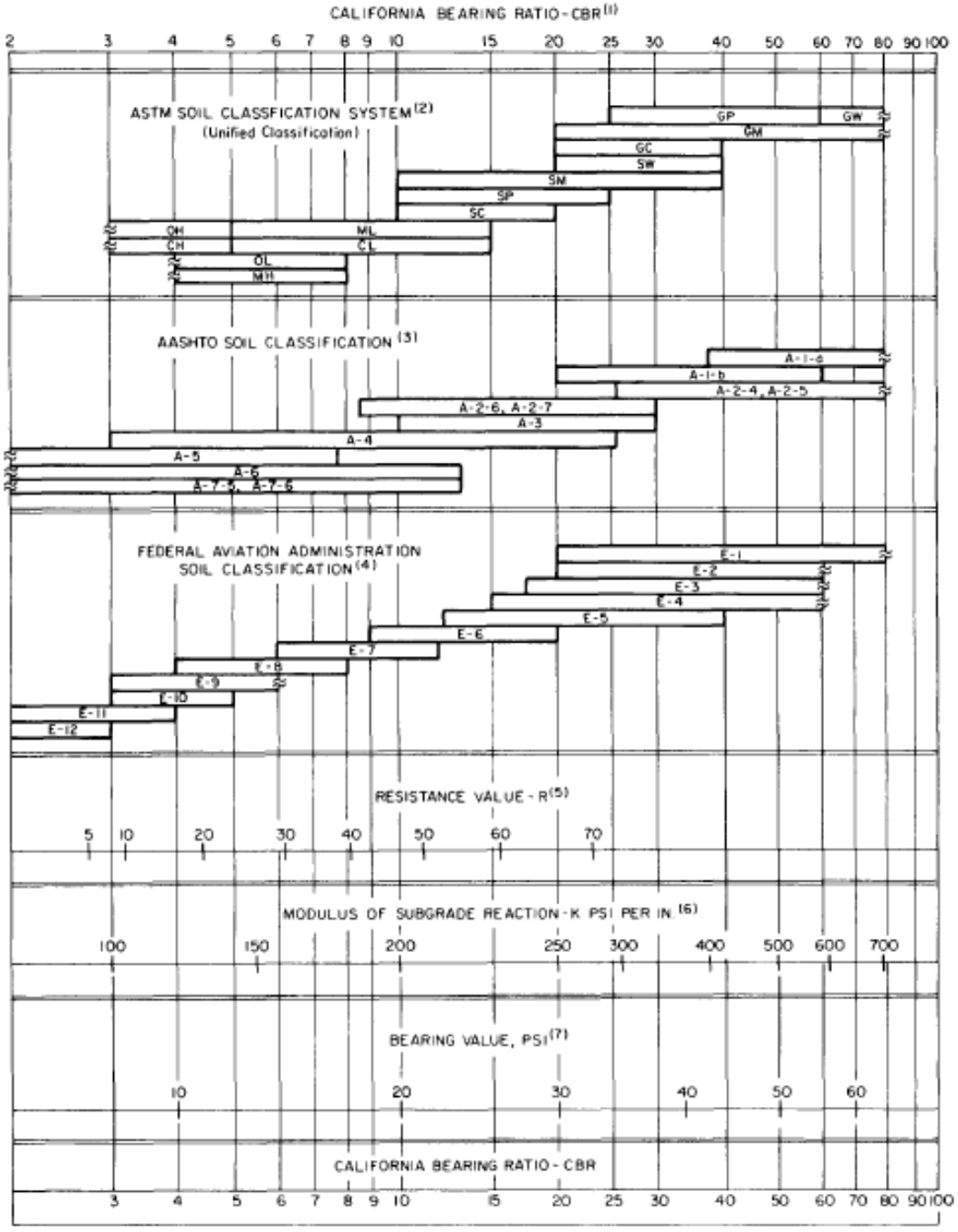

(1) For the basic idea, see O. J. Porter, "Foundations for Flexible Pavements," Highway Research Board *Proceedings of the Twenty-second Annual Meeting*, 1942, Vol. 22, pages 100-136.
(2) ASTM Designation D2487.
(3) "Classification of Highway Subgrade Materials," Highway Research Board *Proceedings of the Twenty-fifth Annual Meeting*, 1945, Vol. 25, pages 376-392.
(4) *Airport Paving*, U.S. Department of Commerce, Federal Aviation Agency, May 1948, pages 11-16. Estimated using values given in FAA *Design Manual for Airport Pavements* (Formerly used FAA Classification; Unified Classification now used.)
(5) C. E. Warnes, "Correlation Between *R* Value and *k* Value," unpublished report, Portland Cement Association, Rocky Mountain-Northwest Region, October 1971 (best-fit correlation with correction for saturation).
(6) See T. A. Middlebrooks and G. E. Bertram, "Soil Tests for Design of Runway Pavements," Highway Research Board *Proceedings of the Twenty-second Annual Meeting*, 1942, Vol. 22, page 152.
(7) See item (6), page 184.

Figure 115. Chart for estimating modulus of subgrade reaction (*k*) from CBR (from PCA 1984)

APPENDIX B: PARTICLE DEGRADATION TEST RESULTS

Degradation of the unbound granular materials (BI values) was calculated to quantify changes in particle size distribution of the tested materials after the permanent deformation tests.

Sample BI Calculation

Area below the particle size distribution curve of untested material is denoted as A and of tested materials is denoted as B. The breakage index (BI) was calculated using Equation A1. Detailed calculation of area between two sieve sizes are summarized in Table 26 and two particle size distribution curves are plotted in Figure 116.

$$BI = \frac{A-B}{B} = \frac{1151.0-1169.6}{1169.6} \times 100\% = -1.59\% \quad \text{(A1)}$$

Table 26. Breakage index (BI) calculation on a subbase sample

	Untested material (A)		**Tested material (B**	
Sieve Size (mm)	**Percent Passing (%)**	**Area between two points (%*mm)**	**Percent Passing (%)**	**Area between two points (%*mm)**
100.0	576.5	100.0	575.6	100.0
77.4	209.7	77.1	210.1	77.4
62.4	235.0	63.0	242.8	62.4
36.6	78.9	39.2	85.4	36.6
29.4	10.4	32.2	11.3	29.4
28.2	28.2	30.8	30.8	28.2
20.8	7.8	22.8	8.6	20.8
16.1	2.6	17.6	2.8	16.1
13.5	1.2	14.5	1.3	13.5
11.5	0.8	12.3	0.8	11.5
9.6	—	10.1	—	9.6
Sum	**A**	**1151.0**	**B**	**1169.6**
BI			**−1.59%**	

Note: — means no value calculated.

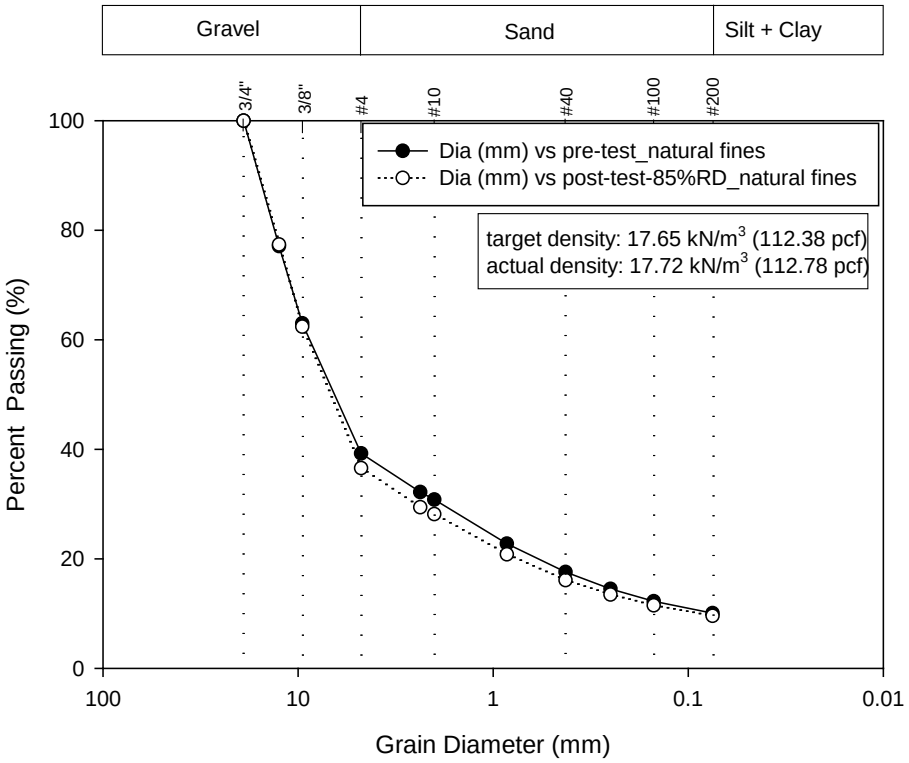

Figure 116. Particle size distribution change of a subbase sample

Particle Size Distribution Changes of All Samples

For each permanent deformation test sample, wash sieve analyses were conducted on all materials from each sample and particle size distribution curves were plotted to compare with related original particle size distribution curves for calculating breakage index. Figure 117, Figure 118, Figure 119, and Figure 120 shows changes in particle size distribution after NCHRP 598 ε_p test for RPCC/RAP with 3.5%, 0.8%, 6.0%, and 12.4% F_{200} separately.

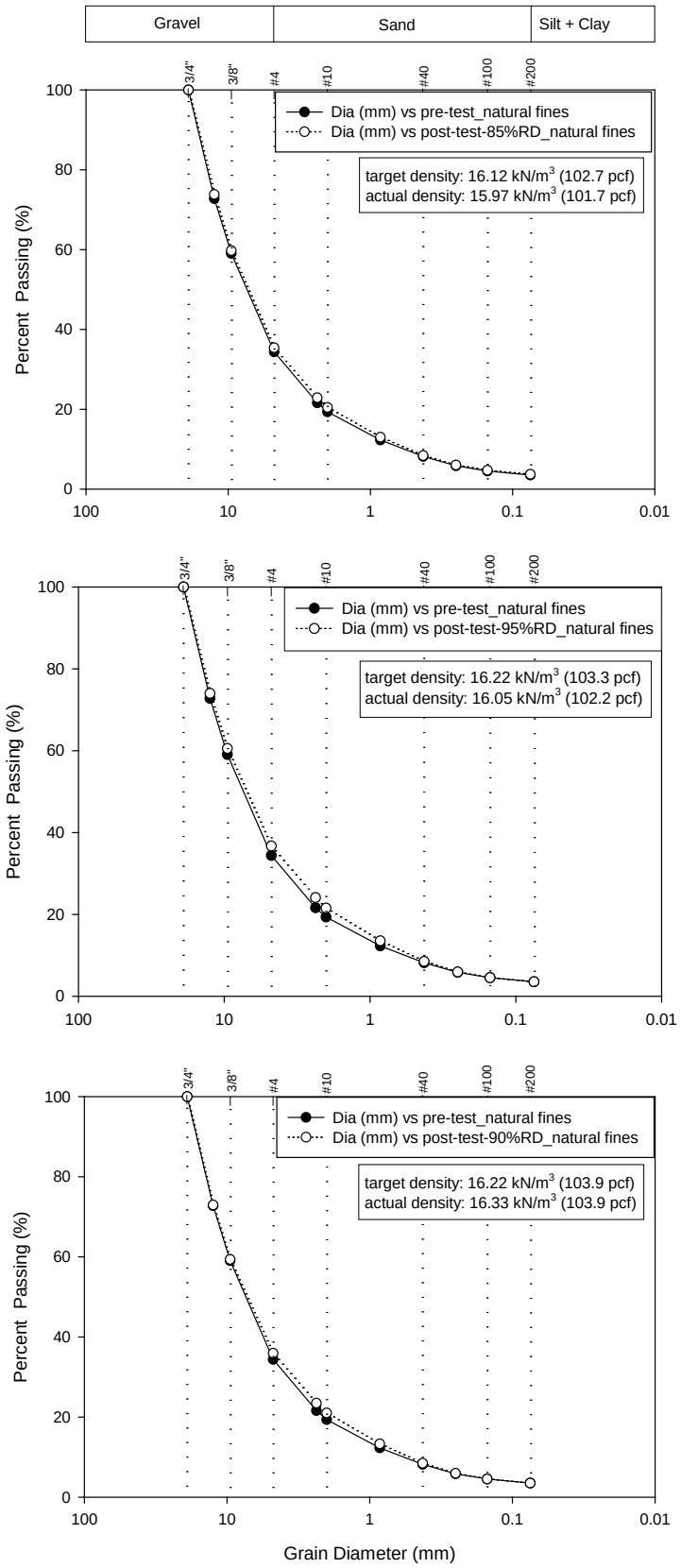

Figure 117. Particle size distributions on RPCC/RAP with 3.5% fines content

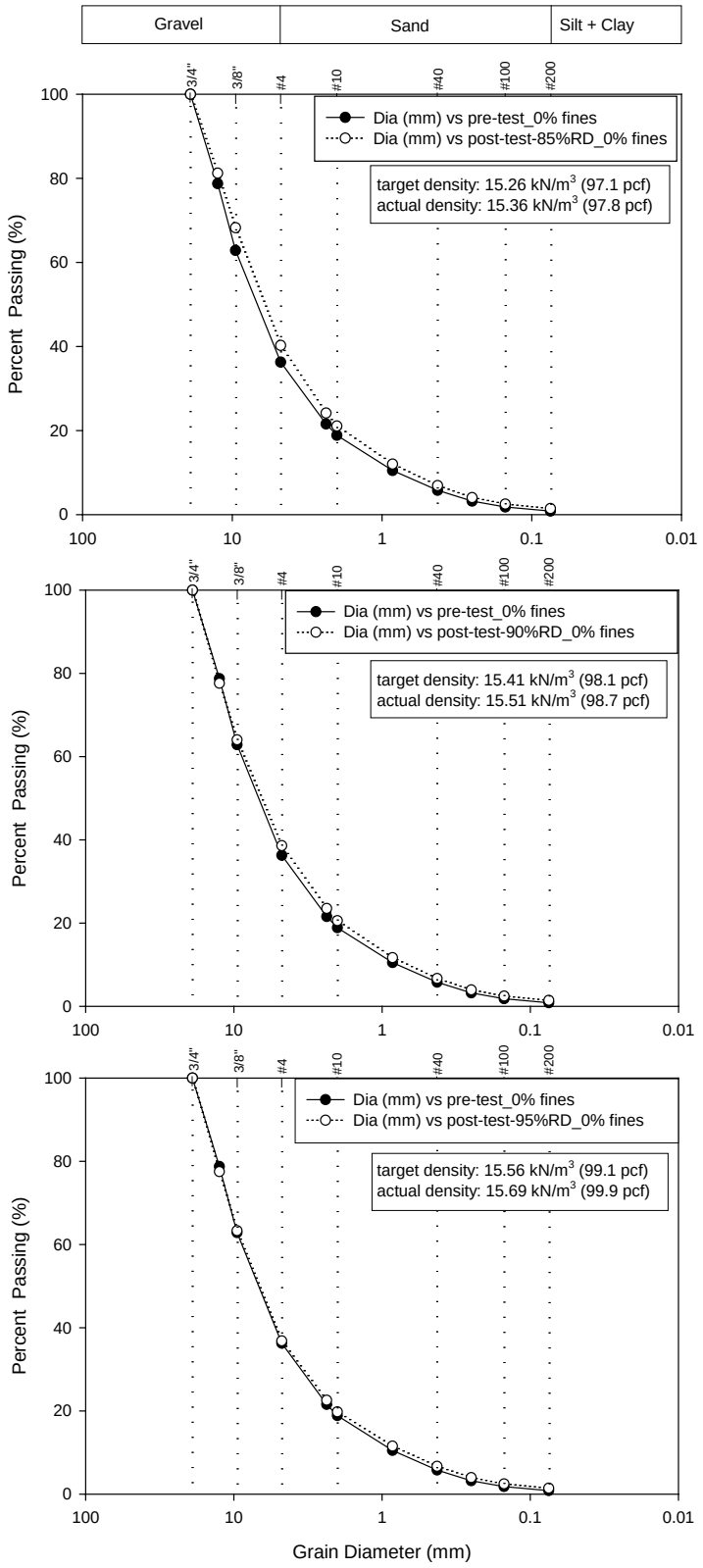

Figure 118. Particle size distributions on RPCC/RAP with 0.8% fines content

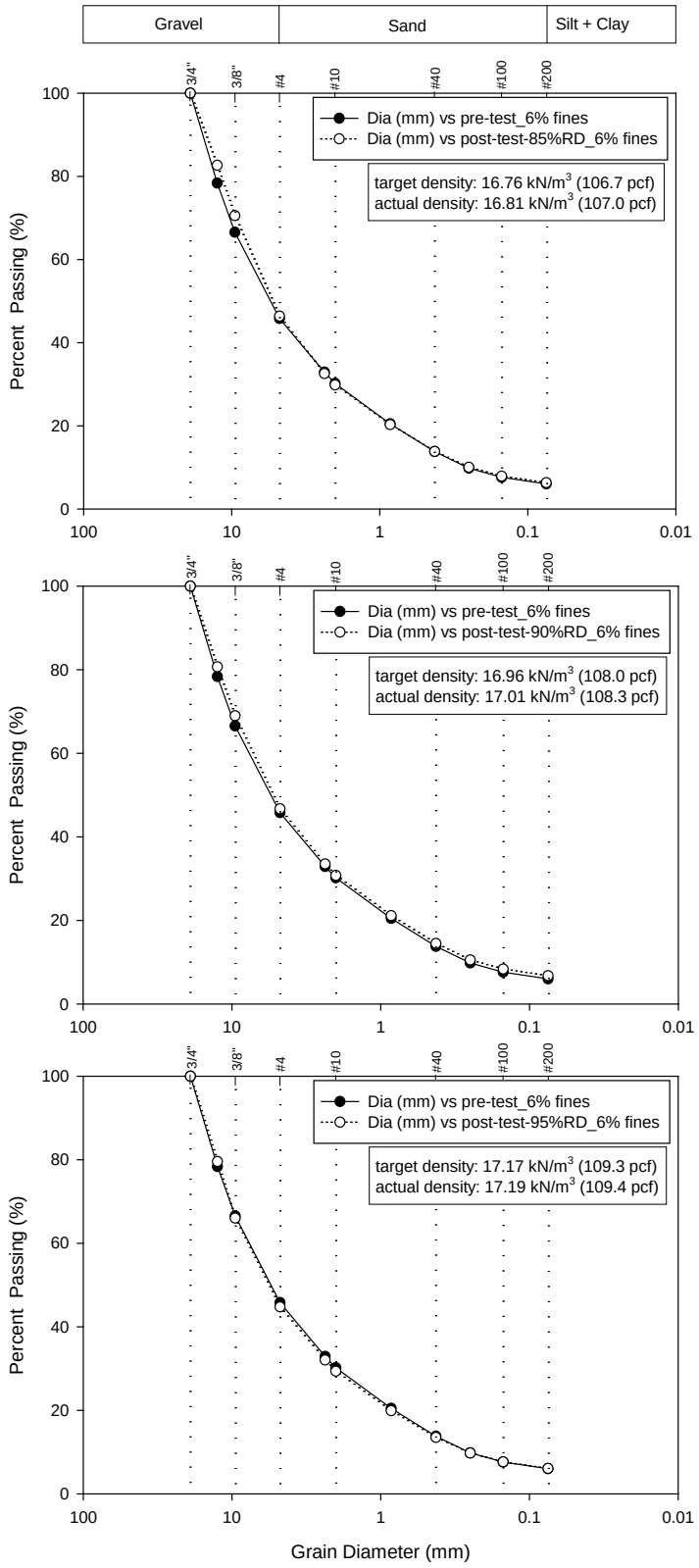

Figure 119. Particle size distributions on RPCC/RAP with 6.0% fines content

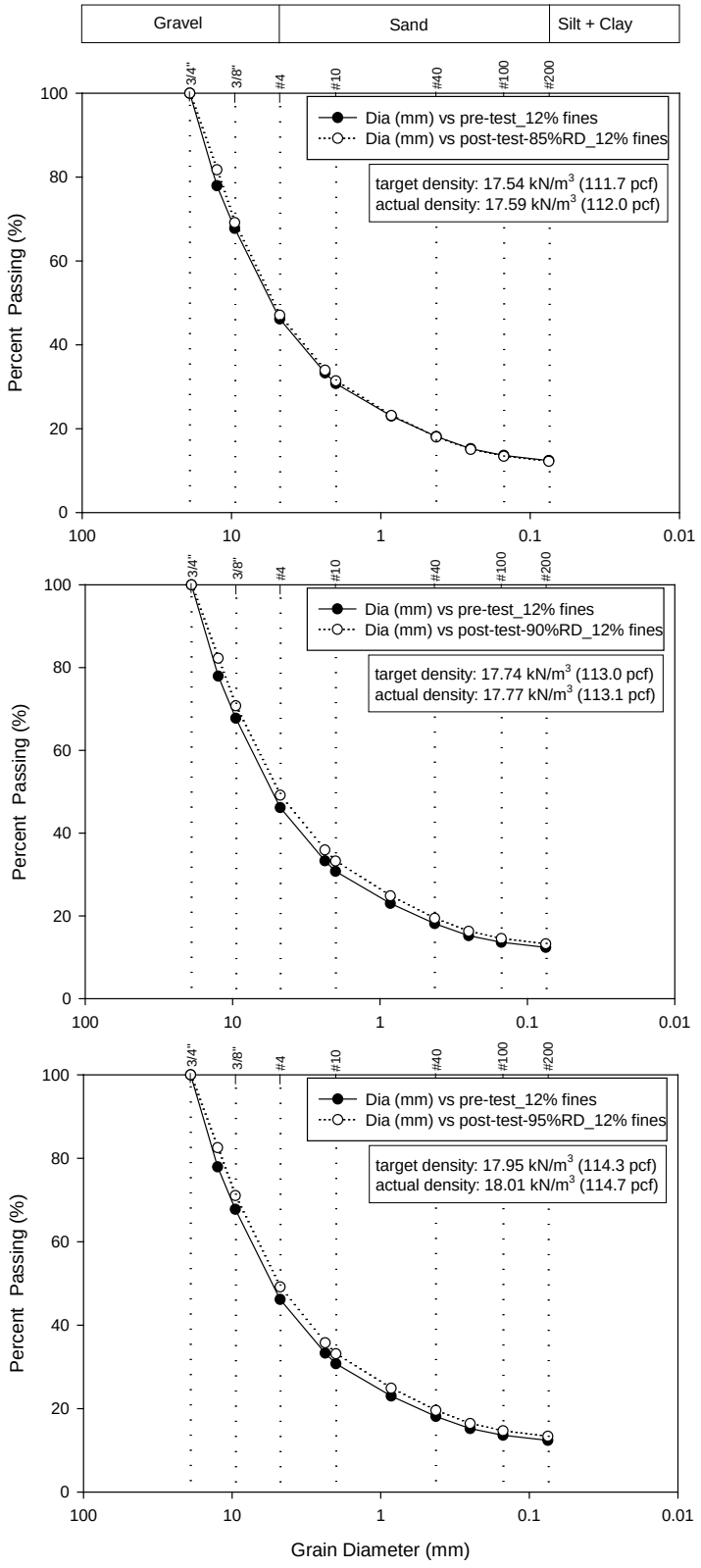

Figure 120. Particle size distributions on RPCC/RAP with 12.4% fines content